Characterization of Amyloid-β Interactions at the Membrane Interface: Implications for Pathogenesis

by

Pamela T. Wong

A dissertation submitted in partial fulfillment
of the requirements for the degree of
Doctor of Philosophy
(Biological Chemistry)
in The University of Michigan
2009

Doctoral Committee:

Professor Ari Gafni, Chair
Professor Carol A. Fierke
Professor Alexander J. Ninfa
Professor Duncan G. Steel
Associate Professor Zhaohui Xu

2009

ACKNOWLEDGEMENTS

I would like to thank everyone that has helped me along the way. I would especially like to express my gratitude to my advisor, Ari Gafni, who has been always been extremely supportive and encouraging throughout my time in graduate school. I have learned a great deal not only about science, but also about how to be a good mentor and teacher from working in his lab. I would also like to thank Duncan Steel who has also been an encouraging mentor throughout my graduate career. From him, I learned a lot about how to look at biological problems from a very different perspective. I feel very lucky to have two extremely understanding and supportive mentors during graduate school who care a great deal about their students. I would also like to thank the rest of my dissertation committee: Carol Fierke, Alex Ninfa, and Zhaohui Xu for their advice and feedback over the years.

I am also extremely grateful for having the privilege to work with so many extraordinary people in the Gafni-Steel lab. I would like to thank the current members, Kathleen Wisser, Joe Schauerte, Edgar Lee, Hao Ding, Jamie Van Etten, and Robin Johnson and past members, Narin Pattaramanon, Jue Shi, Jeff Brender, and Liz Shtrahman. The lab has always felt like a family, and I am very lucky to have worked with such fun and wonderful people. I would especially like to thank Kathleen Wisser and Joe Schauerte. Kathleen has always been there when I needed help with anything and everything, and I am indebted to Joe for all of his insightful advice and guidance. Both Kathleen and Joe will always drop whatever they are doing to help you, and I am thankful for their friendship over the past several years.

I would also like to thank my good friends that I have met before and during graduate school, especially: Mike Corradetti, Joe Lee, Narin Pattaramanon, June Pais, Jue Shi, Connie Wei, Frank Yang, and Qian Yang. I definitely would not have been able to get this far with out them. Lastly, I am most grateful to my parents and my brother for their love, support, and encouragement always.

CONTENTS

LIST OF FIGURES

Figure

LIST OF TABLES

Tables

LIST OF ABBREVIATIONS

Aβ	Amyloid-β
Aβ40 [Y10W]	Aβ40 with a tyr to trp substitution at position 10; AD Alzheimer's Disease
AFM	atomic force microscopy
AMP	antimicrobial peptide
APP	amyloid precursor protein
CF	5(6)-carboxyfluorescein
Dns-DPPE	*N*-(5-dimethylaminonaphthalene-1-sulfonyl)-1,2-Dipalmitoyl-*sn*-Glycero-3-Phosphoethanolamine)
DPPC	1,2-Dipalmitoyl-*sn*-Glycero-3-Phosphocholine
DPPC/PG	liposomes with equimolar DPPC and DPPG
DPPG	1,2-Dipalmitoyl-*sn*-Glycero-3-[Phospho-*rac*-(1-glycerol)]
DPPS	1,2-Dipalmitoyl-*sn*-Glycero-3-[Phospho-L-Serine]
L:P	lipid to peptide molar ratio
LC	liquid-crystalline
LO	liquid-ordered
LUV	large unilamellar vesicle
NaP_i	sodium phosphate
PFT	pore forming toxin
POPC	1-Palmitoyl-2-Oleoyl-*sn*-Glycero-3-Phosphocholine
POPC/PG	liposomes with equimolar POPC and POPG
POPG	1-Palmitoyl-2-Oleoyl-*sn*-Glycero-3-[Phospho-*rac*-(1-glycerol)]
RT	room temperature
SUV	small unilamellar vesicle
WT	wild-type

ABSTRACT

The 40 and 42 residue amyloid-β (Aβ) peptides are major components of the proteinaceous plaques prevalent in the Alzheimer's disease afflicted brain and have been shown to play an important role in instigating neuronal degeneration. Whereas it was previously thought that Aβ becomes cytotoxic upon forming large fibrillar aggregates, recent studies suggest that soluble intermediate sized oligomeric species cause cell death through membrane permeabilization. In this thesis we examine the interactions between Aβ40 and lipid membranes using liposomes as a model system to determine how changes in membrane composition influence the conversion of Aβ into these toxic species. Aβ40 membrane binding was monitored using fluorescence based assays with a tryptophan substituted peptide (Aβ40 [Y10W]). We extend previous observations that Aβ40 interacts preferentially with negatively charged membranes, and show that binding of nonfibrillar, low molecular weight oligomers of Aβ40 to anionic, but not neutral, membranes involves insertion of the peptide into the bilayer, as well as sequential conformational changes corresponding to the degree of oligomerization induced. Significantly, while anionic membranes in the gel, liquid crystalline, and liquid ordered phases all induce these conformational changes equally, membrane permeabilization is dramatically reduced as the fluidity of the membrane is decreased. These findings demonstrate that binding alone is not sufficient for membrane permeabilization, and that the latter is also highly dependent on the fluidity and phase of the membrane. We

conclude that binding and pore formation are two distinct steps. The differences in Aβ behavior induced by membrane composition may have significant implications on the development and progression of AD as neuronal membrane composition is altered with age.

CHAPTER I

Introduction to Amyloid-β induced neurotoxicity

In studying biochemistry it is easy to overlook just how remarkable it is that simple chains of different combinations of only twenty amino acids can fold into unique, complicated, three dimensional structures with such a diverse range of functions. Protein folding and structure play critical roles in determining function, and slight alterations in the protein either by modifications or sequence alterations can result in significant conformational changes, and have a dramatic impact on function.

Several age-related degenerative diseases are characterized by protein misfolding and aggregation. Degenerative diseases such as Alzheimer's disease, type II diabetes, and Parkinson's disease to name a few, are associated with the accumulation of deposits of aggregates of different proteins that belong to a class of proteins called the amyloid proteins. There are approximately 24 amyloid proteins that have been identified, involved in seemingly unrelated diseases (table 1.1). Interestingly, these proteins share no sequence homology, but are induced to have the same unique highly ordered conformation in the disease state. While the normal functions of most of these proteins are unknown, their aggregated forms are involved in the induction of cellular death in each of their associated diseases.

Disease	Amyloid-forming proteins and peptides
Alzheimer's disease	Amyloid-β
Parkinson's disease	α-Synuclein
Type II diabetes	Islet amyloid polypeptide (amylin)
Senile amyloidosis	Transthyretin
Prion-related diseases	PrP
Familial British dementia	ABri
Dialysis-associated amyloidosis	β_2-Microglobulin
Secondary systemic amyloidoses	Serum amyloid A
Amyotrophic lateral sclerosis	Superoxide dismutase-1

Table 1.1: Examples of diseases caused by amyloidogenesis and the associated amyloid protein or peptide.

The amyloid proteins are characterized by the ability to oligomerize extensively, with the capacity to form extremely high ordered oligomers called fibrils (>1000 mer). Amyloids were in fact first discovered when Alois Alzheimer observed proteinaceous plaques or deposits in the brain tissue from patients with Alzheimer's disease in 1906 (1). Further examination of these plaques revealed that they were composed of aggregates of amyloid fibrils. Fibrils appear as thin filaments visible by electron microscopy, with a diameter of about 10 nm and a variable length that can be 100's of nm in length. The formation of fibrils is an essentially irreversible process. Before a fibril is formed, amyloid oligomers are soluble, and can reversibly exchange subunits. For example, a hexamer can still revert back to a trimer. Fibrilization is thus slow until a critical oligomeric species is reached that can nucleate fibril formation. Fibril growth then occurs exponentially. Once a fibrillar structure is formed, it cannot revert back to a soluble intermediate oligomeric species (figure 1.1).

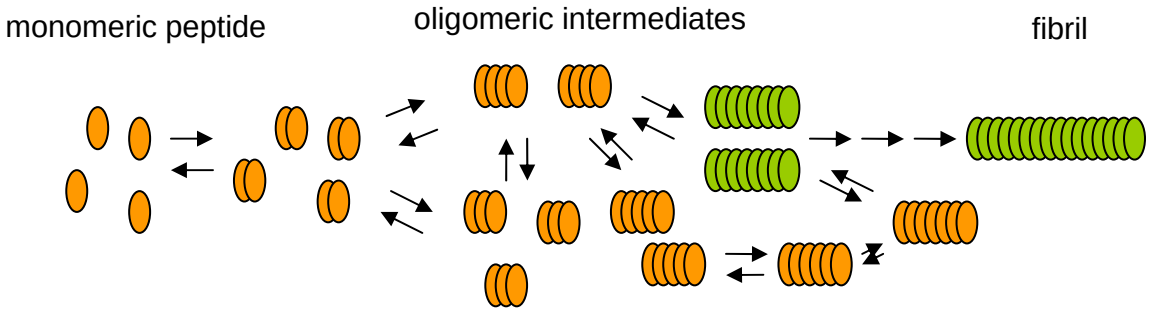

Figure 1.1: The oligomerization of amyloid peptides proceeds from the monomeric state to a fibrillar structure through oligomeric intermediates. The intermediate oligomeric species are in rapid equilibrium, and can exchange subunits until a critical oligomeric species which can nucleate fibril formation is formed (green oligomers).

There is a significant amount of ambiguity of the terminology in the amyloid field. In this thesis, soluble intermediate sized oligomers (> decamer) are referred to as protofibrils, and oligomers smaller than the protofibrils are referred to as low molecular weight oligomers. Fibrils are high in β-sheet content, and contain a unique quaternary structure, termed the amyloid fold. The amyloid fold consists of an intermolecular cross β-sheet structure that spans across more than one molecule, making the fibril a 'β-sheet of β-sheets' (figure 1.2)(2).

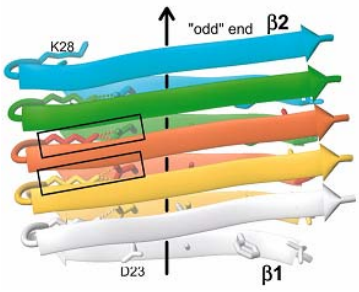

Figure 1.2: NMR structure of amyloid-β. The amyloid fold consists of unique parallel arrangement of in-register intermolecular β-sheets. (reproduced with permission from Luhrs T., et al. (2005) *Proc Natl Acad Sci U S A 102*, 17342-17347. Copyright 2005 National Academy of Sciences, U.S.A.)

Amyloidogenesis is a nucleation dependent process. These proteins begin in solution as monomeric units, and oligomerize reversibly until the critical oligomeric species that can nucleate fibril growth is formed. Fibril growth is thus slow until this species is reached, after which fibril growth occurs exponentially. As mentioned above, there is no sequence homology between the amyloid proteins, demonstrating that specific sequences or side chain interactions are not required to adopt this cross β-sheet structure. In fact, it has been shown that it is possible to induce several non amyloidogenic proteins to form amyloid fibrils through manipulating the conditions *in vitro* (3). Thus fibrilization appears to be a fundamental motif of the polypeptide backbone. Furthermore, antibodies raised against the fibrillar form of one of the amyloid peptides are able to recognize the fibrillar forms of other amyloid forming peptides, demonstrating the structural similarities between these very different proteins (4, 5). All of the amyloid proteins are found in a soluble state under normal conditions, and their levels are not always significantly increased in the disease state. Therefore the question remains as to what induces these proteins to convert from a soluble oligomeric species to the fibril state *in vivo*.

This purpose of this dissertation is to further characterize the amyloidogenic peptide, amyloid-β (Aβ), which plays a key role in the neurodegeneration prevalent in the Alzheimer's disease (AD) brain. This disease affects close to 4.5 million people in the U.S. alone, and this number is rising rapidly as the average expected lifespan increases (6). While AD is a highly age-related disease, it can also occur relatively early on in life (30-40s) in certain cases. AD is a common form of progressive senile dementia that

results in the gradual loss of neurons in the cerebral cortex and hippocampal region of the brain. This loss of cell function gradually leads to the destruction of memory, the ability to learn, reason, make judgments, communicate, and carry out daily activities. Eventually the loss of brain function is fatal. Although AD was first diagnosed over 100 years ago, and has been studied extensively, what causes this disease to develop is still unclear. The first observation made in AD affected brain was the presence of diffuse proteinaceous plaques. These plaques were made up of aggregates of fibrils of the Aβ peptide, pointing to the involvement of this peptide in the pathogenesis of AD. Over the years, evidence has accumulated pointing to the direct involvement of Aβ in AD development. One of the most significant initial observations was the discovery of several point mutations in the Aβ sequence in families with genetically inherited forms of early-onset AD. The Arctic (E22G), Dutch (E22Q), Flemish (A21G), and Iowa (D23N) point mutations were found to increase the propensity of Aβ oligomerization and aggregation. More recently, it was shown that overexpression of the Aβ precursor protein in neuronal cells, or incubation of neuronal cells with Aβ results in cell death (7-10). Furthermore, mice overexpressing the Aβ precursor protein or injected with Aβ demonstrated significant neurodegeneration and cognitive deficits which were reversed upon injection of antibodies against Aβ (11, 12). Thus it is clear that Aβ has a critical role in AD.

Although Aβ has been studied extensively, it is still unclear how Aβ becomes neurotoxic. This peptide is normally present in the body both in the cerebrospinal fluid, and blood, but the physiological role of Aβ is not known. Aβ is found in two forms, a 40

residue form, Aβ40 and a 42 residue form, Aβ42. These two forms of Aβ are formed by the sequential cleavage of the transmembrane protein, amyloid precursor protein (APP), the function of which is also unknown (figure 1.3). APP processing begins when it is cleaved by one of the proteases α-secretase or β-secretase followed by cleavage by another protease, γ-secretase. Cleavage of APP by α-secretase and then γ-secretase yields two relatively benign fragments, P3 and AICD, whereas cleavage by β-secretase and γ-secretase yields Aβ and AICD (figure 1.3). γ-secretase cleavage has some degree of variability, and can yield either the 40 or 42 residue forms of Aβ. The Aβ portion of APP is released extracellularly as a soluble peptide. Aβ40 is presumably cleaved as a monomer from APP, and forms a stable dimeric or trimeric species (13-15). It subsequently oligomerizes to a high degree, eventually forming large insoluble amyloid fibrils. While Aβ40 is much more abundant than Aβ42 in the body, it is less amyloidogenic than Aβ42, which means it does not oligomerize or fibrilize as rapidly as Aβ42. Amyloid plaques are composed of both forms of Aβ. It is interesting that only two extra hydrophobic residues at the C-terminus can change the aggregation properties of the peptide so drastically (figure 1.4). While neurotoxicity has been demonstrated for both peptides, Aβ42 is the more toxic species. This thesis focuses on Aβ40 because it is the more abundant species, and its slower aggregation properties facilitate mechanistic studies of amyloidogenesis and membrane interaction.

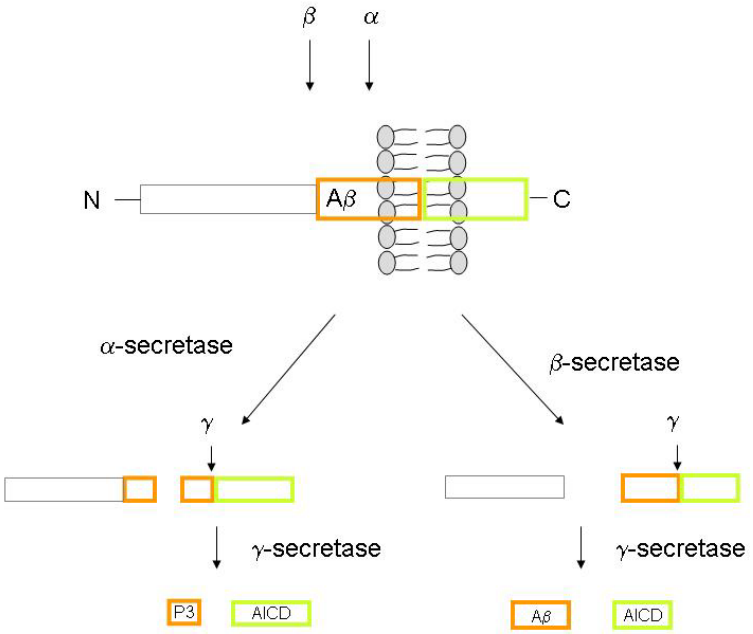

Figure 1.3: Proteolytic processing of APP by secretases yields different peptide products. Cleavage of APP by α-secretase followed by γ-secretase cleavage yields the benign P3 and AICD fragments, whereas cleavage by β-secretase followed by γ-secretase yields either Aβ40 or Aβ42 and AICD.

Aβ40: DAEFRHDSGYEVHHQKLVFFAEDVGSNKGAIIGLMVGGVV
Aβ42: DAEFRHDSGYEVHHQKLVFFAEDVGSNKGAIIGLMVGGVVIA

Figure 1.4: sequence of Aβ40 and Aβ42.

Since Aβ oligomers are in dynamic equilibrium with each other, Aβ exists as a mixture of oligomeric species in solution, making it difficult to determine which species of Aβ is the toxic species, and whether there is just one oligomeric species. Whereas historically it was assumed that Aβ becomes cytotoxic when it forms large insoluble fibrillar aggregates in the brain, recent studies have found little if any correlation between

amyloid plaque load and the clinical severity of the disease. Brain tissue from several patients without dementia or AD have presented with a significant number of amyloid plaque deposits, and brain tissue from several patients with severe AD have shown very few amyloid plaques (16, 17). Furthermore, neuronal abnormalities and cognitive deficits begin to appear well before amyloid plaques are detected in transgenic animals overexpressing APP (18-20). Thus interest has shifted away from studying the fibrils to studying the soluble oligomeric species of Aβ as the potential culprits in instigating neuronal cell death.

Recent studies have provided evidence suggesting that the soluble intermediate-sized oligomeric species of Aβ effectively cause cell death, potentially through membrane permeabilization (21). Indeed, several studies have demonstrated that neurotoxicity is influenced by the interaction of Aβ with membrane lipids (22-28). One of the leading models of how Aβ induces cytotoxicity is the channel or pore hypothesis. In this model, Aβ acts by forming pores or channels in the cell membrane, thereby permitting a rapid unregulated influx of ions such as calcium into the cell (figure 1.4). A recent study demonstrated significant increases in calcium influx into cells upon incubation with Aβ, supporting this model of neurotoxicity (21, 29). Furthermore, increases in membrane conductivity in bilayers treated with Aβ have consistently been shown by several groups (23, 30-33). Lastly AFM images of Aβ bound to lipid membranes revealed annular Aβ structures, supporting the formation of an Aβ channel (32). Calcium influx through these channels structures may subsequently trigger cell death by stimulating apoptosis signaling pathways (34). The increase in ions entering the

cell could also directly lead to cellular stress or death because the cell is forced to pump more ions out of the cell to maintain homeostasis. What specific factors promote conversion of this normally expressed peptide into a neurotoxic entity remains elusive.

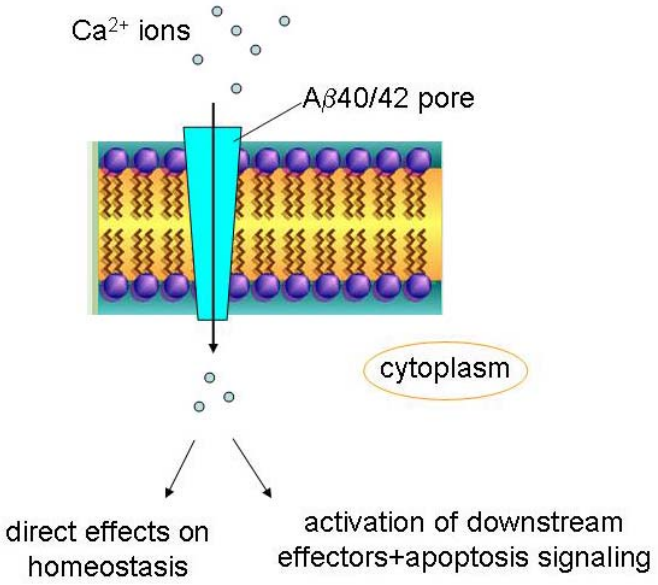

Figure 1.5: Channel or pore model for Aβ induced neurotoxicity. In this model Aβ forms pores or channels in the plasma membrane, leading to an unregulated influx of ions such as calcium into the cell. The increase in calcium can lead to cell death either directly by disruption of cellular homeostasis, or indirectly by activating downstream apoptosis stimulating effectors.

An intriguing aspect of AD is that amyloid plaques are only found in specific regions of the brain, and Aβ is only toxic to certain types of neurons (cerebral cortex and hippocampal cells in particular) and not to other cells in the body (35). There are no post-translational modifications of Aβ that are altered between the AD and non AD states, and as mentioned previously, the level of Aβ in the CSF does not always increase significantly in the disease state. Therefore the development of AD is not just a matter of overexpression. This points to an important role of the local environment, in particular

the plasma membrane, in promoting Aβ toxicity. Therefore changes in the plasma membrane composition may be crucial in the development and progression of AD.

Thesis Summary

This thesis focuses on the characterization of Aβ40 interactions with lipid membranes, in order to determine the mechanism by which a membrane permeabilizing species is formed. Several changes in the neuronal cell membrane composition occur with age, one of the biggest risk factors for developing AD. Therefore we examine how the membrane composition and physical properties, specifically charge and fluidity affect Aβ activity and interaction with the membrane. A number of studies have shown that Aβ can interact with synthetic lipids *in vitro* (32, 36-38), and that the presence of Aβ induces changes in permeability and conductivity across lipid bilayers (23, 30-33). Here we determine the specificity of Aβ membrane binding, and how peptide binding leads to permeabilization, using liposomes as model membranes.

In chapter II, methods for handling Aβ and initial characterization of the aggregation properties of in solution are discussed. The influence of membrane charge as determined by the lipid head group, and membrane fluidity as determined by lipid acyl chain saturation on Aβ40 membrane binding affinity and insertion is characterized using various fluorescence based assays with a tryptophan substituted peptide (Aβ40 [Y10W]). Chapter III describes the changes in conformation and oligomerization of Aβ upon

interaction with various membranes. Two well studied groups of peptides whose normal functions are to form pores in cell membranes are the pore forming toxins (PFTs), and antimicrobial peptides (AMPs). These peptides, such as gramicidin, magainin, and melittin can form pores approximately 30 Å in diameter in their target membranes, resulting in cytotoxicity. Interestingly, PFTs and AMPs share several characteristics with Aβ. For example, they are unstructured in the monomeric state, and can oligomerize to form pores. In this chapter, we found a strong dependence of the membrane induced peptide conformation and oligomerization changes on the peptide to lipid ratio, similar to what has been observed for several AMPs and PFTs. Thus greater insight into the mechanism of Aβ membrane interaction may be obtained by comparing the mechanism of action of Aβ with that of AMPs and PFTs. The similarities between Aβ and AMPs/PFTs extend to the process of membrane permeabilization as well, which is discussed in chapter IV. Kinetic analyses of Aβ membrane permeabilization suggest that membrane binding and permeabilization are distinct, separable processes, and have different requirements in terms of membrane composition. Lastly, changes in the membrane cholesterol content have been observed in aged brain. In chapter V, the effects of altering the membrane fluidity by inclusion of cholesterol in the membrane on binding, insertion, conformational changes and permeabilization are examined. Membrane binding and permeabilization are pivotal steps in Aβ toxicity. Therefore determining which factors promote or inhibit these processes is critical to understanding the etiology of AD, and necessary for the development of methods to prevent the progression of AD.

CHAPTER II

Initial characterization of Aβ and the effects of lipid charge and phase on Aβ binding affinity and orientation

2.1 Introduction

One of the defining attributes of the amyloid proteins is the ability to oligomerize and aggregate to a high degree. These proteins begin as soluble monomeric species, and are able to oligomerize extensively, eventually forming fibrillar structures consisting of thousands of subunits. While this characteristic provides an interesting system to study, it makes the characterization of these proteins very difficult. This is because they are constantly being converted back and forth to larger or smaller oligomers, and an untreated sample of amyloid protein is likely to be a mixture of multiple species. Thus dissolving Aβ in solution without any initial disaggregation treatments could yield a mixture of monomers, dimers, trimers, hexamers, dodecamers, and fibrils for example. It is very difficult to effectively characterize the activity of the peptide when the identity of the starting material is so variable and nonhomogenous. Searching through the Aβ literature reveals a large number of discrepancies between the findings from different research groups. The most likely explanation for these discrepancies is that different groups have different methods for the solubilization and treatment of Aβ before beginning their experiments, and thus may each be working with different forms of the peptide when doing the experiments. Furthermore Aβ oligomerization and fibrilization

are highly sensitive to, and are significantly influenced by factors such as pH, peptide concentration, ionic strength, temperature, and agitation. Aβ also has a "memory effect" where different initial treatments continue to influence Aβ activity and oligomerization even if the peptide ends up in the same final conditions. For example, lyophilizing Aβ treated with either hexafluoro-2-propanol (HFIP) or triflouroacetic acid (TFA), and resuspending it in buffer yields two different Aβ populations. Even though all of the solvent was removed, the TFA treated sample oligomerizes much faster than the HFIP one. Therefore it is critical to treat the peptide so that the starting material is one uniform species. The first section of this chapter discusses methods for treating and handling Aβ, and the initial characterization of the oligomerization and aggregation properties of the peptide.

Several studies have provided evidence suggesting that the soluble intermediate-sized oligomeric species of Aβ cause cell death through membrane permeabilization, whether this occurs by a channel or pore like mechanism, or by thinning of the membrane, it is apparent that neurotoxicity is influenced by the interaction of Aβ with membrane lipids. One of the many unexplained aspects of AD is that the associated neurodegeneration is specific to certain types of neurons, affecting only the hippocampal and cerebral cortex regions of the brain. Furthermore, Aβ plaques are found only in these regions of the brain. Thus it is clear that the local environment must have an influential role in determining the toxicity of Aβ. Throughout this thesis, liposomes composed of synthetic lipids are used as the model membrane bilayer. In the second part of this chapter we examine the membrane association of Aβ40, and determine how changes in

the membrane composition influence the strength of this interaction, and the way by which Aβ associates with the membrane (i.e. bound only to the surface, or inserted into the bilayer). Under normal physiological conditions, neuronal cell membranes are composed of a mixture of zwitterionic (neutral), or anionic phospholipids (see chapter I). Neuronal cell membranes contain approximately only 10 % by mass of the anionic phosphatidylserine (PS) lipid. Although this percentage is low, the cell membrane is asymmetric due to the activity of the membrane enzyme flippase, which under normal healthy conditions, maintains most, if not all of the PS in the inner leaflet of the cell membrane. However, upon cell damage or stress, PS is externalized on the outer leaflet. This externalization is often an early indicator of apoptosis. One of the risk factors for developing AD is having experienced previous injury to the brain at some point in life. Thus accumulation of damaged cells with age containing externalized PS could play a significant role in the development of AD.

Here we examine how negatively charged lipids in the cell membrane influence Aβ using liposomes composed of mixtures of the zwitterionic phospholipid phosphatidylcholine, and the anionic phospholipid, phosphatidylglycerol. We also study the role of membrane phase and fluidity on Aβ-membrane association by varying the acyl tail groups of the phospholipids, comparing membranes composed of saturated gel phase lipids to membranes composed of unsaturated liquid crystalline phase lipids.

2.2 Materials and Methods

2.2.1 Aβ40 Monomerization and Solubilization

For all of the studies in this thesis, synthetic human wild-type (WT) Aβ40 peptide was purchased from Anaspec Inc. (San Jose, CA). Mutant Aβ40 [Y10W] peptide was recombinant, and purchased from rPeptide Inc. (Athens, GA). Peptides were dissolved in 50% acetonitrile/water at a concentration of 1 mg/mL, aliquoted into siliconized eppendorf tubes, lyophilized overnight, and stored at -20°C. The peptide was disaggregated by base treatment as described previously (39, 40). Briefly, the lyophilized Aβ40 was dissolved at 0.5 mg/mL in 2.5 mM NaOH, and the pH of the solution was checked to ensure that it was above 10.5. Aβ was then sonicated in a FS20 bath sonicator (Fisher Scientific, Pittsburgh, PA) for 1 minute, relyophilized overnight and stored at -20°C until needed. This procedure has been shown to disaggregate Aβ40 (39, 40). Immediately before each experiment, the peptide was resuspended in double distilled H_2O to a final concentration of 1 mg/mL, and allowed to dissolve for 1 minute before mixing gently by pipetting. An equal volume of 20 mM sodium phosphate (NaP_i) pH 7.4 was added, resulting in a 0.5 mg/mL solution of Aβ40 (125 μM) in 10 mM NaP_i pH 7.4. All Aβ used in this thesis work was treated and dissolved in this manner to ensure homogeneity of the starting material.

2.2.2 Gel Filtration Chromatography

To determine the oligomerization status of Aβ40 after the NaOH disaggregation treatment, and immediately after dissolution in NaP_i buffer, 40 μL of 25 μM Aβ40 was

run through a TSK-G3000SWXL (Tosoh Bioscience, Montgomeryville, PA) gel filtration column at 1 mL/min in 10 mM NaP_i pH 7.4. Absorbance was measured with an in-line UV-Vis detector at 215 nm and 280 nm. To determine molecular weights, the column was calibrated with molecular weight standards (thyroglobulin, γ-globulin, ovalbumin, ribonuclease A, and N-acetyl tryptophanamide (NATA)).

2.2.3 Thioflavin T (ThT) Binding Assay for Fibril Formation.

ThT binding to Aβ fibrils was determined as previously described (41). Briefly, 3 μg aliquots were taken from a 125 μM solution of WT Aβ40 incubated in 10 mM NaPi pH 7.4 in a 25°C water bath at various time intervals over 150 h. The peptide was incubated at a final concentration of 3.8 μM with 2.5 μM ThT in 50 mM glycine-NaOH pH 8.5 for 3 minutes at RT. ThT fluorescence (ex 440 nm, em 478 nm) was measured.

2.2.4 Liposome Formation

Synthetic lipids: 1,2-Dipalmitoyl-sn-Glycero-3-Phosphocholine (DPPC), 1,2-Dipalmitoyl-sn-Glycero-3-[Phospho-rac-(1-glycerol)] (DPPG), 1,2-Dipalmitoyl-sn-Glycero-3-[Phospho-L-Serine] (DPPS), 1-Palmitoyl-2-Oleoyl-sn-Glycero-3-Phosphocholine (POPC), and 1-Palmitoyl-2-Oleoyl-sn-Glycero-3-[Phospho-rac-(1-glycerol)] (POPG) were purchased in chloroform from Avanti Inc. (Alabaster, AL) (figure 2.1). Fluorescent N-(5-dimethylaminonaphthalene-1-sulfonyl)-1,2-Dipalmitoyl-sn-Glycero-3-Phosphoethanolamine (Dns-DPPE) was purchased from Invitrogen (Carlsbad, CA) as a powder, and was dissolved in a 3:1 mixture of chloroform:methanol.

All lipids were stored at -20°C. To form liposomes, lipids were mixed at the desired ratios, and the chloroform/methanol was removed by evaporation in a glass test tube under a gentle stream of nitrogen. The dried samples were placed in a vacuum chamber overnight to remove any traces of solvent. Dried lipid films were rehydrated in 10 mM NaPi pH 7.4 above the lipid transition temperature in a water bath (for DPPC and mixtures of DPPC and DPPG (DPPC/PG) at 45°C, for DPPC/PS at 50°C, and for POPC and POPC/PG mixtures at 25°C) for 2 hours at a concentration of 2.5 mg/mL. Unless otherwise specified, the notation DPPC/PG refers to liposomes composed of an equimolar mixture of two lipids with the same acyl chains but different head groups—in this case, DPPC and DPPG. To form small unilamelar vesicles (SUVs), the lipid suspension was vortexed and then sonicated in an ultrasonic water bath (Laboratory Supplies, Hicksville, NY) until the solution became translucent (ca. 5 min.). Lipid concentrations were determined by the Stewart method (42). All liposome concentrations are expressed as the concentration of total lipid.

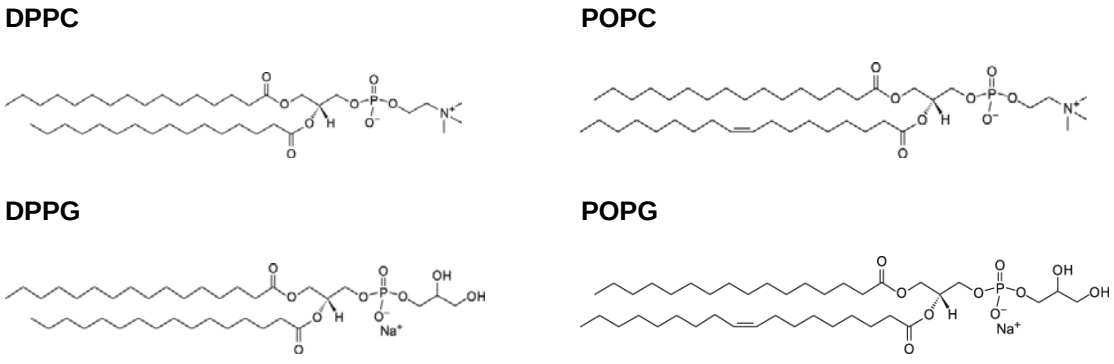

Figure 2.1: Lipids used in forming liposomal membrane bilayers. DPPC and DPPG share the same acyl tail group, but have different hydrophilic headgroups. The same applies to POPC and POPG.

2.2.5 Fluorescence resonance energy transfer (FRET) binding assay

A 5 μM solution of freshly dissolved Aβ40 [Y10W] in 10 mM NaP_i pH 7.4 was titrated with SUVs composed of mixtures of DPPC and DPPG at different ratios and containing 5 mol % Dns-DPPE. In a separate cuvette, the same amount of Dns-SUV was added to buffer only to yield the amount of fluorescence from direct Dns-excitation. Samples were incubated for 10 minutes at room temperature (RT) before taking measurements (no significant increases in fluorescence were seen after 10 min confirming that the sample had reached equilibrium). Fluorescence intensity was measured for both tryptophan at 352 nm and dansyl at 514 nm upon excitation at 280 nm using an FP-6500 spectrofluorometer (Jasco, Easton, MD). The fluorescence change due to FRET was evaluated by subtracting the contribution of direct Dns excitation from the fluorescence signal of Dns-SUV with Aβ40 [Y10W]. The change in fluorescence at 514nm was plotted vs. lipid concentration, and fit to a binding equation (equation 1):

$$\Delta FL = \frac{FL_f}{(1+\frac{K_D}{[lipid]})} \qquad \text{(eq. 1)}$$

where ΔFL is the fluorescence due to FRET, FL_f is the endpoint fluorescence, K_D is the dissociation constant, and [lipid] is the concentration of lipid added.

To follow the effect of Aβ40 incubation time on its membrane binding ability, an aliquot of Aβ40[Y10W] was dissolved at 125 μM in 10 mM NaP_i as described. This sample was incubated at room temperature for 3 days; aliquots were taken at 24 h intervals and their binding to Dns-SUVs was assayed.

2.2.6 Tryptophan emission shift

2.5 μM freshly dissolved Aβ40 [Y10W] in 10 mM NaPi pH 7.4 was incubated with SUVs composed of an equimolar mixture of DPPC and DPPG (DPPC/PG) or POPC and POPG (POPC/PG) at RT for 10 min. before measurements were taken. (Note: significant photobleaching of the trp occurs upon excitation; therefore fluorescence was only measured once for each sample). Tryptophan emission spectra were recorded from 320-370 nm upon excitation at 280 nm. Spectra of liposomes alone at the same concentrations were subtracted. The K_D for the wavelength shift was calculated with a correction for the change in intensity for the 335 nm fully blue shifted fluorescence. The unshifted tryptophan emission at 350 nm and the final shifted emission at 335 nm were individually fit to a single Gaussian curve (Gaussian width=38 nm for both peaks, and the 335 peak had a relative intensity of 1.9 relative to the 350 nm peak). All curves were fit as a linear combination of the initial and final curves and the relative proportion was fit by a simple binding isotherm.

2.2.7 Acrylamide Quenching

5 μM of freshly dissolved Aβ40 [Y10W] in 10 mM NaPi pH 7.4 was incubated with various concentrations of SUVs as above for 10 minutes at RT. Acrylamide was titrated up to 0.25 M from a 5 M stock solution in water. Tryptophan fluorescence was measured immediately (ex 295 em 352). Samples were excited at 295 nm instead of 280 nm to minimize acrylamide absorbance. Stern-Volmer constants (K_{SV}) were determined by equation 2, where F_0 is the fluorescence without quencher, F is the fluorescence with quencher, and [Ac] is the concentration of acrylamide added.

$$\frac{F_0}{F} = 1 + K_{SV}[Ac] \qquad \text{(eq. 2)}$$

2.3 Results and Discussion

2.3.1 Disaggregation of Aβ40 and initial characterization

As mentioned in the introduction, it is extremely important that Aβ is treated so that the starting material is disaggregated and homogenous. Initially different methods of disaggregation were tested. Treatment with 100% TFA, or 50-100% acetonitrile followed by lyophilization before resuspension in 10 mM NaP_i pH 7.4 yielded Aβ40 that aggregated rapidly, or that was incompletely disaggregated respectively (data not shown). Treatment with 100% HFIP did disaggregate the peptide, however sometimes even after lyophilization overnight traces of HFIP would remain, affecting both membrane stability, and the oligomerization properties of Aβ. The pI of Aβ40 is 5.2, therefore when Aβ is initially disaggregated with TFA, the peptide is positively charged in the lyophilized state. Resuspension in pH 7.4 buffer causes Aβ40 to transition through its pI. Passing through the pI makes Aβ more susceptible to aggregation. Thus we decided to use strong basic conditions to disaggregate Aβ so that resuspension at pH 7.4 would not be a transition through the pI. We also found that dissolving Aβ in high ionic strength buffer containing > 100 mM NaCl after base treatment resulted in the immediate formation of higher order oligomers, and the rate of fibrilization as measured by ThT was increased as ionic strength increased. Strong agitation such as vortexing also resulted in the loss of Aβ membrane permeabilization activity, possibly due to agitation induced aggregation.

We thus found that the most effective way of treating of Aβ40 is by incubation in NaOH according to the protocol described in the methods section, lyophilization, and resuspension in 10 mM NaPi pH 7.4 buffer. This resulted in a completely disaggregated peptide solution at the most stable lowest order oligomeric state.

2.3.2 Initial determination of oligomeric state

To determine the oligomeric state of Aβ40 treated with NaOH and freshly redissolved in NaP_i, Aβ40 was run on a gel filtration column, which separates peptides and small proteins based on size. The column was calibrated using various proteins and peptides as molecular weight standards. Aβ40 ran predominantly as a single peak, corresponding to a molecular weight of 27 kDa, or a trimeric or tetrameric species since monomeric Aβ40 has a molecular weight of 4.3 kDa (figure 2.2). This is consistent with previous studies that proposed Aβ exists as a dimer-tetramer (13-15). A smaller peak corresponding a lower molecular weight species was also observed which may be truncated Aβ, or degraded Aβ that remains in the monomeric form.

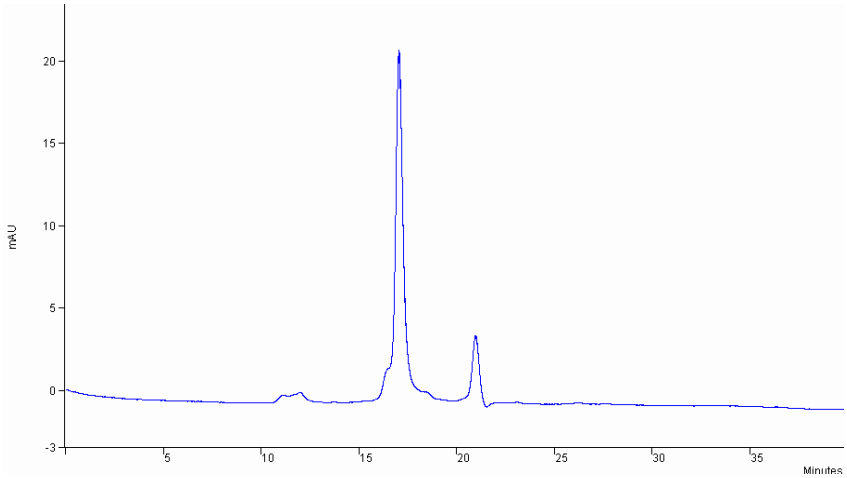

Figure 2.2: Absorbance elution profile at 215 nm of Aβ40 treated with NaOH as described, lyophilized, and redissolved in 10 mM NaP_i pH 7.4 run on a TSK-G3000SWXL gel filtration column in 10 mM NaP_i pH 7.4 buffer at 1 mL/min.

Since insoluble fibrillar Aβ may be present that are too large to enter the column, the absence of fibrils was confirmed by measuring the binding of the fluorescent dye, ThT. ThT is a hydrophobic dye that binds specifically to fibrillar species with the cross β-sheet amyloid fold. This dye has minimal fluorescence in solution, but becomes highly fluorescent upon binding to fibrils. Incubation of Aβ40 freshly dissolved after NaOH treatment and lyophilization showed no ThT binding, confirming the absence of fibrillar species. To follow the fibrilization of Aβ40 and Aβ42 treated with NaOH, these samples was allowed to incubate at 125 μM at RT over several days, and ThT binding was measured periodically. Fibrilization was very slow for Aβ40 in comparison to that of Aβ42, not significantly increasing until after 50 h of incubation, whereas Aβ42 ThT binding began to increase only after 6 h of incubation (figure 2.3). Both Aβ40 and Aβ42 exhibited the initial lag phase before the exponential increase in fibrilization (although the lag phase for Aβ42 was much shorter), indicative of a solution free of seeds, species capable of nucleating rapid fibril growth.

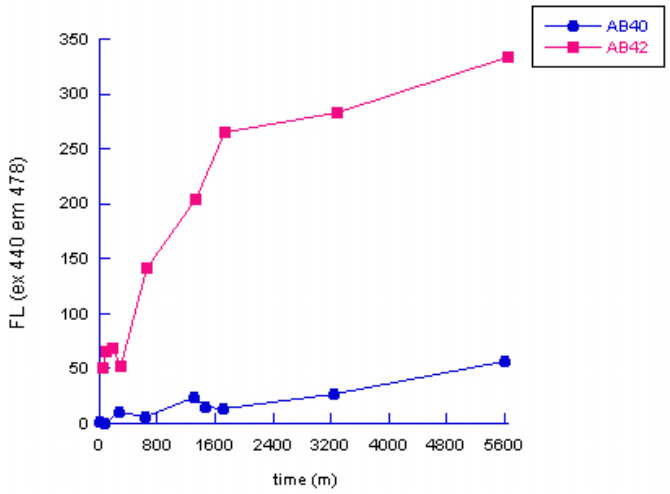

Figure 2.3: ThT binding time course measuring fibrilization of Aβ40 and Aβ42. NaOH treated Aβ was resuspended to 125 μM in 10 mM NaPi pH 7.4, and was incubated at RT. Samples were taken at various time points, and assessed for ThT binding by measuring ThT fluorescence.

2.3.3 Effects of negative lipids on Aβ40 membrane binding affinity

To determine the lipid specificity of Aβ membrane binding, a FRET based assay was used. SUVs containing mixtures of the two lipids DPPC and DPPG at different ratios and 5 mol % Dns-DPPE were made. DPPC is a neutral zwitterionic lipid, whereas DPPG is an anionic lipid with a net negative charge of 1. WT Aβ contains a single tyrosine at position 10. To maximize the spectral overlap and thus the FRET efficiency between the donor (Aβ) to the acceptor (Dns), a tyrosine to tryptophan substituted peptide Aβ40 [Y10W] was used. It has been shown that this mutation does not significantly alter the properties of Aβ40, and that WT and Aβ40 [Y10W] can oligomerize and fibrilize in a similar fashion (13, 14). 5 μM Aβ40 was titrated with 0-100 μM SUVs composed of DPPC, DPPG, or mixtures of the two with increasing ratios of DPPG to DPPC. Incubation of Aβ40 with SUVs containing a percentage of lipids with a Dns fluorophore attached to the phospholipid head resulted in an increase in Dns and a decrease in

tryptophan emission upon excitation of the tryptophan at 280 nm, confirming the occurrence of FRET and the association of Aβ40 with the membrane. Dissociation constants were determined by fitting the binding curves to a simple bimolecular association model (equation 1) where it was assumed that the binding affinity was independent of total peptide concentration.

Increasing the relative amount of DPPG to DPPC elevates the net negative charge of the liposome. Titration of Aβ40 with SUVs containing various molar ratios of DPPC:DPPG showed that Aβ40 binds with greater affinity to liposomes with a larger net negative charge, interacting only weakly with pure DPPC liposomes (table 2.1). The preferential interaction with anionic lipids confirms what has been reported by several groups using other techniques to follow the binding of Aβ40 and other amyloid proteins (36-38, 43-47). Our results show that the K_D of Aβ40 lipid binding decreases dramatically with increasing relative amounts of DPPG, and appears to be saturable. Binding affinity reaches a maximum at 70:30 DPPC:DPPG (K_D= 38.8 ± 7.0 μM) when the Aβ40 concentration is 5 μM, and remains about constant thereafter with increasing amounts of DPPG (table 2.1). Because Aβ lipid binding/insertion in different membrane types (see below) has different effects on tryptophan emission, the fraction bound was determined by normalizing the fluorescence data to the maximum Dns fluorescence intensity for each membrane type. Another factor to consider is that as the relative DPPG levels increase, changes in Aβ40 conformation or oligomerization state could be induced, producing additional changes in the tryptophan emission by self-quenching as previously observed by others for tyrosine (48). Thus, the Aβ40 binding species may be different

when the fraction of DPPG present is changed. Due to these reasons, treating Aβ binding as a simple bimolecular reaction is simplistic, and yields only apparent dissociation constants.

Table 2.1: Dependence of Aβ40 [Y10W] binding affinity on membrane composition assessed by FRET. 5 μM Aβ40 [Y10W] was titrated with SUVs composed of mixtures of various ratios of DPPC and DPPG and 5 mol % Dns-DPPE. Binding as reflected by the increase in Dns fluorescence at 514 nm due to FRET from the tryptophan excited at 280 nm was measured. Dissociation constants were calculated by fitting to eq. 1.

DPPC:DPPG molar ratio	Apparent K_D (μM)
100:0	NA [a]
90:10	NA [a]
80:20	148.8 ± 26.5
70:30	38.8 ± 7.0
50:50	44.5 ± 10.5
20:80	44.1±8.5

[a] SUVs composed of high proportions of DPPC showed minimal binding, resulting in large fit errors.

The experiments discussed above were all done with Aβ40 freshly dissolved from a NaOH disaggregated lyophilate. Aβ40 treated and dissolved in this manner initially is soluble as a low molecular weight species (monomer-trimer) as seen by size exclusion chromatography, and glutaraldehyde crosslinking (chapter III), and lacks amyloid fibrils as evidenced by the lack of ThT binding. To assess the dependence of membrane binding affinity on the oligomerization state of Aβ40, 125 μM Aβ40 was incubated with no added lipid in solution at room temperature for 3 days. Samples were taken each day, and

binding to SUVs of equimolar DPPC:DPPG was measured. Dissociation constants were similar and did not change significantly over the 3 days (figure 2.4a). However, the final Dns fluorescence decreased over this time period (figure 2.4b), suggesting that the extent of binding diminishes (the trp fluorescence of Aβ did not decrease over time (data not shown)). Fibril formation as assessed by ThT binding begins to increase after 48h (figure 2.4b). Because the Y10W mutant does not bind ThT very well (or ThT is not as fluorescent when bound to Y10W fibrils), the ThT signal is very low, and WT Aβ was used for measuring fibril formation rates. The Y10W mutant and WT Aβ40 have previously been shown to fibrilize similarly by electron microscopy (13, 14). Furthermore, from the ThT fluorescence signal, Y10W fibrilization rates are similar to WT (data not shown). From these results we conclude that the species capable of binding to the membrane is present immediately after dissolution, and is diminishing over time due to conversion to larger oligomers or fibrils that no longer bind.

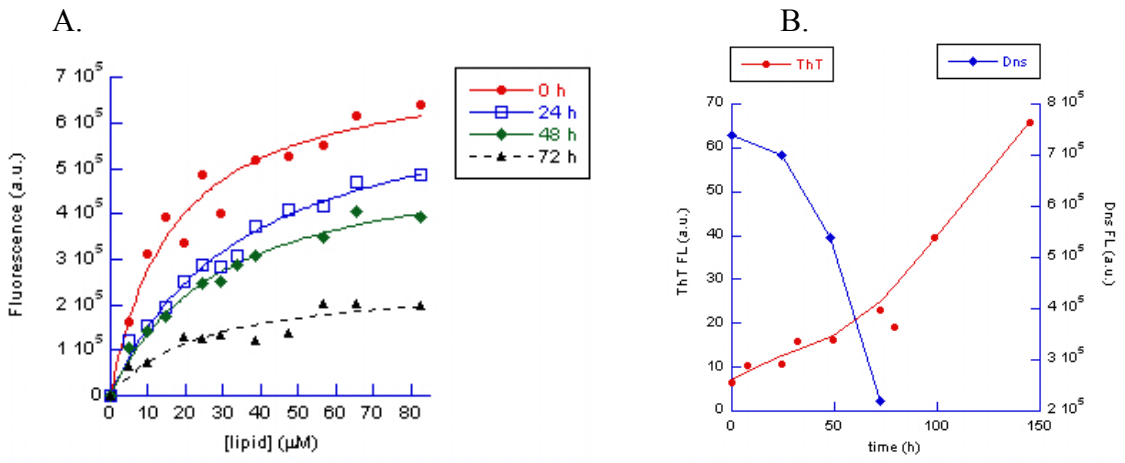

Figure 2.4: Time evolution of Aβ40 [Y10W] membrane binding ability and fibrilization. (A) Aβ40[Y10W] membrane association was measured as an increase in Dns fluorescence at 514 nm due to FRET from the tryptophan excited at 280 nm. Aβ40[Y10W] was dissolved at 125 μM in 10 mM NaPi pH 7.4 and incubated at 25ºC over 72 h. 5 μM aliquots were then titrated with Dns-SUVs composed of equimolar DPPC/DPPG. (B) WT Aβ40 incubated at 125 μM as in (A) was assayed for fibril formation by ThT binding. ThT fluorescence emission intensity was measured at 485 nm upon excitation at 440 nm. Endpoint Dns emission from the titrations in (A) are plotted alongside this data for comparison. The amount of bound Aβ decreases as fibrils begin to appear.

2.3.4 Influence of membrane charge on the orientation of Aβ in the bilayer

While the FRET binding experiments demonstrate tighter binding of Aβ40 to anionic membranes, they do not distinguish between surface binding and penetration of the peptide into the bilayer. Since tryptophan fluorescence emission upon partitioning into a hydrophobic environment is blue shifted and frequently enhanced in intensity relative to that in aqueous solution due to solvent dipole reorientation, membrane insertion was measured by a shift in Aβ tryptophan emission. Another interesting factor to look at is how membrane phase and fluidity influence insertion. 5 μM Aβ40 [Y10W] was allowed to bind to SUVs containing DPPC or POPC, or the mixtures DPPC/PG or POPC/PG. POPC and POPG possess the same lipid head groups as DPPC and DPPG

respectively, but are in the liquid crystalline (LC) phase at room temperature (due to an unsaturated acyl chain), whereas DPPC and DPPG are in the gel phase. For each point in the titration, Aβ40 was incubated with the SUVs before measuring the emission spectrum of Aβ40. The spectra were fit to Gaussian curves as described in materials and methods to determine the fraction of Aβ inserted as a function of lipid concentration. K_Ds obtained this way were similar to those found by FRET (figure 2.5d).

Aβ40 binding to SUVs containing DPPC/PG or POPC/PG (spectra not shown) at low lipid levels (low L:P ratios) resulted in an initial quenching of fluorescence intensity as well as a blue shift in tryptophan emission (figure 2.5b). While there is no dramatic drop in fluorescence intensity at the low concentrations of DPPC/PG as seen for DPPC, there is quenching present. This is because membrane inserted Aβ is much more fluorescent than peptide in solution. Thus in figure 2.5b, Aβ bound to 10 μM DPPC/PG should have a higher quantum yield, and thus fluorescence intensity than Aβ alone. However it is equivalent, demonstrating that self-quenching is occurring for Aβ bound to DPPC/PG as well. As the lipid concentration was increased the initial quenching for both DPPC and DPPC/PG bound Aβ was reversed, and the fluorescence intensity increased while the peak wavelength continued to shift towards shorter wavelengths. Binding of Aβ40[Y10W] to DPPC/PG SUVs resulted in a 15 nm blue shift in the emission maximum wavelength at only 70 μM lipid, reflecting significant insertion of the peptide into the bilayer. In contrast, binding to DPPC SUVs even at 170 μM lipid resulted in only a 3 nm blue shift, but also demonstrated an initial quenching of fluorescence at low L:P, which was reversed as lipid levels were increased (figure 2.5a). POPC/PG showed

the same magnitude shift as DPPC/PG for the same amount of lipid added (figure 2.5c). These results confirm what was found by FRET that Aβ40 binds preferentially to negatively charged lipids, but still interacts weakly with neutral lipids.

A.

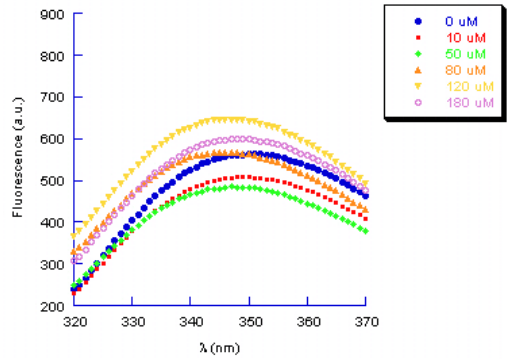

B.

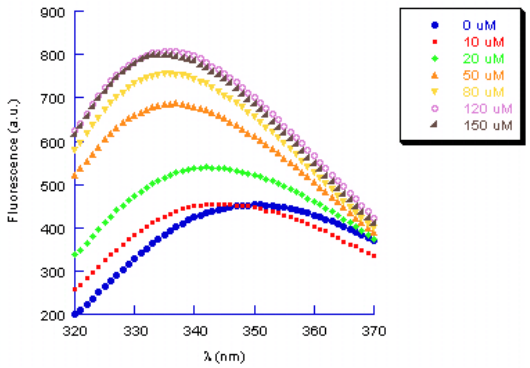

C.

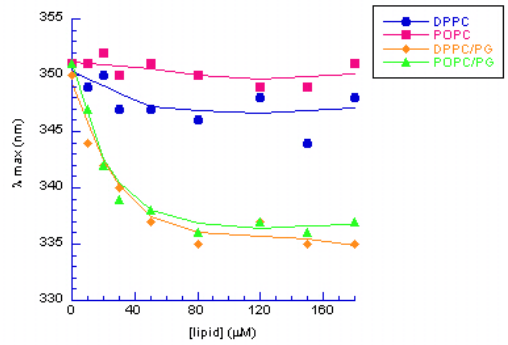

D.

Aβ40 [Y10W] (μM)	K_D DPPC (μM)	K_D DPPC/PG (μM)
0.1	----	0.70±0.15
1.0	NA[a]	4.25±1.0
2.5	NA[a]	18.5±3.5

Figure 2.5: Effect of lipid binding on tryptophan emission spectra. 2.5 μM Aβ40 [Y10W] was titrated with SUVs containing either (A) DPPC or (B) an equimolar mixture of DPPC:DPPG. Peptide was allowed to bind to the liposomes as in the FRET experiments, and tryptophan fluorescence emission spectra were measured upon excitation at 280 nm. (C) Plot of the emission maxima wavelengths versus lipid concentration for DPPC and DPPC/PG binding demonstrated a strong dependence on membrane charge for peptide insertion depth. (D) Apparent K_D's were calculated for various concentrations of Aβ by the fraction of tryptophan emission shift. [a]Minimal binding was observed for DPPC liposomes, and DPPC bound Aβ did not induce a shift to 335 nm due to shallower insertion, resulting in large errors.

Since there is no PG in mammalian cell membranes, liposomes containing DPPC/PS or POPC/PS which have the same net charge as DPPC/PG and POPC/PG were examined as well. These membranes resulted in a similar shift and quenching of fluorescence (data not shown). Thus Aβ40 membrane insertion depth is highly dependent on the negative charge of the membrane. It is interesting to note that although there is only a small shift in tryptophan fluorescence for DPPC alone, the fluorescence still undergoes the same initial quenching seen at low concentrations of DPPC/PG and DPPC/PS. Addition of up to 50 μM DPPC SUVs results in a 15% decrease in fluorescence, and subsequent addition of lipid results in an increase in fluorescence that is saturable (figure 2.5a, 2.5b), indicating that the observed quenching and fluorescence increase must be a result of interaction of the peptide with the membrane. These results could possibly be explained by the presence of at least two different kinds of Aβ-membrane interactions that are dependent on membrane charge.

Similar tryptophan shift experiments with Aβ40 have been reported, however in contrast to our findings, no shift was observed for neutral POPC or anionic POPS liposomes (49). This is not due to differences in buffer conditions (10 mM NaPi pH 7.4 in this study compared to 10 mM NaPi pH 7.4, 150 mM NaCl) since increasing the NaCl concentration up to 150 mM, did not abolish Aβ40 binding to the membranes, although the affinity was slightly decreased at higher ionic strength (unpublished results). The differences may be due to differences in peptide disaggregation methods, since the authors used hexafluoroisopropanol (HFIP) instead of NaOH to disaggregate Aβ. We

have found that it is sometimes difficult to remove HFIP completely from Aβ, and that trace amounts of HFIP are enough to result in membrane instability.

Apparent dissociation constants for membrane binding were determined for different concentrations of Aβ using a tryptophan emission maximum wavelength of 335 nm as representative of a fully bound, fully inserted peptide. Interestingly, the apparent K_D was highly dependent on Aβ concentration, demonstrating a linear relationship at those concentrations of Aβ where the fluorescence could be measured accurately (figure 2.5d). This is indicative of limiting surface area on the liposome membrane, resulting in a higher estimate of the K_D than the actual value at the higher peptide concentrations (see discussion section). Since the workable peptide concentration was limited by fluorescence detection limits, we can only conclude that the actual K_D is at least as tight as the apparent K_D calculated at 100 nM peptide.

2.3.5 Confirming Aβ40 membrane insertion by measuring susceptibility to dynamic quenchers

To confirm that the shift in tryptophan fluorescence was in fact due to Aβ40 insertion, the ability of liposomes to provide protection to the tryptophan from a collisional quencher, acrylamide, was measured. Aβ40 [Y10W] was allowed to bind to various concentrations of SUVs, and the tryptophan emission was measured with increasing concentrations of acrylamide. The Stern-Volmer constants (K_{SV}) were determined using equation 2. DPPC/PG dramatically decreased the Aβ K_{SV} (97% reduction at 100 μM lipid), compared to only 73% at 100 μM DPPC, indicating a large decrease in the solvent accessibility of the tryptophan in anionic membranes (figure 2.6a,

b). This provides further evidence supporting insertion of Aβ40 into DPPC/PG, and a less embedded conformation of the peptide when bound to DPPC. A peptide bound only to the surface of the membrane is also expected to show a small degree of protection from quenching since the membrane blocks solvent access to one face of the peptide even if it is not embedded. The K_{SV} for free tryptophan and RNaseA did not change upon addition of liposomes, and the tryptophan remained readily quenchable and unprotected (data not shown).

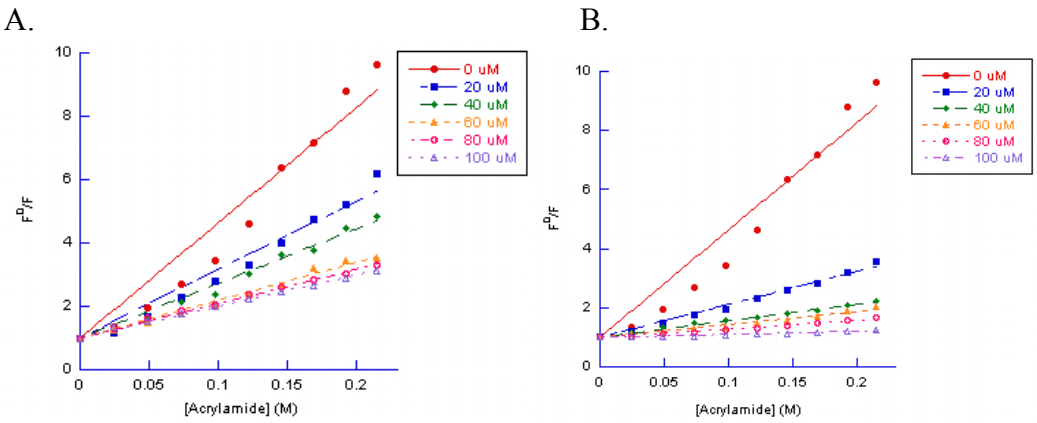

K_{SV} (M^{-1})

lipid (μM)	DPPC	DPPC/DPPG
0	36.4±1.9	36.4±1.9
20	21.6±0.8	11.2±0.2
40	17.2±0.4	5.6±0.1
60	12.0±0.3	4.4±0.1
80	10.8±0.1	2.9±0.1
100	10.0±0.1	1.0±0.1

Figure 2.6: Acrylamide quenching of Aβ40 [Y10W] in the presence of SUVs. 5 μM of peptide was allowed to bind to SUVs composed of either (A) DPPC only, or (B) 1:1 mixture of DPPC:DPPG and titrated with acrylamide. Stern-Volmer plots are shown. Stern-Volmer constants (K_{SV}) were calculated using a linear fit of the plots. A sharper drop in the K_{SV} values for DPPC/DPPG with respect to lipid concentration reflects greater protection of the tryptophan from quenching as compared to DPPC.

2.4 Conclusions

Several studies have pointed to the importance of membrane interactions in Aβ toxicity. Previous studies have shown that negatively charged lipids have a role in mediating these interactions and in influencing the neurotoxic effects of Aβ. In this chapter, we examined Aβ40 membrane binding, and looked at the influence of membrane charge and fluidity/phase on this process. DPPC, DPPG, DPPS, POPC and POPG containing liposomes were used to determine the influence of negatively charged lipids on these interactions. Specifically, we found that Aβ40 membrane binding affinity increases with the net negative charge of the membrane, soluble low order oligomers (<10-mer) are the primary membrane binding species, and binding affinity is independent of the fluidity of the membrane. Furthermore, Aβ40 membrane insertion depth is highly dependent on the negative charge of the bilayer, and independent of fluidity and phase of the membrane. The preferential interaction of other amyloid proteins and antimicrobial peptides with anionic membranes has been reported in several studies, pointing to similarities between the mechanism of membrane interactions of these proteins and Aβ (50, 51).

The FRET binding experiments here demonstrated that as the net negative charge (DPPG content of the membrane) increased, Aβ40 binding affinity became progressively higher. We show that this effect on the apparent binding affinity was saturable, reaching a plateau at 70:30 DPPC:DPPG, with no additional increase in affinity seen upon further raising the levels of DPPG. It is necessary to consider if the true affinity is reflected by the plateau in the K_D, or alternately if the value of the apparent K_D may be attributed to a

limited number of sites available for binding Aβ40 on the liposome surface. A rough estimate of the surface area of a 40 amino acid helical peptide is about 600-700 $Å^2$ (based on estimates of melittin (52) while the surface area of a single lipid molecule is approximately 70 $Å^2$ (52). Therefore one expects that available binding sites on the liposome would be limited at L:P ratios below approximately 10:1. The limiting apparent K_D of 40 μM for 5 μM total Aβ40 suggests that determination of the Aβ40 binding affinity to liposomes with higher DPPG proportions may not reflect true affinity but rather limited surface availability for binding. A better estimate of the true affinity shown by binding studies at higher L:P ratios discussed below.

While some studies found little or no interaction of Aβ with neutral membranes (38, 49), others reported binding to PC membranes (53, 54). Our findings reveal loose binding to PC membranes. Furthermore, increasing the ionic strength of the solution slightly reduced but did not abolish Aβ40 binding to PC/PG membranes (data not shown). This indicates that the Aβ-lipid interaction is not solely electrostatic, but also contains a hydrophobic component.

Immediately after disaggregation and solvation in aqueous buffer Aβ forms stable oligomeric species, mostly dimers and trimers that are able to bind to the lipid membrane. However, we found that the binding decreased over time as oligomerization of Aβ to larger species was allowed to proceed, with very little binding observed for samples in which fibrils had formed. Therefore once Aβ40 progresses past a certain oligomeric state it can no longer undergo the initial step of binding to the membrane.

Insertion of Aβ40 into the bilayer accompanies binding as seen by a blue shift in the tryptophan fluorescence spectra of Aβ40[Y10W] bound to DPPC, POPC, DPPC/PG and POPC/PG SUVs. Much larger blue shifts were observed for anionic membranes, indicating deeper peptide penetration into the bilayer than for neutral membranes since the more hydrophobic the environment is (deeper insertion), the greater the magnitude of the shift. Notably the insertion was similar for both gel phase and liquid crystalline phase membranes, demonstrating that insertion is mediated by initial interactions with the phospholipid head groups and not the hydrophobic tail. It is also possible that the tryptophan environment becomes more hydrophobic due to the oligomerization of Aβ induced by interaction with anionic liposomes, contributing in part to the shift (see chapter III). The insertion of Aβ into the lipid bilayer was confirmed by the observed decrease in susceptibility of the tryptophan to dynamic quenching by acrylamide upon binding to anionic liposomes, and to a lesser extent in neutral liposomes. These data suggest that while Aβ40 is tightly bound and inserted into the bilayer for anionic membranes, a looser, more superficial surface binding exists for neutral membranes. The slight shift in trp emission and the increased protection from quenchers in solution for Aβ on neutral PC membranes is consistent with a surface bound peptide (since only one face of the peptide is accessible to the quencher). Another observation made in measuring the fluorescence spectra of Aβ40[Y10W] bound to SUVs was that at very low L:P ratios where the peptide was in large excess over lipid, the fluorescence was initially quenched below its value in solution. This was seen for both neutral and anionic membranes, and is possibly due to initial weak nonspecific interactions among Aβ molecules coating the

liposome surface at the high local concentrations of peptide, leading to self-quenching of the tryptophan. As the L:P ratio is increased, this quenching is relieved by dilution of the peptide on the membrane surface, and the fluorescence increases well above that of Aβ in solution.

Notably, the K_D for Aβ binding to SUVs evaluated by the shift method was linearly dependent on Aβ concentration, suggesting that under these conditions the measured K_D is higher than the actual value because all of the sites on the liposomes are occupied, sterically blocking the association of Aβ that would otherwise be able to bind. Thus binding is limited by the number of available lipid binding sites, and the calculated K_D values are larger than the real values under these conditions. However, because the fluorescence below 100 nM Aβ is weak, accurate binding measurements could not be made below this concentration of peptide. Therefore the apparent K_D at 100 nM Aβ of 600 nM provides an upper limit for the actual dissociation constant, with the actual K_D value likely being much smaller in the tens of nM range. Thus association of the low order oligomers of Aβ with anionic membranes is very tight. Since the K_D (where half of the peptide is bound) is consistently 6-12 times greater than the Aβ concentration, and since approximately only two thirds of the lipid is available for binding on the SUV exterior, this suggests that each Aβ peptide requires 8-16 lipids to bind. This is consistent with the surface area calculations mentioned previously. Although PG is not found in mammalian cell membranes, it is commonly used as a model for anionic membranes, and repeating these experiments with PS lipids, an anionic lipid found in mammalian systems showed very similar results to what was seen with PG.

In summary, while Aβ binding and insertion are both highly dependent on the initial interactions with the membrane phospholipid head, these processes are not influenced significantly by the phase or fluidity of the membrane as determined by the lipid acyl tail groups.

CHAPTER III

Influence of membrane charge and fluidity on Aβ structure and oligomerization

3.1 Introduction

In the previous chapter it was shown that membrane binding affinity and insertion depth are increased significantly with the inclusion of negatively charged lipids in the membrane, and that membrane fluidity has no significant effect on these processes. In this chapter we examine the role of charge and fluidity on the conformation and oligomerization state of Aβ upon interaction with the membrane.

Once inserted into the membrane, the local environment of a protein or peptide is significantly altered. Because it is energetically costly to transfer charged or highly polar compounds into the hydrophobic core of membrane bilayers, it is thermodynamically unfavorable for peptides to partition from an aqueous environment into the membrane in an unfolded state. Thus it is expected for peptides to undergo significant conformational rearrangements in order to minimize the free energy, and find the most stable state in the membrane. In order to minimize the free energy of membrane insertion membrane proteins have a larger percentage of non-polar amino acid side chains in their transmembrane regions. Furthermore, to overcome the cost of having polar carbonyl and amino groups of the peptide backbone in the hydrophobic core, membrane proteins

undergo conformational changes to form α-helices or β-sheets where these groups can participate in hydrogen bonding with each other. The free energy reduction per residue for peptides accompanying secondary structure formation is approximately -0.5 kcal/mol. This dramatically reduces the peptide's partitioning free energy, making insertion into the membrane much more favorable, and tightly couples the folding and partitioning processes. Here we wanted to examine whether interaction with the bilayer induces conformational changes in Aβ, and determine what conformation the potential Aβ pore is. Because the interface of the bilayer (head group region) is the first site of contact between the peptide and the membrane, it likely plays an important role in influencing folding and insertion. In this chapter we use circular dichroism to determine the secondary structure of Aβ bound to liposomal membranes, and study how membrane charge and fluidity affect this.

Another approach membrane proteins have for reducing partitioning energy is through protein-protein interactions, or oligomerization of the inserted protein. By forming oligomers in the membrane, hydrophilic areas on the protein are further buried and shielded by other subunits from the hydrophobic lipid tails. Recent AFM studies have revealed the presence of annular ring-like structures of Aβ that appear to be made up of multiple monomeric units of Aβ bound to membrane bilayers (27, 32). The membrane binding species and the active membrane permeabilizing species are therefore likely to be an oligomeric species. In this chapter we discuss the determination of the oligomeric order of these membrane binding species, and determine whether these membrane bound oligomers form in solution prior to insertion or are assembled in the

membrane after initial insertion of monomeric Aβ. The high local concentrations of Aβ on the membrane surface leads to crowding, and can influence whether protein-protein interactions or protein-lipid interactions are more favorable. Here we examine the effects of the ratio of lipid to peptide (L:P) on both the conformation of Aβ, and the oligomerization state.

3.2 Materials and Methods

3.2.1 Circular Dichroism

Circular dichroism was measured using a J-715 spectropolarimeter (Jasco, Easton, MD) with temperature control at 22°C using a cuvette with a 1 mm pathlength. Spectra of liposomes in buffer were subtracted for each lipid concentration used. 25 μM of freshly dissolved WT Aβ40 in 10 mM NaPi pH 7.4 was titrated with concentrated stocks of SUVs composed of DPPC, POPC, DPPC/PG, or POPC/PG. After each addition, the sample was allowed to equilibrate at 25°C for 10 min. before beginning the scans. Scans were taken at 50 nm/min with a response time of 2 sec. and a bandwith of 5 nm from 195-260 nm. Each spectrum was the result of averaging 5 consecutive scans. The amount of lipid that could be added was limited due to scattering effects. Secondary structure was evaluated from the spectra using CONTINLL algorithms within the CDPro analysis software (55). The reference basis set used in the analysis was SMP56 which includes membrane proteins (55).

3.2.2 Glutaraldehyde Crosslinking

To determine whether association with the membrane induces changes in oligomerization, the peptide was chemically crosslinked with glutaraldehyde to determine the oligomerization state. 5 μM WT Aβ40 was incubated with increasing concentrations of SUVs at room temperature for 10 minutes in 10 mM NaPi pH 7.4. Peptide crosslinking was initiated by addition of 0.01% glutaraldehyde, and allowed to proceed for 40 min. at RT. Reactions were quenched with 100 mM glycine for 30 min. at RT. 4x SDS-PAGE loading buffer (250 mM Tris pH 6.8, 8% SDS, 40% glycerol, 4% β-mercaptoethanol) was added, and samples were incubated at 100°C for 5 min. Samples were run on a 10-20% SDS Tris-Tricine Ready Gel (Bio-Rad, Hercules, CA) and immunoblotted on a nitrocellulose membrane with a mouse monoclonal α-Aβ antibody (6E10) (Abcam Inc., Cambridge, MA). Bound antibody was visualized with a horseradish peroxidase conjugated α-mouse immunoglobulin and ECL (Bio-Rad, Hercules, CA).

3.2.3 ThT binding with liposomes

To determine whether fibrilization rates are increased for peptide on the liposome membrane, ThT binding was measured for Aβ40 incubated with SUVs of DPPC or DPPC/PG at RT over several days. 125 μM Aβ40 was incubated with 800 μM SUVs in 10 mM NaPi pH 7.4, and samples were periodically removed and measured for ThT binding as described in chapter II. The ThT signal for samples with SUVs only were also measured and subtracted from each time point since SUVs alone slightly increase the ThT fluorescence.

3.3 Results

3.3.1 Influence of membrane charge and phase on Aβ conformation

The effects of anionic and neutral liposomes on Aβ40 conformation were studied using far-UV CD in the range of 190-260 nm. The spectrum of freshly prepared 25 μM WT Aβ40 revealed primarily random coil structure, with a large negative peak at 200 nm (figure 3.1). The peptide was allowed to bind to the liposomes for 10 min. prior to taking the measurements, and this initial spectra did not change over the time of the experiment ca. 3 hr. (data not shown). Addition of either gel phase DPPC SUVs or LC phase POPC SUVs to Aβ40 did not produce any significant changes in the conformation of the peptide, even at concentrations greater than 500 μM lipid (at which the loose binding to the neutral membrane has reached saturation) as seen in figure 3.1 a, c. In contrast, progressive addition of SUVs containing either DPPC/PG or POPC/PG induced a dramatic two step transition from random coil to β-sheet to α-helical structures. The spectra were analyzed for secondary structure composition. At intermediate L:P ratios (~10:1-20:1) β-sheet structure is induced. The percent β-sheet structure in peptide alone is less than 35%, but increases to 45% upon addition of 500 μM DPPC/PG SUVs (L:P of 25:1) or 300 μM POPC/PG SUVs (L:P of 15:1) (figure 3.2 a, b). Further increasing the levels of DPPC/PG or POPC/PG SUVs to high L:P ratios where Aβ is presumably diluted on the liposome, resulted in a decrease in the percentage of β-sheet structure, and an increase in α-helical structure from 5% with no SUVs to 18% with DPPC/PG SUVs and to 35% with POPC/PG SUVs at L:P of 80:1 (figure 3.2 a, b). In contrast, no change in any of these structural components was seen for DPPC or POPC SUVs. These results

further distinguish the interactions between Aβ40 with neutral and anionic membranes. Notably, the induced changes in conformation are independent of the phase and fluidity of the membrane, depending solely on the identity of the lipid head groups. Increasing the ionic strength by including NaCl in the buffer reduced the magnitude of the structural changes in the peptide, however the same random coil-β-sheet-α-helix transitions were seen (data not shown), supporting the involvement of more than just electrostatic interactions in Aβ membrane association.

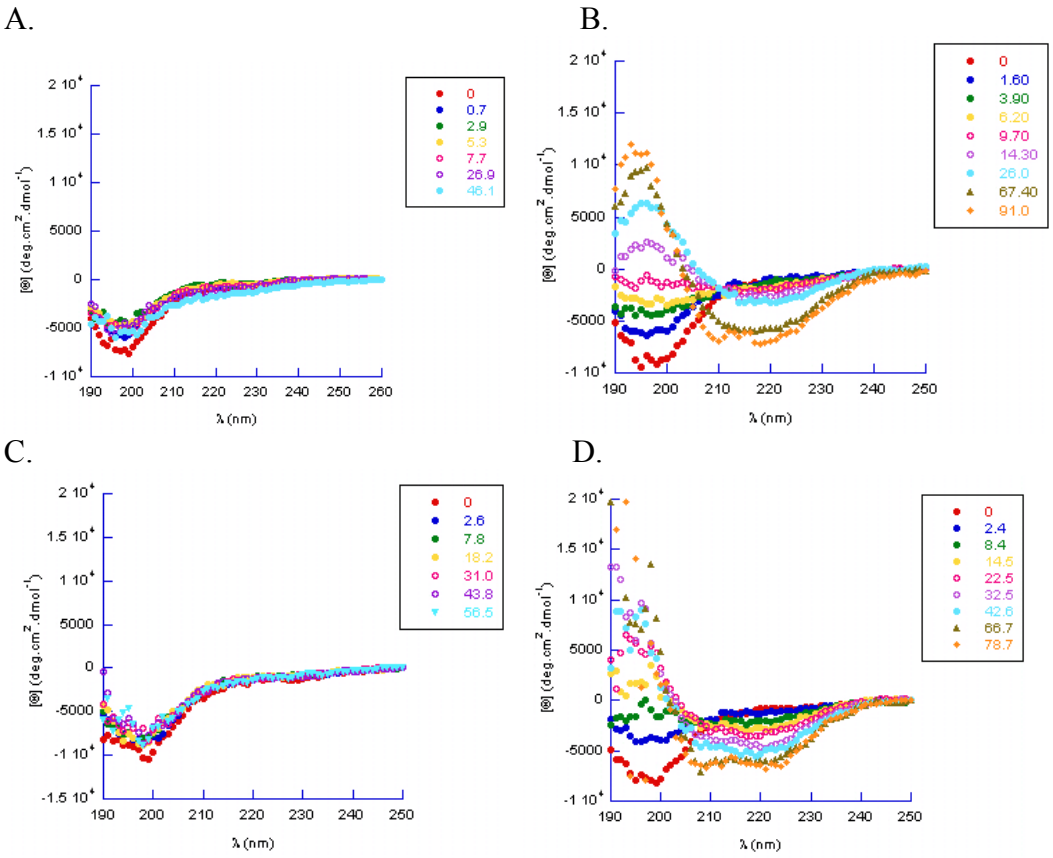

Figure 3.1: Conformational changes in WT Aβ40 upon binding to lipids. Aβ40 at an initial concentration of 25 μM was titrated with and allowed to bind to SUVs composed of gel phase (A) DPPC, (B) DPPC/DPPG, or liquid-crystalline phase (C) POPC, and (D) POPC/POPG at increasing L:P ratios (shown in legend). Spectra were corrected for contributions from the liposomes, as well as for dilution.

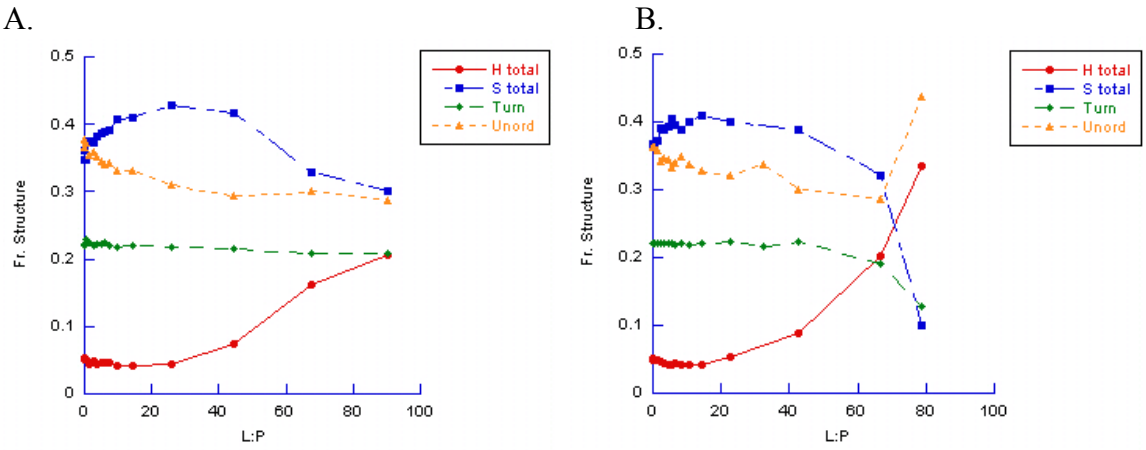

Figure 3.2: Analysis of secondary structure composition of CD spectra from figure 3.1 using CONTINLL with the SMP56 basis set. α-helical (Htotal), β-sheet (Stotal), β-turn (Turn), and random coil (Unord) content for Aβ40 bound to (A) DPPC/PG or (B) POPC/PG SUVs are plotted vs. lipid to peptide ratio (L:P).

3.3.2 Oligomerization changes upon interaction with the membrane

As Aβ binds to the membrane, its local concentration becomes much higher than in solution, which may help promote oligomerization. To measure oligomerization, crosslinking studies were done with glutaraldehyde, (a crosslinker that reacts selectively with primary amines such as lysine residues and the amino-terminus) that has been widely used to assess the oligomeric state of proteins. 5 μM WT Aβ40 was incubated with increasing concentrations of SUVs under the conditions used for the tryptophan shift experiments before addition of crosslinker. Crosslinked oligomers were separated by SDS-PAGE. Crosslinking of freshly dissolved Aβ40 in the absence of phospholipid revealed the presence of trimers, dimers, and monomers (figure 3.3). While it cannot be

determined from this data alone whether all these species are present in solution, (trimers may appear as dimers due to incomplete crosslinking), gel filtration chromatography shows a single tight peak corresponding to an approximately 15 kDa species suggesting that only a single species exists in the freshly dissolved sample (figure 2.1). Incubation with SUVs of DPPC/PG induced further oligomerization of Aβ40, forming additional crosslinked oligomers ranging from tetramers to octamers at low-intermediate L:P ratios (4:1-40:1) (figure 3.3). Oligomerization past trimers was detectable at 20-500 μM DPPC/PG, being maximal around 200 μM. Although 500 μM lipid was able to induce formation of a tetrameric species, no higher order oligomers were detected. Furthermore, incubation with 1 mM lipid (high L:P) did not induce much oligomerization beyond trimer, resulting in a crosslinking pattern similar to that of Aβ40 alone but with a faint band corresponding to tetramer. Thus the intermediate L:P ratios that induced β-sheet structure also promote higher order oligomerization, whereas the higher L:P ratios that induce α-helical structure stabilize the tetrameric or trimeric states. In contrast, addition of up to 1 mM DPPC did not induce significant oligomerization beyond what was present initially. Some bands corresponding to tetramers-hexamers could be detected in the 1 mM DPPC sample. Upon extended film exposure, faint bands were detected in the lower DPPC samples in the tetramer-hexamer range, but it was clear that the predominant species present were trimer and smaller. Similar results were seen for POPC/PG vs. POPC SUVs (data not shown). These results are consistent with the CD analysis, in that only anionic membranes induce a conformational change in Aβ40, favoring oligomerization.

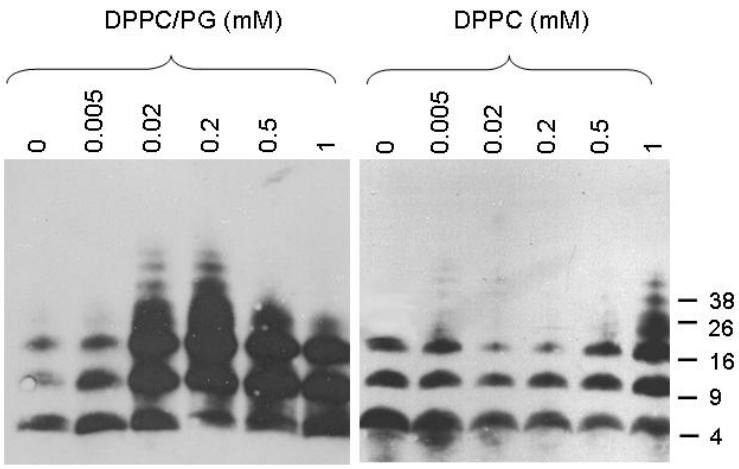

Figure 3.3: Glutaraldehyde crosslinking of Aβ40. 5 μM Aβ40 was incubated with increasing concentrations of 1:1 DPPC/PG or DPPC only SUVs before crosslinking with 0.01% glutaraldehyde. Reactions were quenched with glycine, and boiled in loading buffer before separation by SDS-PAGE. The gel was immunoblotted, and probed with a mouse monoclonal α-Aβ antibody (6E10). The molecular weight of monomeric Aβ40 is 4.3 kDa.

3.3.3 Fibrilization rates are increased upon membrane association

There are limitations to consider when crosslinking proteins in the membrane due to the greater likelihood of nonspecific crosslinking of peptide crowded but not necessarily oligomerized on the surface. However we observed acceleration of fibrilization rates as measured by ThT when Aβ40 was incubated with DPPC/PG SUVs at the intermediate L:P ratios where the larger crosslinked oligomers were observed, and inhibition of fibrilization at the very high L:P ratios where the larger oligomers were not seen (figure 3.4). This, along with the corresponding changes in conformation from the CD experiments at these L:P ratios lead us to believe the crosslinked species are truly oligomers and not just artifacts of glutaraldehyde crosslinking. Furthermore although the

fibrilization rate was not as accelerated upon interaction with the neutral DPPC membranes as with DPPC/PG, there was still significant acceleration in the fibrilization rate. Since at higher concentrations of peptide, peptide-peptide interactions become more favorable than peptide-lipid interactions, the slower fibrilization rate observed for DPPC could be due to less Aβ40 being bound on the membrane surface, due to the weaker affinity to neutral membranes. The acceleration could also be due to DPPC/PG induced conversion of the peptide to β-sheet structure, an intermediate on the pathway to fibril formation, thereby catalyzing the fibrilization process.

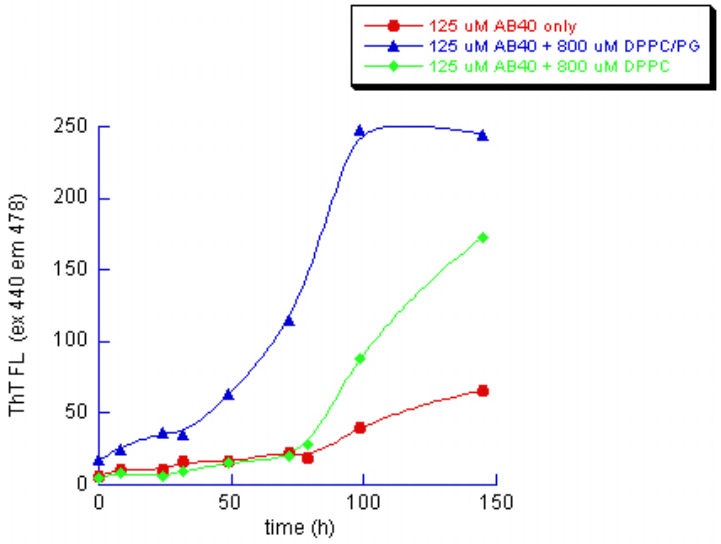

Figure 3.4: ThT binding time course for Aβ40 incubated with DPPC/PG or DPPC SUVs in 10 mM NaP_i pH 7.4 revealed acceleration of fibrilization rates upon interaction with the membrane.

3.4 Discussion

Immediately after disaggregation, Aβ40 in aqueous buffer solution has a random coil structure, and remains unstructured in the presence of neutral SUVs. However, upon

binding to anionic SUVs either in the gel phase (DPPC/PG) or the liquid crystalline phase (POPC/PG), β-sheet structure is rapidly induced at intermediate L:P ratios. As the concentration of lipid is increased, the β-sheet content diminishes and the peptide is converted to mostly α-helical structure (figure 3.1). The selectivity for anionic membranes in terms of inducing structure is similar to what is seen for several antimicrobial peptides, further relating Aβ to these peptides (51, 56, 57). In the β-sheet or α-helical conformation, the peptide is able to adopt an amphipathic configuration, placing hydrophilic and hydrophobic residues in favorable positions to interact with the solvent/lipid head region or the hydrophobic interior of the bilayer respectively. The two-step transition in secondary structure induced upon interaction with anionic liposomes is similar to what was observed by Terzi et al. for Aβ in POPG liposomes (37). Here we further expanded this to examine the role of membrane phase as well as charge on the structural transitions, and found that there is little if any influence of membrane phase on the induction of secondary structure. While illustrations tend to depict lipids in phospholipid bilayers with an insignificantly sized head group relative to the phospholipid tail, in actuality the thermodynamic thickness of the membrane lipid head group interface is approximately 15 Å which is comparable to the 30 Å of the hydrophobic core (58, 59). Thus a significant portion of the membrane protein mass contacts the interface, and it is not surprising that the conformational changes are dictated predominantly by the identity of the phospholipid head group and not by the acyl tail group.

Interestingly, the induced structure also correlates with oligomerization as detected by chemical crosslinking experiments. Oligomerization was induced in the presence of anionic liposomes only, with higher order oligomers (up to octamers) present only at the intermediate L:P ratios where β-sheet structure was prevalent. This order of oligomerization is consistent with the number of subunits observed in the annular membrane bound Aβ structures observed by Quist et.al. by AFM (32). From these results it appears that oligomerization does not occur in solution prior to membrane association, and is induced on the membrane. Insertion is likely cooperative and coupled to conformational changes and oligomerization. This coupling has been observed by CD and IR spectroscopy for several synthetic peptides (58, 59). Higher L:P ratios that induced α-helical structure did not induce significant oligomerization beyond what was seen for Aβ in solution. As Aβ binds to the membrane surface, the local concentration of peptide increases significantly. On the membrane, there is a constant equilibrium between peptide-lipid interactions and peptide-peptide interactions. At low L:P ratios, the local concentration of peptide is high on the membrane surface, making peptide-peptide interactions more energetically favored than peptide-lipid interactions, driving the formation of oligomers. However, as more liposomes are added, the density of Aβ on the membrane surface is lowered, resulting in a lower number of available peptide-peptide interactions, shifting the equilibrium to favor peptide-lipid interactions. Thus while Aβ levels are not significantly increased in the diseased brain, the presence of factors that would cause localized increases in concentration or accumulation of Aβ on neuronal cell membranes could lead to the formation of toxic species.

Extending the oligomerization studies, in this chapter we also found that the rate of fibrilization was enhanced in the presence of both anionic and neutral membranes, but to a greater extent in anionic membranes. However this depended on the L:P ratio. Fibrilization was accelerated at the intermediate L:P ratios where DPPC/PG induced maximal oligomerization and β-sheet structure, but was inhibited at high L:P ratios where oligomerization was minimal, and α-helical structure was predominant. This can be explained ag ain by the increased local concentration of Aβ on the membrane driving oligomerization and subsequently fibrilization, and also by our finding that interaction with the membrane at intermediate L:P ratios induces conformational changes to β-sheet structure, an intermediate structure on the way to forming fibrils (figure 3.5). It cannot be determined from the data in this chapter alone which state of Aβ on the membrane is the toxic pore species--the β-sheet species, the α-helical species, or both. We examine these possibilities further in chapter IV.

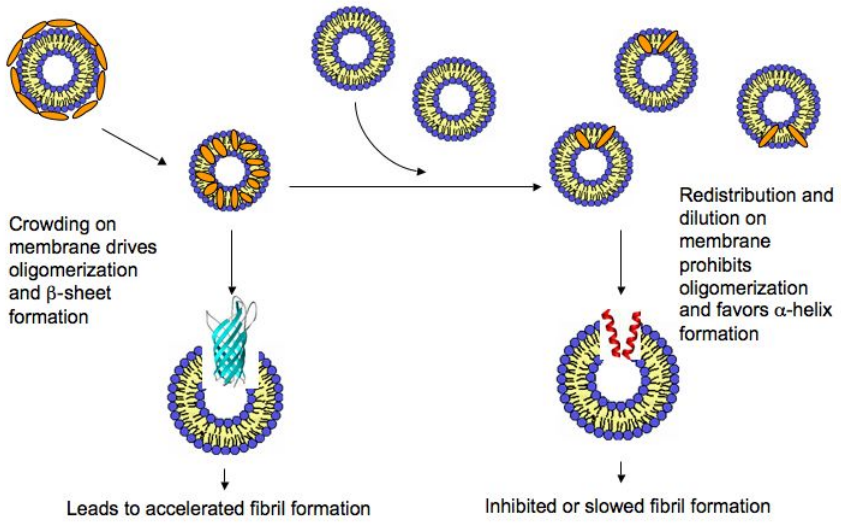

Figure 3.5: Model of crowding and redistribution of Aβ on the membrane surface.

In the previous chapter we demonstrated that fibrillar Aβ formed in solution does not interact with the membrane, however here the fibrils are formed on the membrane starting from peptide already bound to the membrane. Some Aβ researchers suggest that fibril formation actually is a protective mechanism, serving to sequester the toxic soluble oligomers into insoluble plaques so that they can no longer interact with other cells. Thus while we can not determine which species are the toxic species from the data in this chapter alone, it is clear that membrane composition, and the density of peptide on the membrane are critical determinants of Aβ structure and oligomeric status, which is directly related to the formation of cytotoxic structures. The membrane therefore is not simply a static scaffold, but rather plays a dynamic role in influencing Aβ activity.

CHAPTER IV

Aβ Membrane Permeabilization and the Influence of Fluidity and Cholesterol

4.1 Introduction

While Aβ has been studied extensively for several decades, it is still unknown how this peptide exerts its neurotoxic effects. As mentioned in chapter I, Aβ is present both in the cerebrospinal fluid and blood under normal conditions, however the physiological role of this peptide is unknown. One of the predominant models in the field of Aβ research of how Aβ becomes cytotoxic is the channel model suggested by Lashuel and Lansbury (26). In this model, Aβ becomes cytotoxic upon forming channels or pores in neuronal cell membranes, thereby allowing a rapid influx of ions such as calcium into the cell. This rapid influx of ions could result in cell death by disruption of the ionic balance within the cell, forcing the cell to work harder to maintain homeostasis, resulting in chronic cellular stress. Increased calcium in the cell can also lead to the activation of apoptosis signaling pathways, and can lead to cell death indirectly. Physiological extracellular calcium levels are close to 2 mM, whereas intracellularly they are in the low μM range. Thus cell membrane leakage has the potential to dramatically alter cellular calcium levels.

While it is unknown which form of the peptide is the pathogenic agent, recent studies, as discussed in chapter I, have provided evidence to support the involvement of soluble intermediate sized oligomeric species of Aβ (20, 28, 60-63). In a recent study, it was shown that incubation of neuronal SH-SY5Y cells with Aβ oligomers causes a significant rise in cellular calcium levels (21). Furthermore, it has been shown in several studies that the presence of Aβ on membrane bilayers causes a significant increase in conductivity (23, 30-33). Though the increase in conductivity has been demonstrated by several groups including our own, there is still significant debate about whether or not this increase occurs through a pore/channel mechanism, or by a more nonspecific general overall lowering of the dielectric barrier of the membrane (64). A strong piece of evidence supporting a pore or channel mechanism is that the increase in conductivity occurs in discrete steps, characteristic of a channel, rather than a gradual linear increase that would be indicative of overall nonspecific membrane permeabilization (unpublished results from our lab). Furthermore, atomic force microscopy images of Aβ bound to membrane bilayers demonstrate the presence of annular oligomeric structures, which could be the pore unit (32).

Several pore forming toxins (PFTs) and antimicrobial peptides (AMPs) such as gramicidin, magainin, and melittin to name just a few share a similar mechanism of action, forming pores in the cell membrane approximately 30 Å in diameter. These peptides are typically unstructured in solution, and are induced to form α-helical structure in the presence of membrane. Several of these peptides undergo oligomerization to form membrane spanning channels in their target cell membrane, and also have a membrane

charge dependency similar to what was observed for Aβ in the previous chapters. For PFTs and AMPs, the L:P ratio strongly influences the orientation and pore forming activity of these peptides. In chapter II, we also observed a strong dependency of oligomerization order and secondary structure on the L:P ratio. Thus it is likely that much can be learned about the mechanism of Aβ cytotoxicity by comparing Aβ with these peptides.

In this chapter we discuss the effect of charge and fluidity on the ability of Aβ to permeabilize the membrane. In the first section we compare gel phase to liquid crystalline phase membranes, and determine whether conditions that promoted Aβ binding also lead to permeabilization. We examine how the L:P ratios influence the rate of membrane leakage, and relate this to the structural and oligomerization changes we observed in chapter III. While the gel and LC phase membranes provide good models of the extremes, *in vivo* the gel phase does not exist. Rather, the membrane is a mixture of lipids of several different chain lengths, and degrees of saturation. The liquid ordered (LO) phase is the closest phase to gel phase found in the plasma membrane, and is attained by the presence of cholesterol in the membrane. Cholesterol is a member of the polycyclic sterols (figure 4.1.1), and is a ubiquitous component of all mammalian cell membranes. The brain has the most cholesterol in the body, containing roughly a quarter of the total free cholesterol in the human body. The cholesterol hydroxyl group orients the molecule such that the ring structure of cholesterol intercalates in the membrane and interacts with phospholipids such as phosphatidylcholine and sphingomyelin through van der Waals and hydrophobic interactions. Furthermore hydrogen bonding of the hydroxyl

group to the polar head group and interfacial regions of the phospholipids occur. These interactions serve to promote an increase in order, cohesion, and packing in the membrane leading to the more rigid liquid ordered phase. Cell membranes are not homogeneous, and contain regions where cholesterol and sphingomyelin are elevated that are very rigid. These regions are termed lipid rafts. Thus modulating membrane cholesterol content serves as a method by which cells can fine tune the rigidity of the membrane.

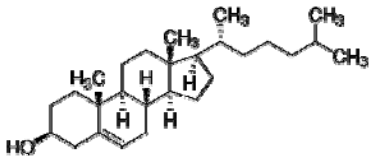

Figure 4.1: Structure of cholesterol

In the second part of this chapter, we examine how the presence of cholesterol affects the fluidity of the membrane, and study how cholesterol affects Aβ membrane binding, insertion, and permeabilization, and the structural, and oligomerization changes induced by membrane association.

4.2 Materials and Methods

Liposome Permeabilization. Liposomes containing 5(6)-carboxyfluorescein (CF) (Sigma-Aldrich, St. Louis, MO) were prepared by rehydrating lipid films at a concentration of 5 mg/mL in 10 mM NaPi pH 7.4 containing 50 mM CF. Lipids were incubated in a water bath above the lipid melting temperature for 2 h. Rehydrated lipid

suspensions were vortexed and subjected to at least 8 freeze thaw cycles from liquid nitrogen to a 60°C water bath. To form LUVs, the lipid solution was extruded 21 times through 2 stacked 100 nm pore size polycarbonate Nuclepore membrane filters (Whatman, Florham Park, New Jersey). Free CF was separated from liposomes containing CF by running the solution through a 10 mL G-50 Sephadex gel filtration column (Sigma-Aldrich, St. Louis, MO) in 10 mM NaPi. For the permeabilization assay, 5 μM freshly dissolved Aβ40 was incubated with increasing concentrations of liposomes. In order to accurately measure fluorescence at high liposome concentrations and avoid inner filter effects due to high concentrations of CF, only 25 μM CF LUVs were included in each sample. Higher lipid concentrations were attained by adding in LUVs not containing CF. CF fluorescence intensity (excitation 490 nm, emission 514 nm) was measured at various time points. Dye leakage from liposomes alone was subtracted. To determine the fluorescence value for maximal dye leakage, 0.2% Triton X-100 was added to the liposomes at the end of the time course. Leakage is expressed as lipid permeabilized as determined by dividing the fluorescence signal by the fluorescence for 1 μM of LUVs permeabilized by triton treatment.

Cholesterol Incorporation. Cholesterol (Sigma-Aldrich, St. Louis, MO) dissolved in chloroform was dried down with POPC/PG at 0, 10, or 25% by mass under a steady stream of N_2, and vacuumed overnight to remove residual chloroform. Liposomes were formed by rehydration at 2.5 mg/mL at 30°C in 10 mM NaP_i pH 7.4 and either sonicated (SUVs) or extruded (LUVs) as described above. As cholesterol was increased, POPC/PG levels were decreased in order to maintain constant total lipid (including cholesterol).

Laurdan General Polarization. Laurdan (Sigma-Aldrich, St. Louis, MO) was dissolved in chloroform. To measure membrane packing density and fluidity, laurdan was mixed with DPPC/PG, POPC/PG, or POPC/PG with various percentages of cholesterol (by mass) at a 5% molar ratio to total lipid and dried down with N_2 and vacuumed overnight. Liposomes were formed by rehydration at 2.5 mg/mL at 30°C in 10 mM NaP_i pH 7.4 and sonicated to form SUVs as described previously. The fluorescence spectrum was measured at an excitation wavelength of 350 nm, and membrane packing was quantified by general polarization (GP) as defined by Parasassi et al. (65) in equation 4.1:

$$GP = \frac{(I_{435} - I_{500})}{(I_{435} + I_{500})} \qquad \text{(eq. 4.1)}$$

where I_{435} and I_{500} are the fluorescence emission intensities at 435 nm and 500 nm upon excitation at 350 nm. A more negative GP value corresponds to a more fluid like, less tightly packed membrane, whereas a positive GP value corresponds to a gel-like, tightly packed membrane.

Tryptophan shift and circular dichroism. Trp shift and circular dichroism experiments and analysis were done as described in chapter II.

4.3 Results

Aβ40 membrane binding, oligomerization, and insertion are not sufficient for permeabilization of gel-phase membranes.

To measure the ability of Aβ40 to permeabilize membrane bilayers, liposomes were made containing high concentrations of the self-quenching fluorescent dye, 5(6)-

carboxyfluorescein (CF). In an intact liposome CF fluorescence is largely quenched; however, upon liposome permeabilization CF is released and diluted, resulting in a large (3-5 fold) increase in fluorescence. Because POPC and POPC/PG SUVs containing high concentrations of CF were unstable, resulting in significant endogenous leakage of dye over time, LUVs were used for these experiments. It is pertinent to note that LUVs and SUVs gave similar results in Aβ binding experiments (data not shown). 5 μM Aβ40 was incubated with increasing concentrations of DPPC, DPPC/PG, POPC, or POPC/PG LUVs containing CF. The dependence of permeabilization activity on the L:P ratio was measured by keeping the Aβ40 concentration constant, and varying the liposome concentration. Because accurate fluorescence measurements of high concentrations of CF LUVs are difficult due to inner filter effects caused by the high concentrations of dye, a constant amount of CF LUVs (25 μM) was used in all samples. Higher lipid concentrations were attained by adding non-dye containing LUVs to the CF LUV solution. No significant Aβ-induced permeability was seen for DPPC or POPC LUVs, as well as for DPPC/PG LUVs (figure 4.2a). However, there was considerable permeabilization of POPC/PG LUVs (figure 4.2b). Even though Aβ was able to bind to liposomes in both the gel and liquid crystalline (LC) phases equally well, permeabilization only occurred in the LC phase. Thus binding and insertion are dependent on the charge of the lipid head groups, whereas permeabilization also depends on the lipid phase (that in turn, depends on the lipid tail group).

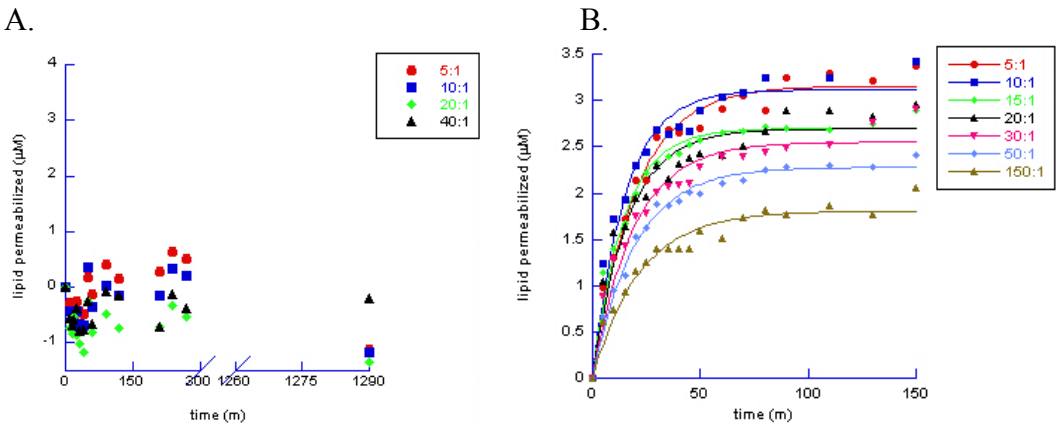

Figure 4.2: Membrane permeabilization assessed by CF leakage. 5 μM Aβ40 was incubated with various concentrations of (A) DPPC/PG or (B) POPC/PG LUVs containing 50 mM CF. Each sample contained 25 μM LUVs with CF, and was brought up to the higher final lipid concentration by adding LUVs of the same composition without entrapped CF (see materials and methods). Permeabilization was measured by an increase in CF fluorescence. Maximal leakage was determined by disruption of the liposomes with 0.02% triton X-100.

Leakage rates found by fitting the fluorescence increase to a single exponential term demonstrated a dependence on the L:P ratio, with the highest rate of leakage seen for low L:P ratios and decreasing as the L:P ratio was increased (figure 4.3c). The differences seen in the leakage rates may be due to the presence of differently sized Aβ pores on the membrane (which has been observed previously through conductivity measurements (23) and unpublished results from our lab), or to different rates of pore assembly. At the low to intermediate L:P ratios (5:1-30:1) where leakage rates are the highest, oligomerization to hexamers-octamers is maximally induced along with β-sheet structure (figures 3.2). Interestingly, the high L:P ratios where dye leakage is minimal also correspond to L:P ratios at which there is minimal oligomerization induced beyond what is observed for Aβ40 alone, and at which α-helical structure is maximal. Additionally, the minimal rate of dye leakage is reached at the same L:P ratio (~ 40:1) where the transition from β-sheet to α-helical structure begins. This further demonstrates

that at least two different classes of bound states of Aβ40 may be present. Concurrent single-molecule fluorescence imaging of fluorescently labeled Aβ40 on a lipid bilayer support this, revealing the presence of at least two classes of pores: large (>dodecameric) high conductance pores, and small, discrete, low conductance pores (<hexameric) (Schauerte, J., unpublished results).

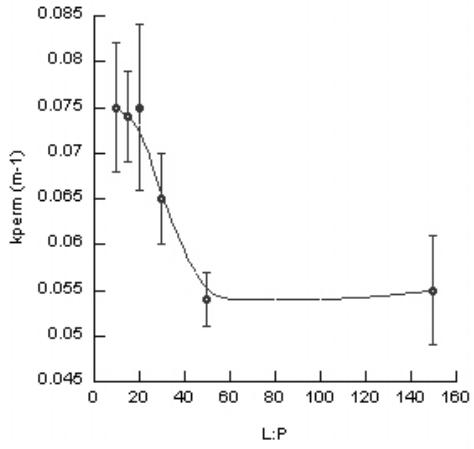

Figure 4.3: Liposome permeabilization rates (k_{perm}) calculated from first order fits to figure 4.2. Data are dependent on the L:P ratio (smooth curve was drawn as a guide).

Another important observation is that dye leakage takes over 1h to reach maximal levels, whereas binding assessed both by FRET and the tryptophan shift assays is complete within 10 minutes. Thus binding alone is not sufficient for membrane permeabilization, and a fast binding step is followed by a slow conversion leading to the formation of a pore.

Modulation of membrane fluidity with cholesterol

While the DPPC/PG membranes provide a good model of a rigid, gel phase membrane, the actual states found in the cell membrane are the LC phase and the less fluid liquid ordered (LO) phase which is of intermediate fluidity in between LC and gel membranes. The liquid ordered phase is formed when cholesterol is present in the membrane, as in lipid rafts where cholesterol is enriched. The fluidity of the LC POPC/PG membrane was decreased by incorporation of 0, 10, or 25% cholesterol into the liposomes. To quantify the packing density, which is directly related to the fluidity of the membrane, the polarity-sensitive fluorescent dye, laurdan was incorporated into the liposome bilayers. Because of its long hydrophobic tail, laurdan is able to intercalate into the membrane such that the naphthalene ring is level with the phospholipid glycerol backbone. The emission spectrum of laurdan in phospholipid bilayers depends upon the phase of the membrane. In the fluid LC phase, lipid head groups are spaced farther apart from each other than in the rigid gel phase membrane. Thus in the LC phase, more water molecules are present in between the phospholipid head groups. Because of this, the fluorescent moiety of the laurdan molecule (the naphthalene ring) is exposed to a more polar environment in the LC phase as opposed to the gel phase. In a polar environment, the laurdan emission spectrum is red shifted due to dipole relaxation in the presence of water dipoles, whereas in a nonpolar environment this spectrum is blue shifted due to the absence of relaxation. Thus membrane fluidity can be measured by comparing the ratio of the laurdan emission maxima. Here we used general polarization as a measure of fluidity.

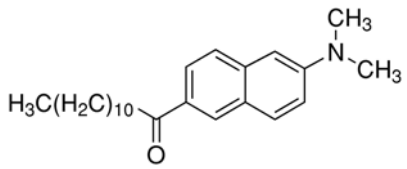

Figure 4.4: Laurdan

As seen in figure 4.5, laurdan has two emission maxima at 435 nm and 480 nm. Incorporation of 10% cholesterol into the LC POPC/PG membrane resulted in a blue shift in the laurdan emission spectrum, resulting in an increase in the 435 nm peak relative to the 480 nm peak, indicative of a more tightly packed, less fluid membrane (figure 4.5a). Further increasing the cholesterol content to 25% resulted in an even larger blue shift and a spectrum that closely resembles that of gel phase DPPC/PG liposomes (figure 4.5b). The GP values for POPC/PG SUVs with 0, 10, and 25% cholesterol were -0.15, 0.14, and 0.38 respectively, compared to a GP value of 0.64 for DPPC/PG. The more negative the GP value is, the more fluid-like the membrane is. Thus LO membranes containing 25% cholesterol are highly rigid, and have a packing density close to what is found in gel phase membranes.

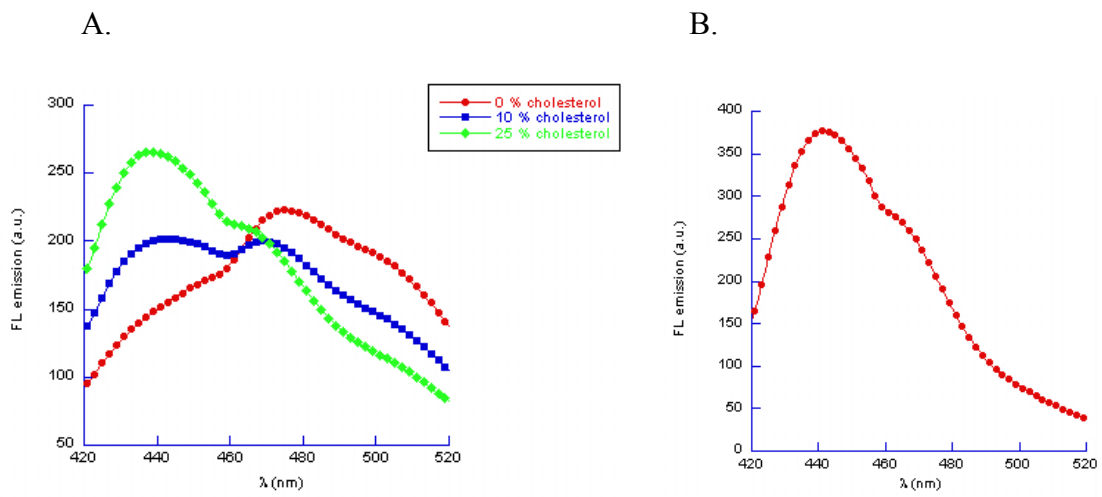

Figure 4.5: Fluorescence emission spectra of (A) POPC/PG SUVs containing 5 % laurdan, and 0-25% cholesterol and (B) DPPC/PG SUVs. SUVs were excited at 350 nm.

To measure how the presence of cholesterol influences binding and insertion, the tryptophan shift experiments with Aβ40[Y10W] were repeated with POPC/PG SUVs containing 0-25% cholesterol (figure 4.6a). No significant differences in the fluorescence λ_{max} curves were observed between 0-25% cholesterol, demonstrating that the insertion depth and binding affinity of Aβ40 are identical in these membranes even though the fluidity is significantly decreased in the presence of cholesterol. CD spectra were taken to determine the effects of having cholesterol in the membrane on Aβ secondary structure. The spectra showed little variance in the α-helical and β-sheet content when SUVs of POPC/PG with 0-25% cholesterol were incubated with Aβ (figure 4.6b). In contrast, CF leakage assays demonstrated that Aβ40 membrane permeabilization was significantly inhibited as the cholesterol content was increased in POPC/PG LUVs, with no leakage occurring at all from LUVs with 25% cholesterol (figure 4.6c). These results support the previously discussed findings with DPPC/PG membranes that Aβ binding,

insertion, and the associated conformational changes depend only on the lipid head groups, whereas permeabilization is inhibited as the fluidity of the membrane is decreased.

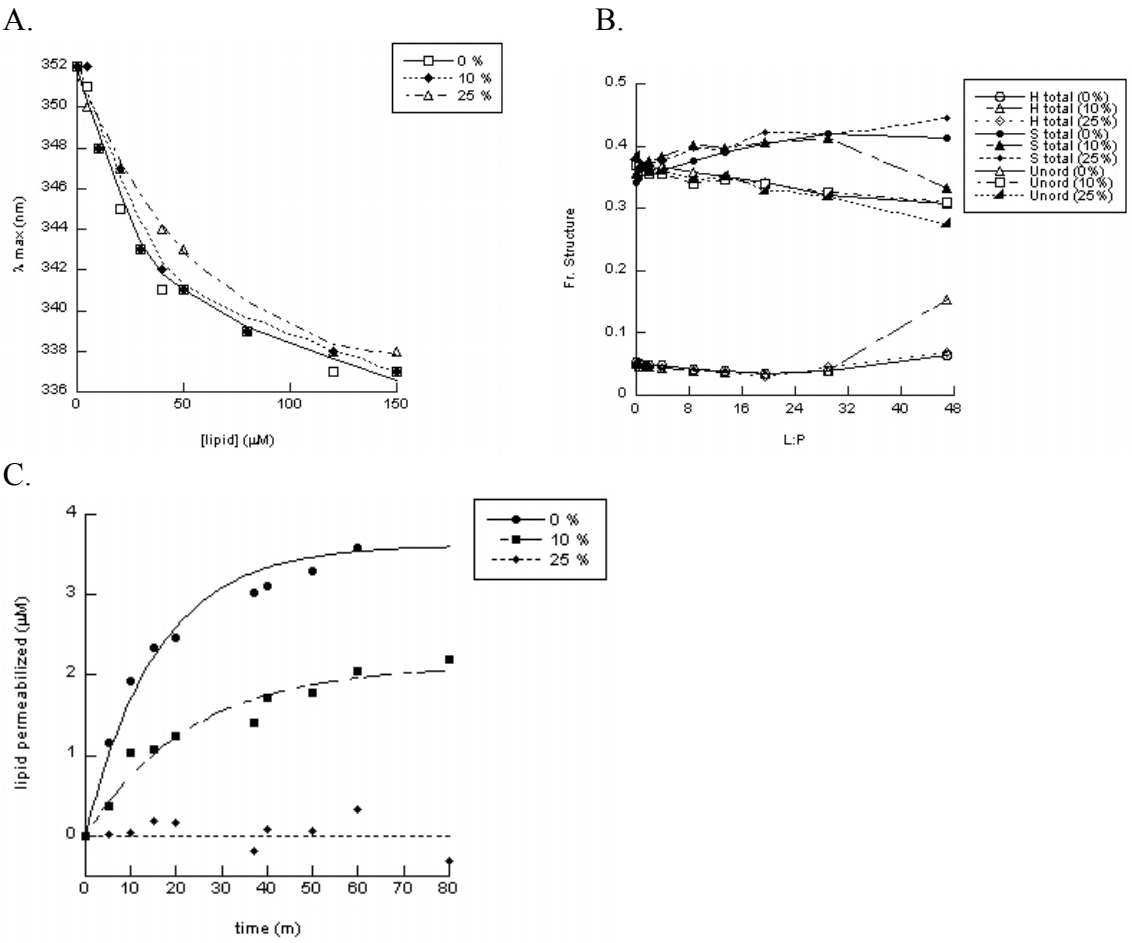

Figure 4.6: Effects of varying membrane fluidity and packing by addition of cholesterol on Aβ40 interactions. (A) Tryptophan shift assay. 2.5 μM Aβ40 [Y10W] was incubated with POPC/PG SUVs containing 0, 10, or 25% cholesterol, and the trp fluorescence λmax was determined as in chapter II. (B) Influence of cholesterol on Aβ40 secondary structure. Aβ40 at an initial concentration of 25 μM was titrated with POPC/PG SUVs containing 0, 10, or 25% cholesterol, CD spectra were taken and analyzed for secondary structure composition with CONTINLL as in chapter III. (C) Permeabilization activity of Aβ40 in the presence of cholesterol. 5 μM Aβ40 was incubated with 100 μM POPC/PG LUVs with 0, 10, or 25% cholesterol containing 50 mM CF. Membrane permeabilization was measured by CF fluorescence as in figure 4.3. Legends show the percentage cholesterol incorporated.

4.4 Discussion

While Aβ40-induced permeabilization has been seen in liposomes and bilayers before, many of these studies were done on membranes composed of lipids with mixed tail groups (i.e. phases) or LC phase membranes (31, 66, 67). In this chapter we distinguish between gel, LC, and LO phase membranes. In assessing Aβ40 permeabilization activity by CF leakage from LUVs, we found that although Aβ40 was able to bind equally well to anionic membranes both in the gel and LC phases (with the same structure and degree of oligomerization), this was not sufficient for permeabilization in gel phase liposomes. Permeabilization was only induced by Aβ when bound to fluid liquid crystalline POPC/PG LUVs. No permeabilization was seen for neutral PC membranes either in the gel or LC phase. This demonstrates that while Aβ membrane binding and insertion, and conformation and oligomerization depend only on the membrane charge or identity of the lipid head groups, permeabilization also depends on the fluidity of the membrane, which in this case is regulated by the identity of the hydrophobic tail group.

The increased permeability in LC phase POPC/PG membranes may be due to packing deficits in the membrane since the lipids are not packed as tightly in the liposome bilayer. This is because of the increased disorder resulting from the presence of an unsaturated acyl chain. This would facilitate incorporation of the Aβ pore into the membrane in comparison to the DPPC/PG membrane where the acyl chains are all saturated, resulting in tight packing of the lipids in the bilayer.

Since the cell membrane is composed of either LC or LO but not gel phase lipids, LC membrane fluidity was varied by the incorporation of 0-25% cholesterol to form the less fluid LO phase (a healthy neuronal cell contains 25% cholesterol). Cholesterol is known to decrease the area per phospholipid molecule in the membrane, thereby increasing the cohesiveness of lipids in the bilayer, making it more rigid. Binding affinity, peptide insertion, and the associated conformational changes were unchanged as the fluidity of the membrane was decreased by addition of cholesterol. However permeabilization was significantly decreased at 10% cholesterol, and completely inhibited at 25% cholesterol. This supports the results observed in the gel phase membranes that permeabilization is highly dependent on membrane phase. Because cholesterol is able to intercalate in between lipids, it fills in the spaces in between adjacent phospholipids, resulting in a tightly packed membrane similar to the packing found in the gel phase. In the cell, due to cholesterol's affinity for PC and sphingomyelin, areas on the membrane rich in these lipids and cholesterol form very rigid patches of membrane called lipid rafts. Cholesterol also reduces the membrane defects at the interface between these lipid rafts and the LC phase lipids, promoting membrane stability. When the peptide binds and inserts as a pore, water molecules that occupied the space in between lipid head groups are displaced, resulting in an increase in entropy in addition to the decrease in energy due to hydrophobic interactions between the peptide and lipids. The lack of significant gaps would make pore formation less favorable in gel and LO phase membranes since there are fewer water molecules to displace, and the cost of disrupting a stable membrane in order to insert a peptide pore could possibly outweigh the decrease in energy due to entropy and hydrophobic interactions.

Interestingly, while Aβ binding and structural changes were complete within 10 minutes as observed in chapter III, dye leakage reached a maximum only after 1-1.5 hours. Peptide binding is thus not the rate limiting step in pore formation, the latter process requiring a slow conversion step on the membrane to an active pore state. At low-intermediate L:P ratios, where oligomerization, and β-sheet structure are maximal, leakage rates are also maximal. In contrast, at the high L:P ratios where there is little induced oligomerization beyond tetramers and α-helical structure is maximal, leakage rates are decreased but notably do not level off at zero. Since k_{perm} did not decrease to zero at high L:P ratios, this suggests that both the β-sheet and α-helical species can permeabilize the membrane. This supports the presence of differently sized pores. Studies in our lab by Joseph Schauerte using simultaneous conductivity measurements and fluorescence imaging of Aβ structures bound to membrane bilayers confirmed the presence of at least two populations of conducting channels (unpublished results). These pores were of different oligomeric states and resulted in different magnitudes of increases in conductance. Aβ channels corresponding to hexameric peptide that demonstrated small discrete increases in conductance were observed as well as large extended pores corresponding to dodecameric peptide or larger that caused large increases in conductance. Alternatively the reduced permeabilization rate at high L:P could be a result of decreased rates of pore assembly due to the lower peptide density in the membrane.

Aβ40 membrane interactions can possibly be described by the two-state model proposed for antimicrobial peptide-membrane interactions in which the L:P ratio

determines the conformation of the peptide bound on the membrane (52, 68-70). In this model, at very high L:P ratios where the lipid is present at a large excess, initially random coiled peptide is induced to develop α-helical structure, but binds to the membrane parallel to the bilayer surface remaining in an inactive state (figure 4.7). Upon decreasing the L:P ratio, peptide density increases driving the transition to a pore with the helical axis perpendicular to the bilayer surface. This is because at high L:P, the energy level of surface adsorption is lower than for perpendicular insertion (69). However, as the L:P is decreased, pore formation is more energetically favored, possibly due to the oligomerization and conformational changes induced by the increased local concentration of peptide on the membrane surface. When a peptide binds to the interface (in the lipid head region), there is a negative binding energy due to the favorable hydrophobic interactions. However when a peptide resides between lipid headgroups parallel to the bilayer surface, it causes a gap in the membrane underneath the peptide that is filled in by the surrounding acyl chains. This causes a deformation and thinning of the membrane, resulting in a positive change in energy. Studies have demonstrated that when the L:P ratio is low (below the critical L:P), the energy of deformation increases as the L:P decreases, making the inactive parallel binding state less energetically favorable, driving the conversion to the pore state. On the other hand, if pore assembly occurs in the membrane, the decrease in the rate of permeabilization at high L:P could be explained by a slower rate of assembly due to a decrease in density of the peptide on the liposome surface.

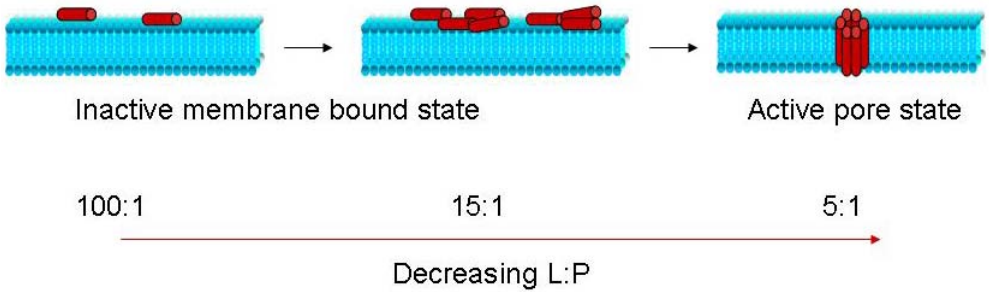

Figure 4.7: Two-state model of peptide-membrane interactions. At very high L:P ratios, the peptide binds to the membrane parallel to the bilayer surface, remaining in an inactive state. Increasing the peptide concentration to yield low L:P ratios below the critical L:P ratio, drives the formation of a peptide pore where the helical axis is perpendicular to the bilayer.

The dependence of Aβ permeablization on the membrane phase and fluidity is another similarity between Aβ and the pore forming toxins. For example, the pore forming activity of the toxin melittin has been shown to be highly dependent on membrane fluidity, and is greatly reduced as the concentrations of cholesterol in the membrane are increased (71). There are several related factors to consider when evaluating different membranes, such as lipid packing density, compressibility and bending moduli, and membrane curvature, which are also likely to play an important role in the formation of a pore. For instance, cholesterol is also known to induce negative curvature in the membrane, which inhibits peptide induced thinning of the lipid bilayer. This further inhibits the formation of toroidal pores where the lipid bilayer must bend such that the lipid headgroups form part of the lining of the pore. The toroidal pore has been observed for melittin, and since Aβ pore formation is also inhibited by cholesterol, this may suggest that the Aβ pore is toroidal as well (71).

While we cannot determine the size of the pore from the experiments in this chapter alone, we can estimate that the internal diameter of Aβ channels is at least 10 Å. This is because the diameter of the CF dye molecule is 10 Å at its widest span. The size of the Aβ pore is thus comparable to that of pores formed by melittin and other pore forming peptides.

Interaction of Aβ with lipid membranes is clearly a complex process, dependent on several factors. Here we show that charge is important in the initial membrane binding and oligomerization steps, however permeabilization depends on membrane fluidity as well. These results may provide insight into how Aβ becomes cytotoxic *in vivo*. Under normal conditions, most of the negatively charged lipids are found on the inner leaflet of the membrane (70). However recent studies have shown that damage by aging or disease can alter the outer membrane composition resulting in increased charge density on the outer leaflet (28, 72). While there are no significant changes in Aβ levels in AD affected brain, the presence of negatively charged lipids in the membrane could cause a large localized increase in peptide concentration leading to the changes described in these chapters. Furthermore, differences in cholesterol content and distribution in an aging brain (73, 74) may also contribute to changes in Aβ membrane permeabilization activity due to alterations in the fluidity of the membrane. Cholesterol has been shown to decrease in cellular membranes with age. Additionally, several oxidized forms of cholesterol are present in the aged brain, which may alter the ability of cholesterol to promote membrane integrity. The different types of membrane interactions described in

this chapter that depend on charge and fluidity may help explain some of the differences in Aβ activity in the healthy brain versus those in the AD brain.

CHAPTER V

Conclusions

5.1 Introduction

In this thesis, the interplay between lipid membrane bilayers and the amyloid-β peptide was studied. We found that the interactions between peptide and membrane are dynamic, and that the composition of the membrane is a strong determinant of Aβ activity, structure, and conformation. In the first part of this chapter, the data presented in this thesis are summarized. The second part of this chapter discusses possible future directions and the implications of our results in the pathogenesis of Alzheimer's disease.

5.2 Thesis summary

While several point mutations have been found that lead to inherited forms of early onset AD, it is still unknown how late onset "sporadic" AD arises. One of the most significant risk factors for developing AD is age. The incidence of AD increases from 10% in adults over 65 to 50% for adults over 85 (6). Another significant risk factor for developing AD is previous head injury (6). As cells age or are damaged, the composition of the cell membrane is altered. Most significantly, the distribution of the negatively charged lipid phosphatidylserine, normally localized primarily on the inner leaflet of the membrane, changes such that much of the PS is externalized to the outer membrane.

Furthermore, cholesterol levels in the membrane are different between young and aged cells. Thus we wanted to look at the role of charge and membrane phase and fluidity as determined by membrane lipid saturation and cholesterol content in determining the toxicity of Aβ.

In chapter II, the basic characterization of Aβ40 is discussed. Treatment of Aβ40 with NaOH effectively solubilizes and disaggregates the peptide, yielding a fibril and aggregate free low molecular weight species. This species is either a trimeric or tetrameric species, because of the glutaraldehyde crosslinking pattern shown in figure 3.3. Through FRET binding assays, we showed that this species is capable of binding to anionic PC/PG membranes at a high affinity, and does not bind significantly to neutral PC membranes. While oligomerization is induced upon binding to the membrane, we observed that the trimer/tetramer is capable of the initial interaction with the membrane. By allowing Aβ to oligomerize towards fibrils in the absence of lipids, we demonstrated that the species capable of binding to the membrane is a low molecular weight oligomeric species that is present immediately after dissolution of the peptide. Oligomerization past this low molecular weight species in solution prior to membrane exposure results in reduced membrane binding ability. Thus only the low molecular weight oligomers have the ability to initially bind to the membrane, although these bound species can go on to form higher order oligomers and fibrils on the membrane.

We also show that not only does Aβ40 bind tighter to anionic membranes, but the peptide is also inserted into the hydrophobic regions of these anionic bilayers. This is

seen by a blue shift in the tryptophan fluorescence of the Aβ40[Y10W] mutant bound to anionic but not neutral membranes, reflecting a more hydrophobic environment of the tryptophan residue. This was confirmed by a large decrease in the susceptibility of Aβ to collisional quenchers in solution when bound to anionic liposomes. Interestingly varying the fluidity and phase of the membrane by using liposomes composed of lipids with saturated (DPPC/PG) or unsaturated (POPC/PG) tail groups did not change the binding affinity of the peptide for the membrane, or the degree of insertion. Thus binding and insertion are processes that depend only on the identity of the lipid head group and the initial oligomerization state of Aβ40.

In chapter III, we demonstrated that interaction with anionic membranes either in the fluid LC or rigid gel phases induce higher order oligomerization, as well as significant changes in conformation. A two-step transition on secondary structure was observed upon binding to the anionic membranes from random coil to β-sheet to α-helical structure depending on the lipid to peptide ratio. At intermediate L:P ratios, β-sheet structure was induced. However, as the L:P ratio was increased further, α-helical structure became predominant. These changes corresponded to the degree of oligomerization. At intermediate L:P ratios where β-sheet structure was maximal, oligomerization up to hexamers and octamers was induced, and at very high L:P ratios where α-helical structure was maximal, only trimers and tetramers were present. At high L:P ratios the density of peptide on the membrane is low, and peptide-lipid interactions are favored. However, at lower L:P Aβ binds and accumulates on the anionic membrane, increasing the local concentration of peptide. The high local concentration of peptide

shifts the equilibrium to favor peptide-peptide interactions over peptide-lipid interactions, driving oligomerization of the peptide. No differences were observed between the induced oligomerization and conformational changes when cholesterol was included in the LC liposomes to yield liquid ordered phase membranes in chapter IV. Thus these processes are also only dependent on the lipid head group, and not on the fluidity or phase of the bilayer.

Chapter IV demonstrated that membrane permeabilization, unlike binding, insertion, oligomerization, and the conformational changes are not only dependent on the identity of the lipid head group, but are dependent on the phase and fluidity of the membrane as determined by the degree of lipid acyl tail group saturation and membrane cholesterol content. Aβ40 bound to gel and liquid ordered phase membranes were unable to induce membrane permeabilization, while a significant amount of permeabilization was observed in fluid LC membranes upon interaction with freshly dissolved Aβ. The rate of permeabilization was highly dependent on the L:P ratio. The highest rates of permeabilization were observed for low and intermediate L:P ratios where the peptide density on the membrane is high. This rate decreases dramatically as the L:P is increased (peptide density decreases). This supports the possibility that Aβ pore formation can be explained by the two-state model proposed for pore forming toxins and antimicrobrial peptides by Huang et al. in which peptides bind parallel to the membrane bilayer embedded in the lipid head group region in an inactive state until a critical concentration of peptide is reached on the surface of the membrane (69). At this critical concentration, oligomerization of the peptide is induced, driving conformational changes, and promoting

the conversion to an active pore in which the axis of the peptide is perpendicular to the bilayer plane.

The preferential interaction of Aβ40 with anionic membranes may seem unlikely because the pI is 5.5 (39), and at pH 7.4 the overall charge of the peptide is negative. However, close examination of the amino acid sequence of the peptide reveals the presence of clusters of basic residues (figure 1.4). In the structured β-sheet or α-helical oligomeric state, these residues may be localized and clustered on the same face of the peptide, allowing for the initial electrostatic attraction to the membrane. After this initial recruitment to the membrane interface, additional hydrophobic interactions can occur. We showed in this thesis that membrane surfaces are not an inert platform, but can act as promoters of aggregation. Thus changes in the membrane can have a significant impact on the pathogenesis of Aβ40.

5.3 Significance and Future Studies

The results presented in this thesis correlate well with work that has been published. A few studies have demonstrated that soluble low molecular weight oligomers of Aβ are able to inhibit learned behaviors and long term potentiation in mice and rats (18, 19, 75, 76). The reports vary however, as to the identity of the actual potent oligomer, ranging from dimers and trimers (75), to tetramers (19) to a 56 kDa species (18). We observed in our experiments that a trimeric or tetrameric species was the most stable unit of Aβ in solution. We showed that the trimeric/tetrameric species appear to be

the initial membrane binding species. While we do not know from our data whether the trimer/tetramer oligomerizes concomitantly with membrane binding, or after association with the membrane into the hexameric-octameric species that we observed, we found that larger oligomers preformed in solution prior to incubation with the membrane are unable to undergo the initial steps leading up to membrane binding. Thus, we do not know the oligomeric identity of the pore forming species, however we know this species is formed upon membrane association, since oligomers formed in solution are less able to interact with the membrane.

In this thesis we present data demonstrating that membrane binding alone is not sufficient for permeabilization, and that these are separable processes. This may allow us to target these steps, and attempt to block the progression towards membrane permeabilization and cell toxicity. Our results suggest a protective role of cholesterol in preventing membrane permeabilization. However, the role of cholesterol in AD is complex. Studies have demonstrated that higher cholesterol levels promote the cleavage of APP (77-79). Furthermore, some evidence points to the beneficial effects of the cholesterol lowering drugs, statins in the prevention of AD (79). While these correlations may seem contradictory to our findings that there is less permeabilization with membranes containing cholesterol, it is important to note that statins lower LDL cholesterol specifically, while maintaining HDL levels. In fact, recent studies have shown that there are links to memory deficits and dementia in patients with lower levels of plasma HDL, the predominant form of cholesterol in the brain (80). Furthermore, HDL has been shown to transport Aβ both in the CSF and plasma, leading to clearance.

While our model system is a much simplified *in vitro* system and the actual role of cholesterol in AD pathogenesis is likely to be multifaceted, our characterization demonstrates another potential role of cholesterol in AD.

We realize that in our system, the amount of negatively charged lipid and cholesterol used are greater than what would be observed under physiological conditions. We don't believe the electrostatic interactions are the sole mediators of Aβ interactions with the membrane. The cell membrane is a very complex mixture of proteins and lipids, and it is likely that since Aβ interacts *in vivo* with membranes with much lower concentrations of negatively charged lipids, and a much lower concentration of Aβ is cytotoxic, there must be other components that it can bind to. It would be interesting to study how changing the membrane charge content and fluidity of neuronal cells affects their susceptibility to Aβ induced toxicity *in vivo*. The work in this thesis focused on the physical disruption of the membrane by Aβ. Several other changes are induced in the cell as well. Examination of cell death signaling pathways in response to Aβ membrane interaction may provide us with a better understanding of the mechanism of Aβ induced neurodegeneration (ex. calcium dependent or independent cell death). It would also be useful to determine the exact identity of the oligomeric species that forms a pore in the membrane. Studies are underway in our lab to combine conductivity measurements with single-molecule fluorescence spectroscopy to quantify the oligomeric order of the conducting pore forming species on lipid bilayers. Lastly, in the AD brain, Aβ is found both in the 40 and the 42 residue forms. We focused our studies on Aβ40 because it is the more abundant form found in AD brain, and cell toxicity of Aβ40 has been

demonstrated (22, 29). Furthermore, the slower aggregation properties of Aβ40 allowed us to study and characterize the early steps leading up to pathogenesis such as oligomerization and membrane binding which we found difficult to resolve within the faster time scale of Aβ42 aggregation. However, it is important to study Aβ42 interactions with both Aβ40 and the membrane as well. Gaining a better understanding of the early stages of Aβ interactions will help us develop more effective methods to block these processes, and could lead to the development of a greatly needed treatment for AD.

APPENDIX

Regulation of Heat Shock Transcription Factor 1

A.1 Introduction

Cells are constantly challenged by exposure to potentially damaging conditions from the environment. Prolonged exposure to these insults can result in the destruction or damage of the proteins critical to proper cellular function through processes such as denaturation, aggregation, and misfolding. Several of these stressful conditions such as heat shock, oxidative stress, radiation, hypoxia, and ischemia, activate a cellular response known as the heat shock response (HSR). In the HSR, cells rapidly induce the expression of a large group of proteins called heat shock proteins (Hsps). Hsps are molecular chaperones that protect cellular proteins by preventing them from becoming damaged upon exposure to harmful conditions, and by repairing them after they become damaged. The HSR is induced under several disease states such as inflammation, heart disease, stroke, and Alzheimer's disease, as well as by several compounds used as pharmacological agents (2,4). Recently it was shown that overexpression of Hsps leads to better survival and recovery rates of ischemic heart and brain tissue (2). Thus a better understanding of how the HSR is regulated may lead to more effective methods of reducing cellular damage and increasing survival from several diseases.

One of the primary heat shock proteins highly expressed under stress is Hsp70. Hsp70 plays a major role in protecting cellular proteins by blocking nonproductive folding interactions such as aggregation, solubilizing denatured protein aggregates, and by facilitating the renaturation of denatured proteins (2). The expression of Hsp70 is tightly regulated by the transcription factor, heat shock factor 1 (HSF1). Under cellular stress HSF1, which primarily resides in the cytosol trimerizes and migrates to the nucleus. In the trimeric state, HSF1 has a high affinity for cis-acting DNA sequence elements called heat shock elements (HSEs) in the promoter region of heat shock protein genes. The HSE consists of a repeating array of the 5-bp sequence nGAAn, where each repeat is inverted relative to the immediately adjacent repeat (2, 5). All heat shock promoters, from different genes and diverse organisms share this same 5-bp repeat motif.

HSF1 is a 57kDa protein made up of several highly conserved functional domains. The amino-terminus contains an approximately 100 amino acid long helix-turn-helix DNA binding domain (DBD). The DBD is followed by a trimerization domain made up of three arrays of hydrophobic heptad repeats which can form coiled-coils or leucine zippers (LZ) (figure 1a) (3). The first heptad repeat (LZ1) is long and occupies the amino-terminal half of the region, whereas the other two heptad repeats (LZ2, 3) are short. Sequence analysis of the short heptad repeats reveal hydrophobic residues juxtaposed at four positions on one helical face, suggesting potential for hydrophobic interactions with the hydrophobic faces of one or more α helices (2,3,7). The rest of the C-terminal half of HSF1 consists of another short conserved hydrophobic heptad repeat (LZ4) that has been shown to repress trimerization. Mutations in this repeat region result

in constitutive trimerization, and abolish heat-inducible regulation of transcription. Trimerization is thought to occur through a transition from intramolecular interactions possibly between LZ4 and LZ1-3 to intermolecular interactions between the trimerization domains of separate monomers to form a triple stranded α-helical coiled coil (figure 1b) (3,7,8,9,10). The last 100 amino acids of the C-terminal make up the transcriptional activation domain (TAD), and a stretch of residues that spans a portion of the trimerization domain and continues further towards the C-terminus has also been seen to have a negative regulatory role on transcriptional activation (residues 181-227) (figure 1a) (3).

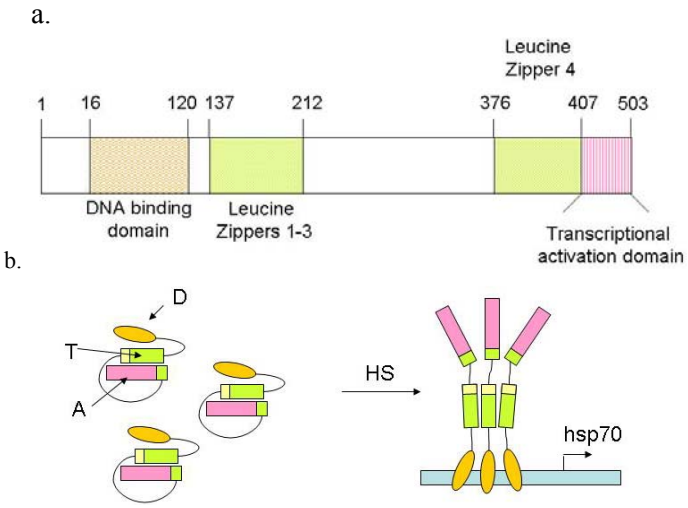

Figure 1. (a) Functional domains of mouse HSF1 (mHSF1). (b) Possible model of the transition that occurs during trimerization. The DNA binding domain (D), trimerization domain (T), and the TAD (A) are shown. In the latent state, intramolecular interactions between leucine zippers 1-3 and 4 keep HSF1 as a monomer. Upon heat shock, these interactions are disrupted, and intramolecular interactions become intermolecular interactions. (Not shown) upon trimerization further conformational changes allow exposure of the TAD.

Although HSF1 has been studied extensively, it is still not known how HSF1 is able to sense stress and undergo trimerization, and how its transcriptional activation activity is regulated. It remains unclear whether it directly senses stress or is regulated by upstream factors. Since trimerization and DNA binding alone are not sufficient for

transcriptional activation (12), at least two levels of regulation control HSF1 activity. A previous study showed that mouse HSF1 could be recombinantly expressed and purified in a monomeric form that could directly sense heat shock stress (22). The authors demonstrated that exposing this isolated HSF1 to high temperatures could induce trimerization, and DNA binding. However, HSF1 has been shown to interact with several proteins, which are likely to have a role in the regulation of HSF1 activity. Therefore we were interested in further characterizing HSF1 regulation using the purified recombinant protein. Our focus was to study HSF1 conformational alterations upon stress using fluorescence based assays along with traditional biochemical techniques to study the effects of protein-protein interactions and various modifications on the trimerization and DNA-binding steps of HSF1 activation.

We were initially interested in studying HSF1 because it was recently shown that the diminished level of Hsp70 expression in aged rat hepatocytes strongly correlates with a decreased ability to recover from stress due to exposure to elevated temperatures, and that this is possibly due to the decreased DNA binding affinity of HSF1 to the Hsp70 promoter (25). Therefore better understanding HSF1 regulation could lead to effective ways to protect aged cells from stress and damage.

In the first part of this chapter, we attempted to recombinantly express and purify monomeric mouse HSF1 in *E. coli*. We then characterized the activity of the isolated protein, measuring its oligomerization status, sensitivity to heat, and DNA binding activity. After several years of work to optimize expression and purification conditions,

we were unable to produce monomeric HSF1 that could be induced to oligomerize and bind DNA upon exposure to stress (ex. heat, oxidation). Rather, purified recombinant HSF1 was trimeric, hexameric, or aggregated to a large species, and constitutively bound DNA containing the HSE. Thus in the second part of this chapter we tried alternate methods of expressing HSF1 such as in reticulocyte lysate and in Sf9 insect cells. In the reticulocyte lysate, other interacting proteins which may keep HSF1 monomeric such as Hsp90 and FKBP52 are present endogenously, and available to interact with HSF1 as it is produced. In the Sf9 cells, the purpose was to coexpress HSF1 with these other proteins in hopes of keeping HSF1 monomeric and soluble. We also wanted to determine which proteins interact with HSF1 under normal, (nonshock (NS)) or heat shocked (HS) conditions by immunoprecipitations in cell lysate with the Sf9 expressed HSF1, and hoped to elucidate what proteins keep HSF1 in an inactive state.

A.2 Materials and Methods

Bacterial Expression and Purification of mHSF1

Mouse HSF1 (accession number X61753) with a GST tag at the N-terminus end and a 6 poly-histidine tag at the C-terminus was overexpressed and purified from BL21(DE3) *E. coli* cells using a plasmid and protocol (22) provided by Dr. Dennis Thiele. Briefly, mHSF1 cloned into a pGEX6p-1 vector was transformed into BL21(DE3) Codon Plus *E. coli* cells. A 1 mL culture of the transformed cells was grown in 2xYT media containing 100 μg/ml ampicillin, and 34 μg/ml chloramphenicol at 37°C overnight. The culture was added to 1L of 2xYT/ amp/chloramphenicol media, and incubated in a 37°C shaker until the OD at 600 nm was 0.7. Fresh antibiotic was added,

and the culture was then cooled on ice for 1h before induction. To induce protein expression, 0.4 mM IPTG was added, and the culture was incubated overnight at 20°C. After spinning the cells down, a 500 mL culture equivalent of cells were respuspended in 20 mL lysis buffer (50 mM Tris pH 8.0, 300 mM NaCl, 20 mM imidazole, 0.05% β-mercaptoethanol, with protease inhibitors (1 mM benzamidine, 1 mM PMSF, 1μg/mL of each aprotinin, leupeptin, and peptstatin)), and sonicated twice for 60 sec at 90% output, 50% duty cycle. Triton X-100 was added to a final concentration of 0.5%, and insoluble celluar debris was removed by centrifugation at 12,000 rpm for 30 min at 4°C. Ni-NTA agarose His affinity beads (Qiagen, Gaithersburg, MD) were washed in lysis buffer, and incubated with the cell lysate for 2 hr at 4°C. Beads were washed with lysis buffer containing 0.5% Triton X-100, and then with lysis buffer without detergent. To remove bound *E. coli* DNAK protein, the beads were washed with ATP solution (20 mM Tris pH 8.0, 20 mM $MgCl_2$, 5 mM ATP, 300 mM NaCl, 2 mM DTT) at room temperature, and then with lysis buffer. HSF1 was then eluted off the beads for 20 min in 0.5 mL of elution buffer (50 mM Tris pH 8.0, 50 mM NaCl, 200 mM imidazole, 0.05% β-mercaptoethanol, with protease inhibitors) at 4°C. Beads were incubated again in another 0.5 mL of elution buffer to remove all HSF1. To further purify the protein, glutathione-agarose beads (Amersham Biosciences, Piscataway, NJ) were washed in GST lysis buffer (20 mM Tris pH 8.0, 300 mM NaCl, 2 mM EDTA, 2 mM DTT, with protease inhibitors). His purified protein was incubated with the beads for 2 hrs at 4°C. Beads were washed with lysis buffer, resuspended in protease buffer (50 mM Tris pH 7.0, 150 mM NaCl, 1 mM EDTA, 1 mM DTT) and the GST tag was cleaved by adding Precission protease (Amersham Biosciences, Piscataway, NJ) for 10 hrs at 4°C. This protease cleaves the

tag, and is captured by the beads. Therefore another step to remove the protease is not needed. DTT was added to yield a final concentration of 2 mM, and glycerol was added to 25% to the final purified HSF1. HSF1 was frozen in liquid N_2 and stored at -80°C.

Determination of oligomerization status

To assess the oligomeric status of the purified protein, HSF1 was chemically crosslinked with the 16.1 Å spacer arm ethylene-glycol-bis-[succinimidylsuccinate] (EGS), a homobifunctional crosslinker that forms bonds between primary amines. HSF1 diluted in PBS was subjected to heat shock at 42˚C for 5 min, or left on ice (NS) before crosslinking with different concentrations of EGS at 20°C for 20 min. Samples were placed on ice, and quenched by addition of glycine at 75 mM for 15 min. 4x reducing SDS loading buffer was added, samples were boiled for 5 min and run on a 6% Tris/Glycine SDS-PAGE gel. Gels were transferred to nitrocellulose membranes, and immunoblotted with a rabbit polyclonal ab2923 αHSF1 antibody (Abcam, Cambridge, MA), and a horseradish peroxidase (HRP) conjugated secondary antibody. HSF1 was visualized by chemiluminescence.

Electrophoretic mobility shifts (EMSA)

DNA binding of purified HSF1 was examined by EMSA using the Light Shift Chemiluminescence EMSA kit (Pierce, Rockford, IL). Either NS HSF1, or HS HSF1 (incubated at 42˚C for 5 min.) was incubated with a biotinylated, 24 bp double stranded piece of DNA (HSE) (b-HSE) containing 4 of the nGAAn repeats. A typical 25 μL binding reaction contained 100 ng-20 μg (70 nM-14 μM) of HSF1, 10 μg BSA, 0.5 μg of

poly[dI-dC] DNA, and 0.1 ng (0.5 nM) b-HSE in EMSA binding buffer (10 mM Tris pH 7.8, 50 mM NaCl, 1 mM EDTA, 0.5 mM DTT, 5% glycerol). After allowing HSF1 to bind the DNA probe for 20 min at RT, the amount of HSF1 bound DNA was determined by a shift in electrophoretic mobility on a 4% Tris-Borate-EDTA polyacrylamide gel. DNA bound by HSF1 has a lower mobility compared to free DNA. After running the gel, DNA was transferred to a positively charged nylon membrane (Sigma-Aldrich, St. Louis, MO). The position of HSE DNA on the membrane was determined by probing the membrane with HRP conjugated streptavidin and measuring chemiluminescence. For competition samples, non biotinylated HSE was preincubated with HSF1 for 20 min at a before addition of b-HSE. Different methods of detection such as using autoradiography with a ^{32}P labeled HSE or in-gel fluorescence with a fluorescently labeled HSE were also used.

Fluorescent Labeling and Single Molecule Spectroscopy

HSF1 was labeled using the cysteine reactive dye, Alexafluor 488 maleimide (Molecular Probes). Because HSF1 contains 5 Cys residues, the protein was underlabeled to try and get singly labeled protein. Briefly, GST-HSF1 bound to glutathione-agarose beads was incubated with the dye at a 1:20 molar ratio in PBS at RT on a shaker for 2 hrs. Beads were washed with PBS, and the GST tag was cleaved with 5 units of biotninylated thrombin for 1.5 hrs at RT. Thrombin was removed by incubating with streptavidin-agarose beads (Novagen, Gibbstown, NJ) for 30 min at RT. Running this labeled protein on a native gel showed that the labeled protein was a monomer, EMSA also showed the same activity as unlabeled.

For single molecule experiments, molecules were trapped at very dilute concentrations in a thin layer of agarose gel. 12 pmol of NS or HS (incubated at 42˚C for 5 min) Alexa488-HSF1 was diluted in 200 μL of 0.1% agarose in PBS containing 200 mM NaCl, and spincoated onto a quartz coverslip. Individual molecules on the slide were excited by a Ti-Saph laser beam at 450 nm, and the fluorescence was viewed in real-time by a CCD camera. For photobleaching traces, fluorescence was measured with an avalanche photodiode (APD).

A.2.5 *In vitro* transcription translation

Mouse HSF1 cloned into the pGEM1 vector was a gift from Dr. Kevin Sarge at the University of Kentucky. This vector contains a T7 promoter. mHSF1 was transcribed and translated using a rabbit reticulocyte lysate TNT Quick Coupled *in vitro* transcription and translation kit (Promega, Madison, WI). A total reaction volume of 50 μL contained 40 μL of master mix (reticulocyte lysate), 1 μL of 1 mM Methionine, and 45 ng of the pGEX-2T mHSF1 plasmid DNA. The reaction was incubated at 30˚C for 2 hrs, and frozen at -80˚C.

Baculovirus expression of HSF1 in Sf9 cells

Bacmid preparation

To express mHSF1 in Sf9 insect cells, the Bac-to-Bac Baculovirus expression system (Invitrogen, Carlsbad, CA). mHSF1 was cloned from the pGEX6p-1 mHSF1 construct, using primers that added either a $(His)_6$ or FLAG tag to the C-terminus of

HSF1. The forward primer for both His-HSF1 and FLAG-HSF1, 5' GCGAATTCATGGATCTGGC 3' added a 5' EcoRI restriction site. For the FLAG tagged HSF1, the reverse primer was 5' ACC TCG AGT CAC TTG TCA TCA TCG TCC TTG TAG TCG GAG ACA GTG GGG TC 3', introducing a 3' XhoI site after the HSF1 sequence. For the $(His)_6$ tagged HSF1, the reverse primer was identical, except containing the sequence for 6-His residues in place of the FLAG tag. After PCR amplification with vent polymerase, the HSF1 sequence was ligated into a pFastBac (pFB) plasmid (Invitrogen, Carlsbad, CA) at the EcoRI and XhoI sites. pFB-mHSF1-FLAG or pFB-mHSF1-$(His)_6$ was transformed by heat shock into DH10Bac bacterial cells which contain viral genes (ex. polyhedrin) in the genome with transposable elements. Once pFB-mHSF1 is in the DH10Bac bacterial cell, the plasmid recombines with these endogenous elements, creating a plasmid, called a bacmid, which can be transfected into Sf9 cells to produce baculovirus containing the HSF1 gene. Transformed DH10Bac cells were plated onto LB plates containing 7 μg/mL gentamycin, 50 μg/mL kanamycin, and 10 μg/mL tetracycline, with freshly applied BluoGal (Invitrogen, Carlsbad, CA) (similar to X-Gal). Cells were incubated for 2 days at 37˚C, and white colonies (indicative of a successfully recombined bacmid due to disruption of the LacZ gene on pFB upon recombination in the DH10Bac cells) were selected, and replated on fresh plate overnight. Colonies were selected, and grown up in 2 mL cultures for miniprep bacmid isolation.

To isolate the bacmid, cells were spun down, and resuspended in 300 μL TE8 buffer (10 mM Tris pH 8.0, 1 mM EDTA) containing 0.1 mg/mL RNaseA. 300 μL of

0.2 N NaOH and 1% SDS was added, and incubated at RT for 5 min. 300 μL of 3 M potassium acetate pH 5.5 was slowly added and incubated on ice for 10 min, and centrifuged at maximum speed for 10 min. 800 μL of isoproanol was added to the supernatant, incubated on ice for 10 min, and centrifuged for 15 min at RT. The supernatant was removed, and 0.5 mL of 70% cold ethanol (-20˚C) was added. After inversion, the DNA was spun down at maximum speed for 5 min at RT. The ethanol was removed, and the DNA pellet was allowed to air dry in the hood, and resuspended in 40 μL of sterile TE8 buffer.

Transfection of Sf9 Cells

Sf9 cells were seeded at $1x10^6$ cells per well in Sf-900 II serum free media (Invitrogen, Carlsbad, CA) in a 6 well plate, and incubated for 1 h at 27˚C to allow the cells to adhere. 5 μL of the HSF1 bacmid DNA was diluted into 100 μL of media. In a separate tube, 6 μL of Cellfectin (Invitrogen, Carlsbad, CA) was diluted into 100 μL of media, and allowed to sit for 2 min. The diluted bacmid was added to the cellfectin, and incubated in the hood at RT for 45 min. Cells were then rinsed with media, and 800 μL of fresh media was added to each well. The bacmid/cellfectin mixture was added to the cells dropwise, and incubated at 27˚C for 4 hrs. 1 mL of media containing 4% fetal bovine serum was added, and cells were incubated at 27˚C for 5 days.

Harvesting Baculovirus and Cytosolic/Nuclear Extract Preparation

Cells were detached from plate by pipetting. The cells were spun down at 730xg for 5 min at RT, and the supernatant containing the baculovirus was saved on ice (can

save for months at 4˚C). Cell pellet was washed two times with 1 mL of cold TBS (10 mM Tris pH 7.5, 150 mM NaCl), and spun at 730xg. Resuspended cells in 200 μL (per 6 wells) of ice cold Buffer A (10 mM HEPES pH 7.9, 10 mM KCl, 0.1 mM EDTA, 0.1 mM EGTA, 0.1 mM DTT, 0.5 mM PMSF), and swelled cells on ice for 15 min. To lyse cells further, 0.05% NP40 was added, and the solution was vortexed. The nuclear fraction was spun down for 30 sec at 35,000 rpm. The supernatant contained the cytosolic extract. The nuclear pellet was resuspended in 25 μL of 20 mM HEPES pH 7.9, 400 mM KCl, 1 mM EDTA, 1 mM EGTA, 10 % glycerol, 0.1 mM DTT, and 0.1 mM PMSF. This was incubated on ice for 15 min, and the nuclear debris was spun down at 25,000 rpm for 10 min at 4˚C. To determine the optimal titer and time of infection for HSF1 expression, incubated Sf9 cells with various concentrations of baculovirus for various time points, and checked protein expression levels.

A.2.7 Reconstitution/immunoprecipitation of Hsp90-HSF1 complex

To determine whether HSF1 expressed in *E. coli* or Sf9 cells could interact with the Hsp90 chaperone complex, 0.25 mg/mL of HSF1 in 20 mM Tris pH 8.0, 2 mM EDTA, 150 mM NaCl, 2 mM DTT, 25 % glycerol was centrifuged at 100,000 x g to remove aggregated protein for 30 min. 100 μL of the supernatant was diluted to 300 μL in TENa300 buffer (10 mM TES pH 7.6, 50 mM NaCl, 4 mM EDTA). HSF1 was incubated at 0.15 mg/mL with 5 μL rabbit reticulocyte lysate (RL) (Green Hectares, Oregon, WI), and an ATP-regenerating system (ARS) (50 mM ATP, 250 mM creatine phosphate, 20 mM magnesium acetate, and 100 units/ml creatine phosphokinase) at a

total volume of 50 μL in TENa300 with 100 μM PMSF, and a Complete mini protease inhibitor tablet (Roche, Indianapolis, IN) for 20 min at 30˚C. 0.1 mg/mL of nonimmune IgG, or 0.1 mg/mL rat aHSF1 O.N.318 antibody and 70 mL of a 20% slurry of protein-A-sepharose was added to a total volume of 300 μL in TENa300, and incubated at 4˚C for 1.5h on a rotator. Beads were washed 4 times with TEGM buffer (10 mM TES, pH 7.6, 50 mM NaCl, 4 mM EDTA, 10% glycerol, 20 mM sodium molybdate). Beads were boiled in SDS-PAGE loading buffer, and run on a SDS-PAGE gel, transferred to a PVDF membrane, and probed with antibodies against Hsp90 (AC88), Hsp70 (N27F3-4), FKBP52 (UPJ30), and CyP40 (PA3-022), and HSF1(ab2923).

A.3 Results and Discussion

A.3.1 Purification and characterization of recombinant mHSF1

In order to eventually study endogenous HSF1 activity at the single molecule level, initial work focused on developing these fluorescence techniques using recombinant mouse HSF1 overexpressed in and purified from *E. coli*. A previous study done by Ahn and Thiele (22) demonstrated that monomeric HSF1 (with no DNA binding activity) can be obtained in this manner, and that these monomers can be induced by exposure to heat shock to form trimers (or higher order oligomers) capable of binding DNA. Following the published protocol (22) we were able to express and purify mHSF1 to a high degree of purity. To assess the oligomeric status of the purified protein, HSF1 was crosslinked with EGS, a crosslinker that forms bonds between primary amines with a 16.1 Å spacer arm. HSF1 was subjected to heat shock at 42˚C for 5 min (HS), or left on ice (NS) before crosslinking with different concentrations of EGS. Initially, even

without exposure to HS, the majority of HSF1 molecules were found to crosslink as trimers and higher order oligomers (figure 2a). Upon exposure to HS, no significant change in the proportion of monomer to trimer was seen at intermediate crosslinker concentrations. However at high EGS, HS HSF1 appears to be a very large species (aggregate), unable to enter the gel. No significant differences were seen at higher or lower HS temperatures, shorter or longer HS times, and different buffer conditions such as salt concentration and pH (data not shown). The presence of trimers and larger oligomers and aggregates prior to HS was confirmed through native gel electrophoresis as well as gel filtration and light scattering experiments (figure 2b).

In order to optimize the procedure to get active monomeric HSF1, an extensive number of factors were varied including culture growth/induction temperatures and times, *E. coli* cell lines, cell lysis methods and conditions, and compositions of the various buffers used at each step of the protocol. Finally, a different plasmid was provided by Dr. Kevin Sarge (University of Kentucky) containing only an N-terminal GST tag. Using this plasmid, the same problems were encountered. Eventually, a complex set of conditions was identified using this plasmid (lowering the growth and induction temperature to 20˚C, lowering the amount of gene expression, lysing the cells by sonication for less than 10 seconds at the lowest power output setting, increasing NaCl to 200 mM, and increasing glycerol to 10%) that yielded HSF1 that crosslinked less under NS conditions (figure 2a). The purified protein ran as a single band at the expected position of the monomer on a native gel detected by western blotting against HSF1. Upon exposure to HS, trimers and very large oligomers or aggregates (likely denatured protein)

could be seen after crosslinking. The intensity of the monomeric band on native gels also decreased significantly, and a new band appeared at the position corresponding to 600 kDa (figure 2b). Although these experiments confirm that oligomerization can be induced by HS *in vitro*, it did not show whether or not the oligomeric species are active.

To determine whether the oligomeric HSF1 species are active species, DNA binding of the purified HSF1 was examined by EMSA. Either NS HSF1, or HS HSF1 (42˚C, 5 min) was incubated with a biotinylated, 24 bp double stranded piece of DNA (HSE) containing 4 of the nGAAn repeats, and run on a TBE-polyacrylamide gel as done before (22, 24). DNA bound by HSF1 has a lower mobility compared to free DNA. Surprisingly, the amount of HSF1 bound HSE DNA in the NS samples was several times greater than that in the HS samples. In fact, HS appeared to consistently abolish DNA binding (figure 2c). Because these results are in contradiction with previous work (22,24), several conditions of the assay were varied such as HS temperature, length of HS, exposure to a different stress (ex. H_2O_2), pH of the binding buffer, composition of the binding mixture (ex. buffer base, salt concentration, nonspecific DNA competitors), and binding reaction temperature. Different molar ratios of HSF1 to DNA were also tried. Lastly, different methods of detection such as autoradiography with a ^{32}P labeled HSE or in-gel fluorescence with a fluorescently labeled HSE were attempted. None of these made a significant difference in the results. For controls, DNA probes with only 3 or 2 nGAAn repeats were also tested. Previous work has shown that HSF1 requires at least 3 nGAAn repeats for binding (5). For the 3 repeat DNA, NS samples still bound more than HS, but the amount of binding for both were less than that of the 4 repeat DNA, and as

expected no binding was seen for the 2 repeat DNA. The signal from the HSF1-DNA shifted complex could be competed away with unlabeled HSE DNA, but not by a non HSE containing oligo, demonstrating that this binding is specific (data not shown).

One possible explanation for these results is although crosslinking and native gel experiments showed mostly monomeric HSF1, there actually are active (DNA-binding) trimers present in these preps and EMSA has a lower detection limit. Although the former experiments show that HS promotes oligomerization, these could actually be inactive aggregates of denatured protein. In an attempt to remove any preformed trimers, purified protein was passed through either a 100 kDa cut off centricon filter, or a gel filtration or anion exchange column which eliminated any oligomers present. A DNA-affinity column was also made with the same HSE DNA fragment to remove DNA-binding protein from the NS sample. Even after these steps, a significant amount of constitutive DNA binding was seen which was further diminished by HS. Lastly, to eliminate the possibility of differential processing and modification in *E. coli*, a different source of recombinant HSF1 was tried. HSF1 was in vitro transcribed and translated in rabbit reticulocyte lysate (RL). While there did seem to be a slight increase in DNA binding for RL generated HSF1, there was still a significant amount of binding without heat shock (data not shown).

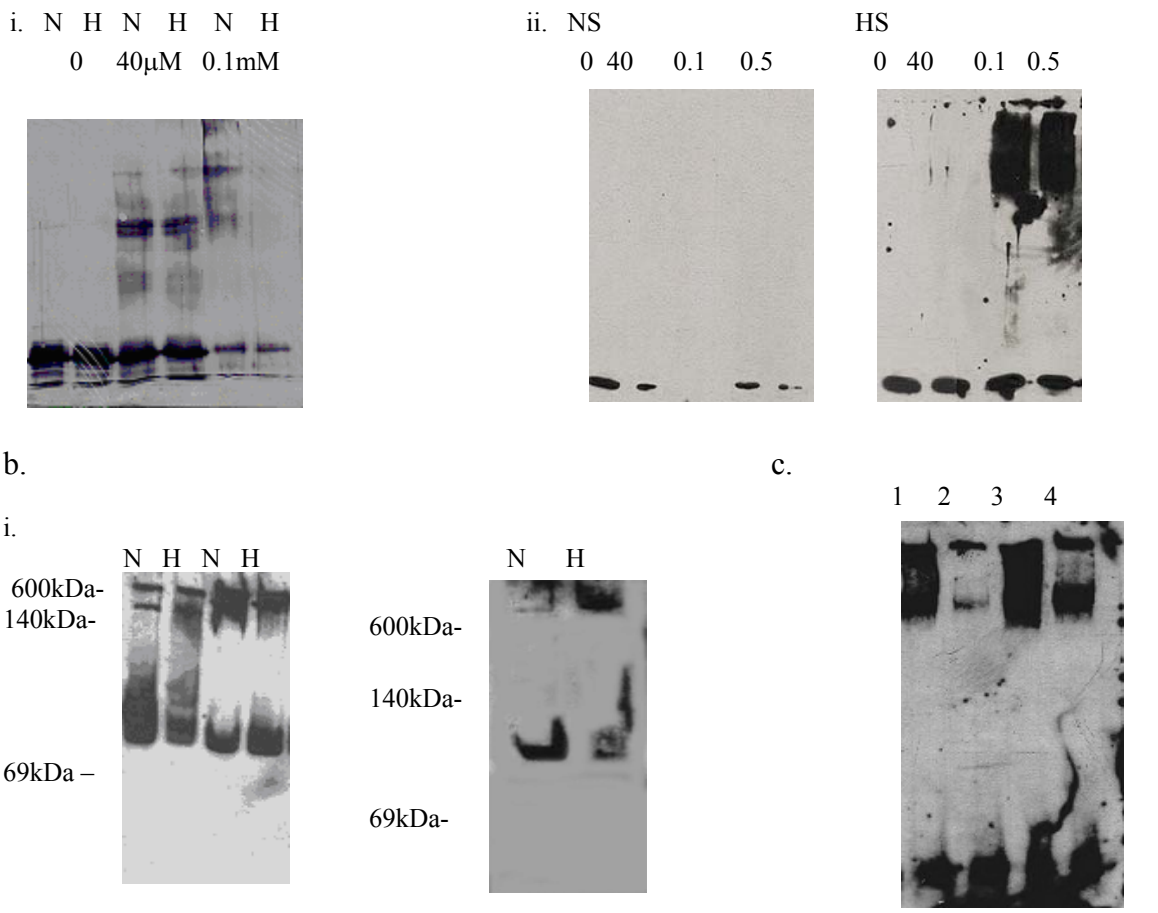

Figure 2: (a) NS (N) and HS (H) (42˚C, 5min.) different samples of initial preps (i) or optimized preps (ii) of HSF1 were crosslinked with the indicated concentrations of EGS, and detected by western blotting for HSF1. (b) Native gels of two initial (i) and final (ii) preps detected by western blotting with an αHSF1 antibody. (c) EMSA of NS or HS HSF1 binding to a biotinylated HSE probe. Complexes were resolved on a 4% 0.5xTBE, transferred to a membrane and detected with HRP-streptavidin. Lanes 3-4 contained twice the amount of HSF1 as 1-2.

It is widely accepted that HSF1 only binds DNA as a trimer *in vivo* (30, 2, 5, 7, 8, 23) but only two papers (22, 24) have demonstrated that trimerization and subsequent DNA binding of recombinant HSF1 can be heat induced *in vitro*. From these results, we conclude that HSF1 is not monomeric in the purified state, and cannot be induced *in vitro* to form an active DNA binding trimer by direct exposure to heat. A few groups propose

that Hsp90 and/or Hsp70 and the cochaperones, FKBP52 and p23 play an important role in regulating HSF1 trimerization and DNA binding (4, 26). Thus from these experiments, a possible explanation for the observed results is that the HSF1 monomer may form a trimer and bind DNA in the absence of HS *in vitro* because of the absence of these regulators. However, *in vivo,* interactions with the chaperone complex hold HSF1 in a monomeric state, preventing trimerization and DNA binding. This questions the validity of studying HSF1 in a purified *in vitro* system.

A.3.2 Single molecule fluorescence imaging of HSF1

Single molecule fluorescence spectroscopy (SMFS) allows us to observe and analyze individual molecules, without the loss of information due to averaging in the ensemble. In our setup HSF1 molecules were trapped at very dilute concentrations in a thin layer of agarose gel on a quartz coverslip, and the fluorescence of the individual molecules was measured. Monomers can be distinguished from trimers and larger oligomers by following the fluorescence time trace for photobleaching steps. A single monomer labeled with only one dye will display a single photobleaching step, whereas a trimer with three dyes will show three steps (figure 3b). Our end goal was to measure trimerization and DNA binding affinity using SMFS.

A488 labeled NS recombinant 'monomeric' mHSF1 was viewed under the single molecule fluorescent microscope in preliminary studies. 12 picomoles of A488-HSF1 caged in agarose was coated onto a coverslip, and excited at 450nm. Individual

molecules could be detected (figure 3a). Following the intensity of individual spots over time revealed that the majority had a single photobleaching step, confirming the fact that these were monomeric. An aliquot of the same protein was subjected to HS at 42˚C for 5 min. as done for the EMSA, caged in agarose, and viewed similarly. The results revealed the presence of huge protein species (most likely aggregates) several orders of magnitude larger than a trimer (figure 3a) with several photobleaching steps (figure 3b). This helps explain the aberrant EMSA results, demonstrating that *in vitro* HS resulted in inactive aggregates.

a. i. ii.

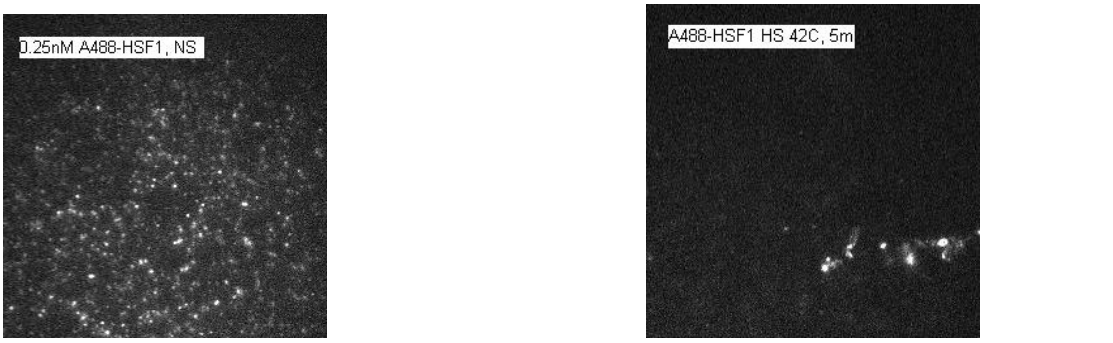

b. i. ii.

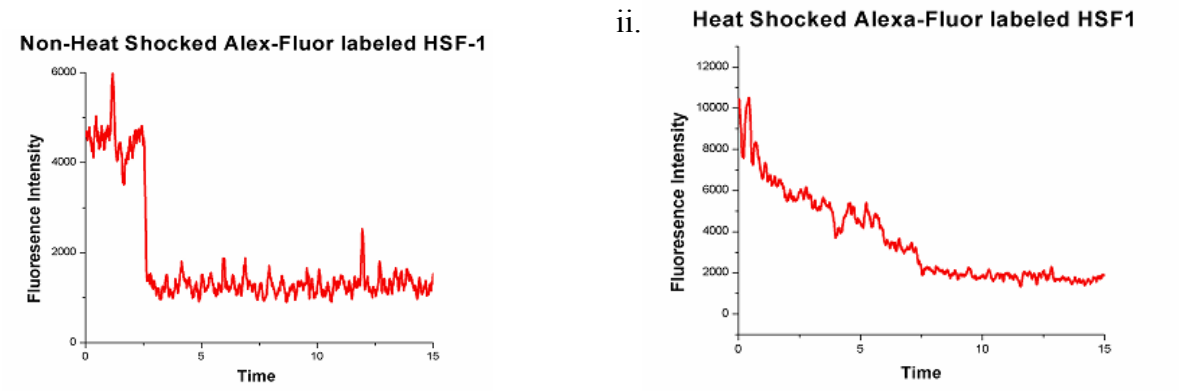

Figure 3: (a) i. NS A488 labeled HSF1 that appeared monomeric on native gels as viewed under a confocal single molecule fluorescence microscope. Each individual bright spot represents a single monomer. ii. The same A488 HSF1 was HS before caging in agarose. Large oligomers or aggregates are seen. (b) i. Fluorescence time trace of a single spot of the NS sample showed a single photobleaching step, whereas multiple indiscriminate steps are seen in the HS sample ii. (time traces done by Brender, J)

A.3.3 Reconstitution of HSF1/Hsp90 chaperone complex

To determine whether the reason why purified recombinant HSF1 is constitutively trimerized and able to bind DNA without HS is because of the absence of other regulatory proteins (figure 4a.), the Hsp90 complex was reconstituted *in vitro*. Transcriptional regulation by the same foldosome complex has been seen in the steroid receptors (27). In collaboration with Dr. Bill Pratt and Dr. Yoshihiro Morishima (University of Michigan), similar techniques published for assembling the Hsp90 complex on the glucocorticoid receptor (GR) were used for HSF1. To first determine whether the chaperones can interact with recombinant HSF1 produced in *E. coli,* HSF1 was immunoadsorbed onto sepharose beads either by α-HSF1 or α-GST antibodies, and incubated with rabbit reticulocyte lysate (RL)-which contains a high concentration of chaperone components. The pulled down complex was analyzed by western blotting for the presence of each of the components previously found to interact with the GR: (Hsp90, FKBP52, Cyp40, and Hsp70).

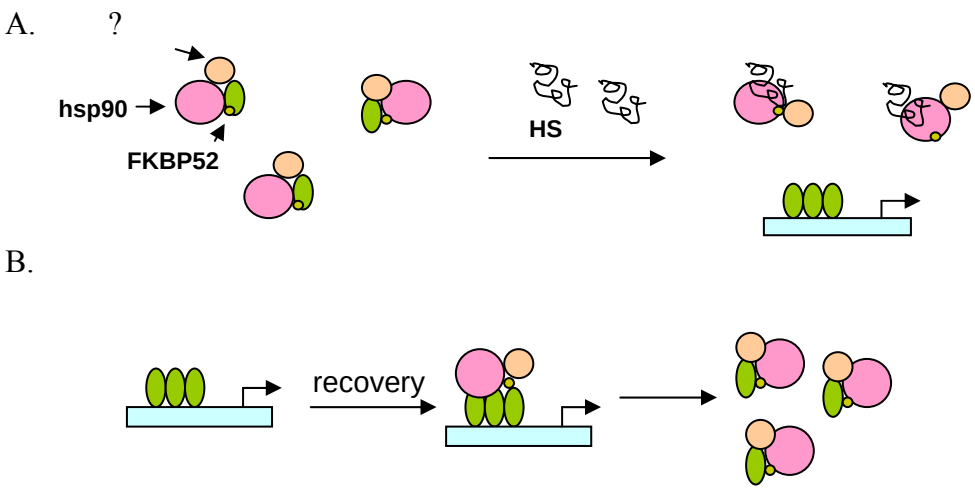

Figure 4: (a) Possible mechanism of the hsp90 chaperone complex regulation of HSF1 trimerization and DNA binding. Under normal conditions HSF1 is kept monomeric by interactions with the hsp90 complex. Upon HS, hsp90 binds unfolded and denatured proteins damaged by the stress, releasing HSF1 and allowing it to trimerize and bind DNA. (b) Another possible function of the hsp90 complex is in attenuation of HSF1 activity after HS. During the recovery stage, trimeric HSF1 may be disassembled by the chaperone complex through unfolding or remodeling.

We found that HSF1 would adsorb to both nonimmune and immune (specific for HSF1 or the GST tag) antibodies bound to sepharose beads equally well. The presence of aggregates in the purified HSF1 was found to be a contributing factor in this nonspecificity. Removing these aggregates by ultracentrifugation or by detergent solubilization (NP40) reduced nonspecific binding slightly, but there was still a significant amount of nonspecific binding. This was most likely due to the formation of new aggregates in solution during the time it takes to immunoadsorb HSF1.

Because of these problems, we tried adding in the chaperone machinery in the form of RL along with an ATP regenerating system (ARS) to see whether these aggregates and non-functional higher order oligomers could be pulled apart to a functional form by the chaperones prior to immunoadsorption. This technique also

allows for the simultaneous coimmunoprecipitation of the Hsp90 complex components that may interact with HSF1. Pre-incubation with RL decreased the amount of aggregated HSF1 as detected by ultracentrifugation and slightly improved the specificity of HSF1 immunoprecipitation. However when the pulled down proteins were analyzed for the presence of the Hsp90 complex components: Hsp90, Hsp70, FKBP52, CyP40, the only component detected was Hsp70 (which has an affinity for denatured or aggregated proteins) (figure 5). It has been shown that Hsp90 and FKBP52 can be coimmunoprecipitated with HSF1 in cell lysate (26). Therefore, either the complex is not stable in these binding conditions, or recombinant HSF1 is somehow folded or processed differently making it nonfunctional.

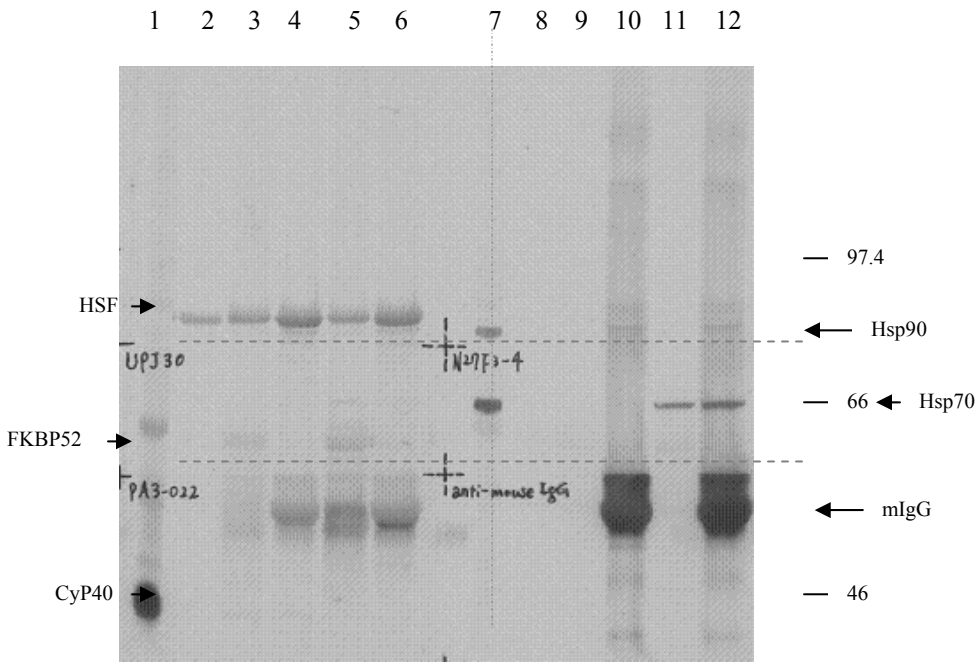

Figure 5: Preincubation of GST-HSF1 with rabbit RL to determine whether the Hsp90 complex can dissociate HSF1 oligomers and aggregates to a functional form, and whether these components coimmunoprecipitate with HSF1. Samples were western blotted by cutting the membrane, and probing with antibodies against Hsp90, Hsp70, HSF1, Cyp40, and FKBP52. Lanes: 1, 7: RL, 2, 8: GST-HSF1. GST-HSF1 was pre-incubated with either binding buffer (lanes 3, 4, 9, 10), or RL (lanes 5, 6, 11, 12) and ARS at 30ºC for 20min. and immunoadsorbed to protein G sepharose beads with either a control nonimmune rat IgG (lanes 3, 9, 5, 11) or an αGST antibody (lanes 4, 10, 6, 12) . (Morishima, Y.)

Since there was an improvement in the ability to immunoprecipitate recombinant HSF1 after incubation with RL and ARS, corresponding most likely to a decrease in aggregation, the same preincubation step with RL was done prior to submitting the sample to an EMSA. This was to see whether the possible decrease in aggregation and nonfunctional oligomers also translated into decreased DNA binding activity before HS. If the complex was successfully reconstituted and can dissociate the trimer and aggregates, one would expect DNA binding under NS conditions to be diminished in the RL incubated samples relative to the unincubated samples. Taking the samples incubated

with RL and subjecting them to HS would then restore DNA binding activity to a greater or equal level as before incubation. These experiments were done, comparing recombinant HSF1, recombinant HSF1 preincubated with RL with an ATP source, and recombinant HSF1 preincubated with RL without an ATP source (as a control since Hsp90 and Hsp70 require ATP for remodeling activity) (figure 6).

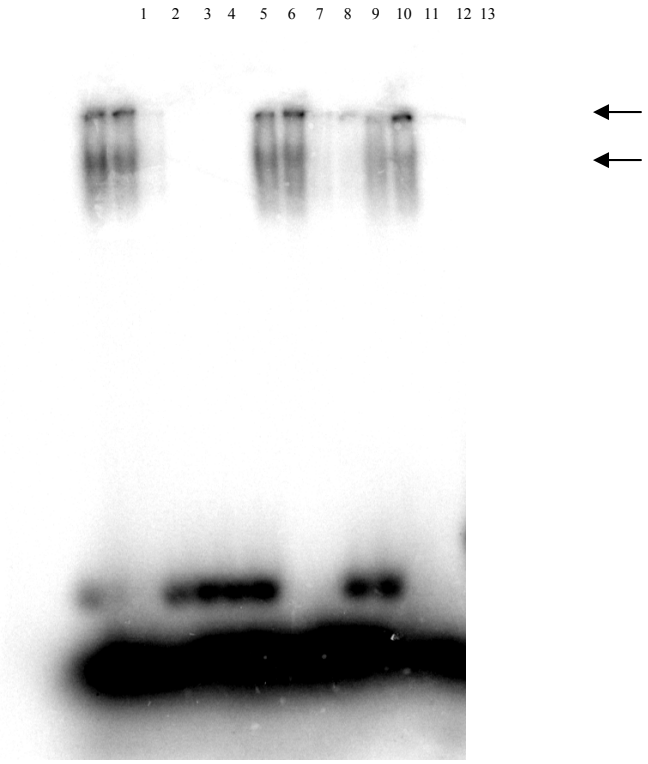

Figure 6: Preincubation of recombinant HSF1 with RL to determine whether the Hsp90 complex can dissociate preformed DNA binding trimers and unfunctional aggregates of HSF1 to a non DNA binding monomer, and whether this dissociated HSF1 product can be re-induced by HS to bind DNA. HSF1 was preincubated with RL and an ATP regenerating system at 30ºC for 20 min. For HS samples, this mixture was then incubated at 42ºC for 5 min. The mixture of HSF1 and RL was incubated with ^{32}P-HSE DNA at 25º C for 20 min. Samples were run on a native 4% 0.5XTBE gel, and imaged by autoradiography. Free HSE only (lane 1), rHSF1: NS (lane 2), HS (lane 3), NS+ unlabeled HSE competitor (C) (lane4), RL without HSF1: NS (lane 5), HS (lane 6), NS+ C (lane 7), HSF1 preincubated with RL+ARS: NS (lane 8), HS (lane 9), NS+C (lane 10), HS+C (lane 11), HSF1 preincubated with RL –ARS: NS (lane12), HS (lane 13). Top arrow: possibly aggregated HSF1 bound to DNA that was too large to enter gel. Lower arrow: bound trimeric HSF1.

Preincubation with RL, and HS in the presence of RL did not appear to make a significant difference in DNA binding activity of recombinant HSF1. A slight increase in the levels of DNA binding after HS in the preincubated samples could be seen. Also, in the no ATP control samples, very little binding was seen before HS, and a more intense upper band corresponding to aggregates appeared after HS. This suggests that some component in the RL (that requires ATP) may protect the rHSF1, shielding it from aggregation upon HS *in vitro.* Although some effects are seen upon reconstitution of the chaperone machinery *in vitro*, the effects are very small. No detectable complex could be found of HSF1 with Hsp90, FKBP52, or any of the other components that have been shown to coimmunoprecipitate with HSF1 *in vivo*. These results confirm the findings from the initial experiments-- that is, recombinant HSF1 expressed in *E. coli* does not function as it does *in vivo*.

Since recombinant HSF1 behaves differently in the purified system than *in vivo* possibly because HSF1 may be folded or modified differently in *E. coli* versus in the mammalian cell an expression system which more closely mimics the mammalian cell folding and modification processes such as the baculovirus/Sf9 insect cell system was used. Since no significant difference was seen previously when aggregated and trimerized HSF1 was incubated with the Hsp90 complex, adding the Hsp90 chaperone machinery after HSF1 has already aggregated or trimerized in *E. coli* might be too late. HSF1 may need Hsp90 and the cochaperones present immediately as it is being synthesized and folded by the cell to function properly. Sf9 endogenous Hsp70 and Hsp90 have been shown to interact with mammalian glucocorticoid receptor (GR) when

GR is overexpressed in this system. Therefore the baculovirus system would provide chaperones to interact with as HSF1 is being translated, possibly preventing HSF1 from trimerizing and aggregating when it is produced. The insect Hsp90 complex can then be stripped off by incubation at high ionic strength (0.5 M NaCl), and reconstituted with mammalian Hsp90 from RL. The Sf9 system also allows for the possibility of coexpressing HSF1 along with mammalian forms of the Hsp90 chaperone complex.

mHSF1 with a C-terminal FLAG or His_6 tag was cloned into a bacmid, and baculovirus stock containing this HSF1 gene was produced. The His_6 tagged HSF1 was to be used for purification of HSF1 from Sf9 insect cells, and the FLAG tagged HSF1 was used for immunoadsorption studies as discussed above. Mouse GR produced in the Sf9 cells pulled down insect Hsp90 and insect Hsp70 when immunoadsorbed, and could be reconstituted with rabbit Hsp90 and Hsp70 upon incubation with RL after stripping GR of the insect chaperones (figure 7). In contrast, HSF1 did not pull down insect Hsp90 or Hsp70, and the Sf9 lysate containing the expressed HSF1 bound DNA without exposure to stress (figure 8). Also a significant amount of FLAG-HSF1 was precipitated when the Sf9 cytosolic fraction was spun at 100,000xg revealing a significant fraction of aggregated protein. Furthermore, after FLAG-HSF1 was immunoadsorbed onto M2 αFLAG antibody conjugated agarose beads, stripped of any insect chaperones, and incubated in RL with an ARS, no rabbit Hsp90 was pulled down (only rabbit Hsp70 as with the bacterially produced HSF1 discussed above) (figure 8). Interestingly, FLAG-HSF1 ran as a long smear on an SDS-PAGE gel with several bands upon probing with αHSF1 antibodies, suggesting that the protein is degraded or unstable in Sf9 cells (figure

9). Therefore we found again that HSF1 can not be overexpressed even in a more mammalian like system, and the insect chaperones could not interact with mHSF1 and could not prevent it from oligomerizing and aggregating in the cell.

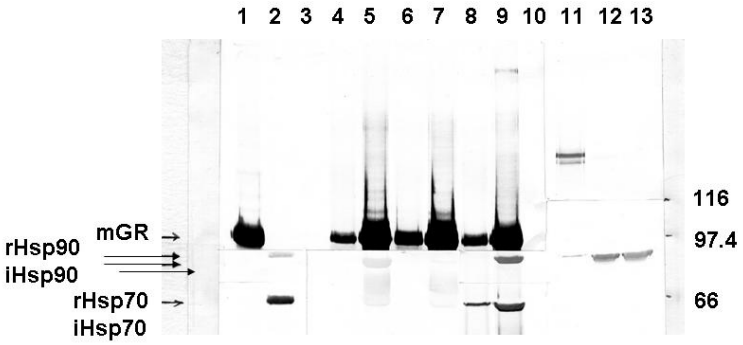

Figure 7: mGR was immunoadsorbed from cytosol from Sf9 cells overexpressing mouse GR, and stripped of insect chaperone proteins with 0.5M NaCl and incubated with RL in the presence of an ARS. Unlike immunoadsorbed HSF1 expressed in Sf9 cells, GR pulled down rabbit Hsp90 and Hsp70. Different portions of the blot were probed with different antibodies and reassembled in the figure. Lanes: 1- mGR-Sf9 cytosol, 2- rabbit RL, 3- nonimmune (NI) adsorbed GR, 4- immune (I) adsorbed GR, 5- NI adsorbed GR stripped of insect chaperones 6-I adsorbed GR stripped of insect chaperones, 7-NI adsorbed and stripped GR incubated with rabbit RL, 8- I adsorbed and stripped GR incubated with rabbit RL. (Morishima, Y.)

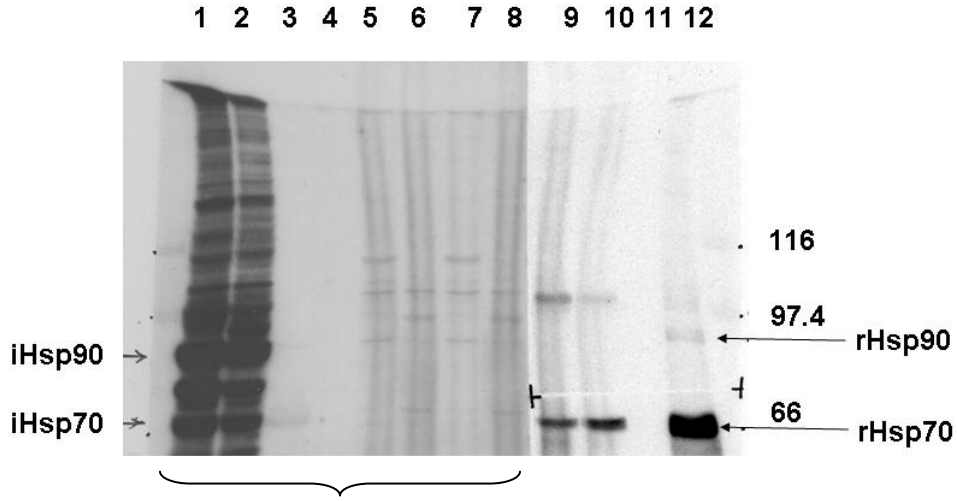

Figure 8: FLAG-mHSF1 was immunoadsorbed from cytosol from Sf9 cells overexpressing mHSF1, and stripped of insect chaperone proteins with 0.5M NaCl and incubated with RL in the presence of an ARS. Immunoadsorbed FLAG-HSF1 expressed in Sf9 cells did not pull down rabbit Hsp90, but did pull down rabbit Hsp70. Different portions of the blot were probed with different antibodies and reassembled in the figure. Lanes: 1- Sf9 cytosol (C-sf9), 2- Sf9 cytosol expressing FLAG-HSF1 (H-sf9), 3- purified recombinant HSF1, 5- C-sf9 immunoadsorbed with α-FLAG antibody, 6- H-sf9 immunoadsorbed with α-FLAG antibody, 7- C-sf9 8-H-sf9 immnunoadsorbed and stripped of insect chaperones, 9- immunoadsorbed C-sf9 or 10- H-sf9 stripped and reconstituted in rabbit RL of insect chaperones. (Morishima, Y.)

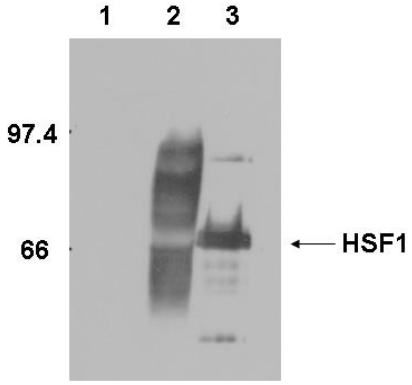

Figure 9: FLAG-HSF1 expressed in Sf9 cells resulted in a long smear on an SDS-PAGE gel when probed with an αHSF1 antibody. Lanes: 1- control Sf9 cytosol, 2- FLAG-HSF1 Sf9 cytosol, 3-recombinantly expressed purified HSF1. (Morishima, Y.)

A.4 Conclusions

An exhaustive amount of work was done using recombinantly expressed HSF1, yet it was not possible to observe heat inducible DNA binding of the purified protein.

Although different growth conditions, purification conditions, assay conditions, and expression systems were tested extensively, monomeric HSF1 could not be obtained. Unlike what has been published (22), the recombinant HSF1 was not a monomer, and could bind DNA even without exposure to heat stress. HS appeared to inactivate HSF1, and decrease DNA binding due to the formation of inactive aggregates. Bacterially produced HSF1 could not interact with the Hsp90 chaperone complex which is known to interact with HSF1 *in vivo*. Switching to a more mammalian-like Sf9 insect cell expression system still resulted in significant aggregation of HSF1, and DNA binding ability without HS. Even with the presence of insect chaperones during HSF1 production, HSF1 was not inhibited from forming trimers and aggregates, attempts to reconstitute Sf9 expressed HSF1 with the rabbit Hsp90 chaperone complex from RL failed to coimmunoprecipitate any of the chaperone complex except for Hsp70 which is known to bind nonspecifically to aggregated proteins. Thus HSF1 does not behave the same *in vitro* in the purified form as it does *in vivo*. Studies have shown that *in vivo* HSF1 binds to several other proteins including Hsp90 and the cochaperones. It has been proposed that these proteins hold HSF1 in the monomeric state, blocking the trimerization domains and preventing the monomers from binding to each other. However, when unfolded proteins are present such as under cellular stress, the Hsp90 releases HSF1 and binds to these unfolded proteins instead, freeing the HSF1 monomer to interact with other monomers and oligomerize to form a DNA binding trimer that can activate transcription.

Studying HSF1 regulation in the purified state *in vitro* is therefore very complicated, and difficult. Thus, purifying endogenous HSF1 from hepatocytes to study heat inducibility of HSF1 activity is not a logical step since HSF1 cannot function alone. Lastly, since attempts to reconstitute the system *in vitro* did not change the activity of HSF1 significantly, work on mHSF1 regulation should be done with endogenously expressed protein where the mammalian chaperones are present at sufficient relative concentrations to keep HSF1 inactive under nonstress conditions.

APPENDIX REFERENCES

1. Zuo, J., Rungger, D., Voellmy, R. (1995) Multiple layers of regulation of human heat shock transcription factor 1. *Mol. and Cell. Biol.* 15, 4319-4330.

2. Morimoto, R., Tissieres, A., Georgopoulos, C. (1984) The Biology of Heat Shock Proteins and Molecular Chaperones. Cold Spring Harbor Laboratory Press, NY.

3. Shi, Y., Kroeger, P., Morimoto, R. (1995) The carboxyl-terminal transactivation domain of heat shock factor 1 is negatively regulated and stress responsive. *Mol. and Cell. Biol.* 15, 4309-4318.

4. Morimoto, R. (1998) Regulation of the heat shock transcriptional response: cross talk between a family of heat shock factors, molecular chaperones, and negative regulators. *Genes & Dev.* 12, 3788-3796.

5. Perisic, O., Xiao, H., Lis, J. (1989) Stable binding of Drosophila heat shock factor to head-to-head and tail-to-tail repeats of a conserved 5 bp recognition unit. *Cell* 59, 797-806.

6. Harrison, C., Bohm, A., Nelson, C. (1994) Crystal structure of the DNA binding domain of the heat shock transcription factor. *Science* 263, 224-227.

7. Peteranderl, R., Rabenstein, M., Shin, Y., Liu, C., Wemmer, D., King, D., Nelson, H. (1999) Biochemical and biophysical characterization of the trimerization domain from the heat shock transcription factor. *Biochemistry* 38, 3559-3569.

8. Zuo, J., Baler, R., Dahl, G., Voellmy, R. (1994) Activation of the DNA-binding ability of human heat shock transcription factor 1 may involve the transition from an intramolecular to an intermolecular triple-stranded coiled-coil structure. *Mol. and Cell. Biol.* 14, 7557-7568.

9. Farkas, T., Kutskova, Y., Zimarino, V. (1998) Intramolecular repression of mouse
heat shock factor 1. *Mol. and Cell. Biol.* 18, 906-918.

10. Newton, E., Knauf, U., Green, M., Kingston, R. (1996) The regulatory domain of human heat shock factor 1 is sufficient to sense heat stress. *Mol. and Cell. Biol.* 16, 839-846.

11. Hilgarth, R., Hong, Y., Park-Sarge, O., Sarge, K. (2003) Insights into the regulation of heat shock transcription factor 1 SUMO-1 modification. *Biochem. and Biophys. Res. Comm.* 303**,** 196-200.

12. Kline, M., Morimoto, R. (1997) Repression of the heat shock factor 1 transcriptional activation domain is modulated by constitutive phosphorylation. *Mol. and Cell. Biol.* 17, 2107-2115.

13. Holmberg C., Hietakangas V., Mikhailov, A., Rantanen, J., Kallio, M., Meinander, A., Hellman, J., Morrice, N., MacKintosh, C., Morimoto, R., Eriksson, J., Sistonen, L. (2001) Phosphorylation of serine 230 promotes inducible transcriptional activity of heat shock factor 1. *EMBO J.* 20, 3800-3810.

14. Hay, R. (2001) Protein modification by SUMO. *TIBS* 26, 332-333.

15. Seeler, J., Dejean, A. (2003) Nuclear and unclear functions of SUMO. *Nat. Rev. Mol. Cell Bio.* 4, 690-699.

16. Gill, G. (2003) Post-translational modification by the small ubiquitin-related modifier SUMO has big effects on transcription factor activity. *Curr. Op. Gen. & Dev.* 13, 108-113.

17. Kroll, M., Conconi, M., Desterro, M., Marin, A., Thomas, D., Friguet, B., Hay, R., Virelizier, J., Arenzana-Seisdedos, F., Rodriguez, M. (1997) The carboxy-terminus of
IKBa determines susceptibility to degradation by the catalytic core of the proteasome.
Oncogene 15, 1841-1850.

18. Subramanian, L., Benson, M., Iniguez-Lluhi, J. (2003) Synergy control motif within the attenuator domain of CCAAT/enhancer-binding protein a inhibits transcriptional synergy through its PIASy-enhanced modification by SUMO-1 or SUMO-3. *J. Biol. Chem.* 278, 9134-9141.

19. Hong, Y., Rogers, R., Matunis, M., Mayhew, C., Goodson, M., Park-Sarge, O., Sarge, K. (2001) Regulation of heat shock transcription factor 1 by stress-induced SUMO-1 modification. *J. Biol. Chem.* 276, 40263-40267.

20. Hietakangas, V., Ahlskog, J., Jakobsson, A., Hellesuo, M., Sahlberg, N., Holmberg, C., Mikhailov, A., Palvimo, J., Pirkkala, L., Sistonen, L. (2003). Phosphorylation of serine 303 is a prerequisite for the stress-inducible SUMO modification of heat shock factor 1. *Mol. and Cell. Biol.* 23, 2953-2968.

21. Drees, B., Rye, H., Glazer, A., Nelson, H. (1996) Environment-sensitive labels in multiplex fluorescence analyses of protein-DNA complexes. *J. Biol. Chem.* 271, 32168-32173.

22. Ahn, S., Thiele, D. (2003) Redox regulation of mammalian heat shock factor 1 is essential for Hsp gene activation and protection from stress. *Genes & Dev.* 17, 516-528.

23. Westwood, J., Wu, C. (1993) Activation of *Drosophila* heat shock factor: conformational change associated with a monomer-to-trimer transition. *Mol. and Cell. Biol.* 13, 3481-3486.

24. Goodson, M., Sarge, K. (1995) Heat-inducible DNA binding of purified heat shock transcription factor 1. *J Biol Chem.* 270, 2447-50.

25. Heydari, A., You, S., Takahashi, R., Gutsmann-Conrad, A., Sarge, K., Richardson, A. (2000) Age-related alterations in the activation of heat shock transcription factor 1 in rat hepatocytes. *Exp Cell Res*. 256, 83-93.

26. Guo, Y., Guettouche, T., Fenna, M., Boellmann, F., Pratt, W., Toft, D., Smith, D., Voellmy, R. (2001) Evidence for a mechanism of repression of heat shock factor 1 transcriptional activity by a multichaperone complex. *J. Biol. Chem.* 276, 45791-45799.

27. Morishima, Y., Murphy, P., Li, D., Sanchez, E., Pratt, W. (2000) Stepwise assembly of a glucocorticoid receptor. Hsp90 heterocomplex resolves two ATP-dependent events involving first hsp70 and then hsp90 in opening of the steroid binding pocket. *J. Biol. Chem.* 275, 18054-60.

REFERENCES

1. Alzheimer, A., Stelzmann, R. A., Schnitzlein, H. N., and Murtagh, F. R. (1995) An English translation of Alzheimer's 1907 paper, "Uber eine eigenartige Erkankung der Hirnrinde", *Clin Anat 8*, 429-431.

2. Luhrs, T., Ritter, C., Adrian, M., Riek-Loher, D., Bohrmann, B., Dobeli, H., Schubert, D., and Riek, R. (2005) 3D structure of Alzheimer's amyloid-beta(1-42) fibrils, *Proc Natl Acad Sci U S A 102*, 17342-17347.

3. Chiti, F., Webster, P., Taddei, N., Clark, A., Stefani, M., Ramponi, G., and Dobson, C. M. (1999) Designing conditions for in vitro formation of amyloid protofilaments and fibrils, *Proc Natl Acad Sci U S A 96*, 3590-3594.

4. Glabe, C. G. (2004) Conformation-dependent antibodies target diseases of protein misfolding, *Trends Biochem Sci 29*, 542-547.

5. Glabe, C. G. (2006) Common mechanisms of amyloid oligomer pathogenesis in degenerative disease, *Neurobiol Aging 27*, 570-575.

6. (2008) Alzheimer's Association.

7. Harper, J. D., and Lansbury, P. T., Jr. (1997) Models of amyloid seeding in Alzheimer's disease and scrapie: mechanistic truths and physiological consequences of the time-dependent solubility of amyloid proteins, *Annu Rev Biochem 66*, 385-407.

8. Selkoe, D. J. (1991) The molecular pathology of Alzheimer's disease, *Neuron 6*, 487-498.

9. Glenner, G. G., and Wong, C. W. (1984) Alzheimer's disease: initial report of the purification and characterization of a novel cerebrovascular amyloid protein, *Biochem Biophys Res Commun 120*, 885-890.

10. LaFerla, F. M., and Oddo, S. (2005) Alzheimer's disease: Abeta, tau and synaptic dysfunction, *Trends Mol Med 11*, 170-176.

11. Chauhan, N. B., and Siegel, G. J. (2002) Reversal of amyloid beta toxicity in Alzheimer's disease model Tg2576 by intraventricular antiamyloid beta antibody, *J Neurosci Res 69*, 10-23.

12. Banks, W. A., Farr, S. A., Morley, J. E., Wolf, K. M., Geylis, V., and Steinitz, M. (2007) Anti-amyloid beta protein antibody passage across the blood-brain barrier in the SAMP8 mouse model of Alzheimer's disease: an age-related selective uptake with reversal of learning impairment, *Experimental neurology 206*, 248-256.

13. Garzon-Rodriguez, W., Sepulveda-Becerra, M., Milton, S., and Glabe, C. G. (1997) Soluble amyloid Abeta-(1-40) exists as a stable dimer at low concentrations, *J Biol Chem 272*, 21037-21044.

14. Garzon-Rodriguez, W., Vega, A., Sepulveda-Becerra, M., Milton, S., Johnson, D. A., Yatsimirsky, A. K., and Glabe, C. G. (2000) A conformation change in the carboxyl terminus of Alzheimer's Abeta (1-40) accompanies the transition from dimer to fibril as revealed by fluorescence quenching analysis, *J Biol Chem 275*, 22645-22649.

15. Chen, Y. R., and Glabe, C. G. (2006) Distinct early folding and aggregation properties of Alzheimer amyloid-beta peptides Abeta40 and Abeta42: stable trimer or tetramer formation by Abeta42, *J Biol Chem 281*, 24414-24422.

16. Klein, W. L., Krafft, G. A., and Finch, C. E. (2001) Targeting small Abeta oligomers: the solution to an Alzheimer's disease conundrum?, *Trends Neurosci 24*, 219-224.

17. Mucke, L., Masliah, E., Yu, G. Q., Mallory, M., Rockenstein, E. M., Tatsuno, G., Hu, K., Kholodenko, D., Johnson-Wood, K., and McConlogue, L. (2000) High-level neuronal expression of abeta 1-42 in wild-type human amyloid protein precursor transgenic mice: synaptotoxicity without plaque formation, *J Neurosci 20*, 4050-4058.

18. Lesne, S., Koh, M. T., Kotilinek, L., Kayed, R., Glabe, C. G., Yang, A., Gallagher, M., and Ashe, K. H. (2006) A specific amyloid-beta protein assembly in the brain impairs memory, *Nature 440*, 352-357.

19. Townsend, M., Shankar, G. M., Mehta, T., Walsh, D. M., and Selkoe, D. J. (2006) Effects of secreted oligomers of amyloid beta-protein on hippocampal synaptic plasticity: a potent role for trimers, *J Physiol 572*, 477-492.

20. Haass, C., and Selkoe, D. J. (2007) Soluble protein oligomers in neurodegeneration: lessons from the Alzheimer's amyloid beta-peptide, *Nature reviews 8*, 101-112.

21. Demuro, A., Mina, E., Kayed, R., Milton, S. C., Parker, I., and Glabe, C. G. (2005) Calcium dysregulation and membrane disruption as a ubiquitous neurotoxic mechanism of soluble amyloid oligomers, *J Biol Chem 280*, 17294-17300.

22. Hertel, C., Terzi, E., Hauser, N., Jakob-Rotne, R., Seelig, J., and Kemp, J. A. (1997) Inhibition of the electrostatic interaction between beta-amyloid peptide and membranes prevents beta-amyloid-induced toxicity, *Proc Natl Acad Sci U S A 94*, 9412-9416.

23. Kourie, J. I., Culverson, A. L., Farrelly, P. V., Henry, C. L., and Laohachai, K. N. (2002) Heterogeneous amyloid-formed ion channels as a common cytotoxic mechanism: implications for therapeutic strategies against amyloidosis, *Cell Biochem Biophys 36*, 191-207.

24. Kayed, R., Sokolov, Y., Edmonds, B., McIntire, T. M., Milton, S. C., Hall, J. E., and Glabe, C. G. (2004) Permeabilization of lipid bilayers is a common conformation-dependent activity of soluble amyloid oligomers in protein misfolding diseases, *J Biol Chem 279*, 46363-46366.

25. Fagan, T., Kagan, B., Corbin, D., Hwang, W., Glabe, C., Nault, L., Lal, R., Teplow, D., Albensi, B., and Sokolov, Y. (2006) Alzheimer Research Forum Live Discussion: Now you see them, now you don't: The amyloid channel hypothesis, *J Alzheimers Dis 9*, 219-224.

26. Lashuel, H. A., and Lansbury, P. T., Jr. (2006) Are amyloid diseases caused by protein aggregates that mimic bacterial pore-forming toxins?, *Q Rev Biophys 39*, 167-201.

27. Lin, H., Bhatia, R., and Lal, R. (2001) Amyloid beta protein forms ion channels: implications for Alzheimer's disease pathophysiology, *Faseb J 15*, 2433-2444.

28. Simakova, O., and Arispe, N. J. (2006) Early and late cytotoxic effects of external application of the Alzheimer's Abeta result from the initial formation and function of Abeta ion channels, *Biochemistry 45*, 5907-5915.

29. Kawahara, M., Kuroda, Y., Arispe, N., and Rojas, E. (2000) Alzheimer's beta-amyloid, human islet amylin, and prion protein fragment evoke intracellular free calcium elevations by a common mechanism in a hypothalamic GnRH neuronal cell line, *J Biol Chem 275*, 14077-14083.

30. Arispe, N., Pollard, H. B., and Rojas, E. (1996) Zn2+ interaction with Alzheimer amyloid beta protein calcium channels, *Proc Natl Acad Sci U S A 93*, 1710-1715.

31. Arispe, N., Pollard, H. B., and Rojas, E. (1993) Giant multilevel cation channels formed by Alzheimer disease amyloid beta-protein [A beta P-(1-40)] in bilayer membranes, *Proc Natl Acad Sci U S A 90*, 10573-10577.

32. Quist, A., Doudevski, I., Lin, H., Azimova, R., Ng, D., Frangione, B., Kagan, B., Ghiso, J., and Lal, R. (2005) Amyloid ion channels: a common structural link for protein-misfolding disease, *Proc Natl Acad Sci U S A 102*, 10427-10432.

33. Arispe, N., Rojas, E., and Pollard, H. B. (1993) Alzheimer disease amyloid beta protein forms calcium channels in bilayer membranes: blockade by tromethamine and aluminum, *Proc Natl Acad Sci U S A 90*, 567-571.

34. Dong, Z., Saikumar, P., Weinberg, J. M., and Venkatachalam, M. A. (2006) Calcium in cell injury and death, *Annual review of pathology 1*, 405-434.

35. Selkoe, D. J. (2006) The ups and downs of Abeta, *Nat Med 12*, 758-759; discussion 759.

36. Terzi, E., Holzemann, G., and Seelig, J. (1995) Self-association of beta-amyloid peptide (1-40) in solution and binding to lipid membranes, *J Mol Biol 252*, 633-642.

37. Terzi, E., Holzemann, G., and Seelig, J. (1997) Interaction of Alzheimer beta-amyloid peptide(1-40) with lipid membranes, *Biochemistry 36*, 14845-14852.

38. Bokvist, M., Lindstrom, F., Watts, A., and Grobner, G. (2004) Two types of Alzheimer's beta-amyloid (1-40) peptide membrane interactions: aggregation preventing transmembrane anchoring versus accelerated surface fibril formation, *J Mol Biol 335*, 1039-1049.

39. Teplow, D. B. (2006) Preparation of amyloid beta-protein for structural and functional studies, *Methods Enzymol 413*, 20-33.

40. Fezoui, Y., Hartley, D. M., Harper, J. D., Khurana, R., Walsh, D. M., Condron, M. M., Selkoe, D. J., Lansbury, P. T., Jr., Fink, A. L., and Teplow, D. B. (2000) An improved method of preparing the amyloid beta-

protein for fibrillogenesis and neurotoxicity experiments, *Amyloid 7*, 166-178.

41. LeVine, H., 3rd. (1999) Quantification of beta-sheet amyloid fibril structures with thioflavin T, *Methods Enzymol 309*, 274-284.

42. Charles, J., Stewart, M. (1980) Colorimetric determination of phospholipids with ammonium ferrothiocyanate, *Analytical Biochemistry 104*, 10-14.

43. McLaurin, J., and Chakrabartty, A. (1997) Characterization of the interactions of Alzheimer beta-amyloid peptides with phospholipid membranes, *Eur J Biochem 245*, 355-363.

44. Alarcon, J. M., Brito, J. A., Hermosilla, T., Atwater, I., Mears, D., and Rojas, E. (2006) Ion channel formation by Alzheimer's disease amyloid beta-peptide (Abeta40) in unilamellar liposomes is determined by anionic phospholipids, *Peptides 27*, 95-104.

45. Ladokhin, A. S., and White, S. H. (1999) Folding of amphipathic alpha-helices on membranes: energetics of helix formation by melittin, *Journal of molecular biology 285*, 1363-1369.

46. Terzi, E., Holzemann, G., and Seelig, J. (1994) Alzheimer beta-amyloid peptide 25-35: electrostatic interactions with phospholipid membranes, *Biochemistry 33*, 7434-7441.

47. Del Mar Martinez-Senac, M., Villalain, J., and Gomez-Fernandez, J. C. (1999) Structure of the Alzheimer beta-amyloid peptide (25-35) and its interaction with negatively charged phospholipid vesicles, *Eur J Biochem 265*, 744-753.

48. Maji, S. K., Amsden, J. J., Rothschild, K. J., Condron, M. M., and Teplow, D. B. (2005) Conformational dynamics of amyloid beta-protein assembly probed using intrinsic fluorescence, *Biochemistry 44*, 13365-13376.

49. Choo-Smith, L. P., Garzon-Rodriguez, W., Glabe, C. G., and Surewicz, W. K. (1997) Acceleration of amyloid fibril formation by specific binding of Abeta-(1-40) peptide to ganglioside-containing membrane vesicles, *J Biol Chem 272*, 22987-22990.

50. Breukink, E., van Kraaij, C., van Dalen, A., Demel, R. A., Siezen, R. J., de Kruijff, B., and Kuipers, O. P. (1998) The orientation of nisin in membranes, *Biochemistry 37*, 8153-8162.

51. Blondelle, S. E., Lohner, K., and Aguilar, M. (1999) Lipid-induced conformation and lipid-binding properties of cytolytic and antimicrobial peptides: determination and biological specificity, *Biochimica et biophysica acta 1462*, 89-108.

52. Lee, M. T., Hung, W. C., Chen, F. Y., and Huang, H. W. (2005) Many-body effect of antimicrobial peptides: on the correlation between lipid's spontaneous curvature and pore formation, *Biophys J 89*, 4006-4016.

53. Ege, C., and Lee, K. Y. (2004) Insertion of Alzheimer's A beta 40 peptide into lipid monolayers, *Biophys J 87*, 1732-1740.

54. Devanathan, S., Salamon, Z., Lindblom, G., Grobner, G., and Tollin, G. (2006) Effects of sphingomyelin, cholesterol and zinc ions on the binding, insertion and aggregation of the amyloid Abeta(1-40) peptide in solid-supported lipid bilayers, *The FEBS journal 273*, 1389-1402.

55. Sreerama, N., and Woody, R. W. (2000) Estimation of protein secondary structure from circular dichroism spectra: comparison of CONTIN, SELCON, and CDSSTR methods with an expanded reference set, *Anal Biochem 287*, 252-260.

56. Wenk, M. R., and Seelig, J. (1998) Magainin 2 amide interaction with lipid membranes: calorimetric detection of peptide binding and pore formation, *Biochemistry 37*, 3909-3916.

57. Zhao, H., Sood, R., Jutila, A., Bose, S., Fimland, G., Nissen-Meyer, J., and Kinnunen, P. K. (2006) Interaction of the antimicrobial peptide pheromone Plantaricin A with model membranes: implications for a novel mechanism of action, *Biochim Biophys Acta 1758*, 1461-1474.

58. White S.H., W., M.C. (1995) *Determination of the structure of fluid lipid bilayer membranes*, CRC Press.

59. White S.H., W., M.C. (1996) *The liquid-crystallographic structure of fluid lipid bilayer membranes*, Cirkhauser, Boston.

60. Zhu, Y. J., Lin, H., and Lal, R. (2000) Fresh and nonfibrillar amyloid beta protein(1-40) induces rapid cellular degeneration in aged human fibroblasts: evidence for AbetaP-channel-mediated cellular toxicity, *Faseb J 14*, 1244-1254.

61. Shankar, G. M., Li, S., Mehta, T. H., Garcia-Munoz, A., Shepardson, N. E., Smith, I., Brett, F. M., Farrell, M. A., Rowan, M. J., Lemere, C. A., Regan, C. M., Walsh, D. M., Sabatini, B. L., and Selkoe, D. J. (2008)

Amyloid-beta protein dimers isolated directly from Alzheimer's brains impair synaptic plasticity and memory, *Nat Med 14*, 837-842.

62. Klein, W. L., Stine, W. B., Jr., and Teplow, D. B. (2004) Small assemblies of unmodified amyloid beta-protein are the proximate neurotoxin in Alzheimer's disease, *Neurobiol Aging 25*, 569-580.

63. Selkoe, D. J. (2008) Soluble oligomers of the amyloid beta-protein impair synaptic plasticity and behavior, *Behavioural brain research 192*, 106-113.

64. Sokolov, Y., Kozak, J. A., Kayed, R., Chanturiya, A., Glabe, C., and Hall, J. E. (2006) Soluble amyloid oligomers increase bilayer conductance by altering dielectric structure, *J Gen Physiol 128*, 637-647.

65. Parasassi, T., De Stasio, G., Ravagnan, G., Rusch, R. M., and Gratton, E. (1991) Quantitation of lipid phases in phospholipid vesicles by the generalized polarization of Laurdan fluorescence, *Biophys J 60*, 179-189.

66. McLaurin, J., and Chakrabartty, A. (1996) Membrane disruption by Alzheimer beta-amyloid peptides mediated through specific binding to either phospholipids or gangliosides. Implications for neurotoxicity, *J Biol Chem 271*, 26482-26489.

67. Hirakura, Y., Lin, M. C., and Kagan, B. L. (1999) Alzheimer amyloid abeta1-42 channels: effects of solvent, pH, and Congo Red, *J Neurosci Res 57*, 458-466.

68. Huang, H. W. (2000) Action of antimicrobial peptides: two-state model, *Biochemistry 39*, 8347-8352.

69. Huang, H. W. (2006) Molecular mechanism of antimicrobial peptides: the origin of cooperativity, *Biochim Biophys Acta 1758*, 1292-1302.

70. Sanderson, J. M. (2005) Peptide-lipid interactions: insights and perspectives, *Org Biomol Chem 3*, 201-212.

71. Allende, D., Simon, S. A., and McIntosh, T. J. (2005) Melittin-induced bilayer leakage depends on lipid material properties: evidence for toroidal pores, *Biophys J 88*, 1828-1837.

72. Balasubramanian, K., Mirnikjoo, B., and Schroit, A. J. (2007) Regulated externalization of phosphatidylserine at the cell surface: implications for apoptosis, *J Biol Chem 282*, 18357-18364.

73. Thelen, K. M., Falkai, P., Bayer, T. A., and Lutjohann, D. (2006) Cholesterol synthesis rate in human hippocampus declines with aging, *Neuroscience letters 403*, 15-19.

74. Wood, W. G., Schroeder, F., Igbavboa, U., Avdulov, N. A., and Chochina, S. V. (2002) Brain membrane cholesterol domains, aging and amyloid beta-peptides, *Neurobiol Aging 23*, 685-694.

75. Cleary, J. P., Walsh, D. M., Hofmeister, J. J., Shankar, G. M., Kuskowski, M. A., Selkoe, D. J., and Ashe, K. H. (2005) Natural oligomers of the amyloid-beta protein specifically disrupt cognitive function, *Nat Neurosci 8*, 79-84.

76. Walsh, D. M., Klyubin, I., Fadeeva, J. V., Cullen, W. K., Anwyl, R., Wolfe, M. S., Rowan, M. J., and Selkoe, D. J. (2002) Naturally secreted oligomers of amyloid beta protein potently inhibit hippocampal long-term potentiation in vivo, *Nature 416*, 535-539.

77. Grimm, M. O., Grimm, H. S., Patzold, A. J., Zinser, E. G., Halonen, R., Duering, M., Tschape, J. A., De Strooper, B., Muller, U., Shen, J., and Hartmann, T. (2005) Regulation of cholesterol and sphingomyelin metabolism by amyloid-beta and presenilin, *Nat Cell Biol 7*, 1118-1123.

78. Wahrle, S., Das, P., Nyborg, A. C., McLendon, C., Shoji, M., Kawarabayashi, T., Younkin, L. H., Younkin, S. G., and Golde, T. E. (2002) Cholesterol-dependent gamma-secretase activity in buoyant cholesterol-rich membrane microdomains, *Neurobiology of disease 9*, 11-23.

79. Puglielli, L., Tanzi, R. E., and Kovacs, D. M. (2003) Alzheimer's disease: the cholesterol connection, *Nat Neurosci 6*, 345-351.

80. Kontush, A., and Chapman, M. J. (2008) HDL: close to our memories?, *Arterioscler Thromb Vasc Biol 28*, 1418-1420.